Role of the cytoskeleton in regulating axonal tension and growth cone traction dynamics

A thesis submitted in partial fulfillment of the requirements for the Degree of Doctor of Philosophy

Sampada P. Mutalik

20123151

Indian Institute of Science Education and Research (IISER), Pune

2018

DECLARATION

I declare that this written submission represents my ideas in my own words and where others' ideas have been included; I have adequately cited and referenced the original sources. I also declare that I have adhered to all principles of academic honesty and integrity and have not misrepresented or fabricated or falsified any idea/data/fact/source in my submission. I understand that violation of the above will be cause for disciplinary action by the Institute and can also evoke penal action from the sources that have not been properly cited or from whom proper permission has not been taken when needed.

Date:

Sampada P. Mutalik

20123151

CERTIFICATE

Certified that the work incorporated in the thesis entitled **"Role of the cytoskeleton in regulating axonal tension and growth cone traction dynamics"**, Submitted by Ms. Sampada P. Mutalik was carried out by the candidate, under my supervision. The work presented here or any part of it has not been included in any other thesis submitted previously for the award of any degree or diploma from any other University or institution.

Date: Dr. Aurnab Ghose

Thesis advisor

ACKNOWLEDGMENTS

I joined IISER Pune as a Ph.D. student in January 2012. Since then it has been a great experience and I have learned a lot in all these years. I take this opportunity to thank everyone who helped me directly or indirectly during this period.

I would like to thank my thesis advisor Dr. Aurnab Ghose for giving me the opportunity to work with him. He always gave me enough freedom to venture into new directions and helped me to grow as an independent researcher. I have learned from him to handle each and every problem patiently and optimistically. He not only helped me to build my communication and writing skills but also to look at any scientific problem in different perspectives and in a larger picture.

I would like to thank my collaborator and co-advisor, Dr. Pramod Pullarkat (RRI, Bangalore) for giving me the opportunity to work in his lab and for helping me throughout the project. His valuable suggestions and constructive criticism have always helped me during my research. I could develop the different kinds of interdisciplinary skillsets in his lab which was not possible otherwise.

I thank our collaborator Dr. Joby Joseph (Hyderabad university) for his timely help with the mitochondria analysis. He helped us immensely to get mitochondria analysis working which was otherwise nearly impossible. I sincerely thank my research advisory committee members Dr. Thomas Pucadyil (IISER Pune) and Dr. Richa Ricky (IISER Pune) for their valuable inputs and suggestions.

I am grateful to Dr. Deepak Barua (IISER Pune) for helping me with the statistical analysis and discussions regarding the mitochondria analysis. I would like to thank Dr. Shamik Sen and Kavitha Sthanam (IIT, Bombay) for the kind help with

stiffness measurements of PAA gels. I acknowledge Dr. David Odde (University of Minnesota) for generously sharing the flow-tracker code and for help with the analysis.

I would like to thank my lab colleagues- Ketakee, Tanushree, Priyanka, Aditi, Devika and Dhriti and Rale. Their inputs and suggestions during lab meetings and journal club have always helped me to do better. Also, I thank them for bearing with me and my bad jokes for such a long time! I thank Ketakee once again, part of her work is complementary to retrograde flow and traction analysis data presented in this thesis and hence have helped to make our case stronger regarding Fmn2 studies and weak clutch.

I thank my previous lab members Abhishek, Ajesh, Girish and Jagruti. Abhishek, Ajesh and Ketakee formed a really nice framework of Fmn2 study which became the basis of work on Fmn2 and weak clutch presented in this thesis. I express my gratitude towards Jagruti and Girish who initiated this project in the lab and have helped in my early days of Ph.D. I would like to thank my RRI colleagues-Giri, Anagha, Renu, Susav Arslan, Serene and Sushil. They made my stay at RRI pleasant and enjoyable. It was fun to work with people with the different backgrounds and perspectives. Thanks to Lakshmi for exploring some of the interesting aspects of the growth cone traction in her master thesis. I would like to thank Amrutha and Raghuram for helping me with some of the experiments and/or analysis.

I made many friends in IISER during my Ph.D. and have shared really great moments with them. No point in being so formal with Manasi, but I take this opportunity to thank her for the fun time we had as well as heating discussions about the science. She was always there to hear out problems and excitement about the new results as well. I would like to thank Sayali, Neerja, Radhika, Mungi, Sukrut

and Devika (TP lab) for their friendship and help. Sayali and I have shared many crazy and joyful moments together, especially in the long, live imaging slots and tea breaks.

I cannot imagine the imaging facility without Vijay Vitthal; he was extremely helpful and I would like to thank him and other staff of imaging facility-Aaditi, Boni and Santosh. All the technical and administrative staff at IISER have been very helpful, especially Mrinalini, Shabnam, Piyush, Kalpesh and Mahesh Rote. I thank IISER Pune for providing me the infrastructure and facility to carry out my work and DBT for the funding.

I express my gratitude towards my family for all the support, they were always ready to handle my mood swings at the end of the day. My mother, My elder brother (Bharadwaj) and sister (Harshada) have been a great support in whatever I could achieve.

Any scientific finding builds on the existing knowledge and research. I am grateful to all those researchers who pioneered and developed the field over the years and inspired young researchers like me to do exciting science.

Contents

List of Figures

ABSTRACT

Functions of neuronal cells are influenced by mechanical forces due to their unique shape and geometry. Neurons are highly polarized cells with thin, elongated axons and motile structures at the tip; growth cones. Directional growth cone motility is required for the formation of precise neuronal connections. Growth cone motility is driven by transmission of actomyosin dependent contractile forces onto the substrate via integrin-ECM complexes. How the F-actin network remodelling and coupling to adhesion sites regulate traction forces in growth cones is understudied. Our lab has recently identified an actin nucleator of formin family, Formin 2 (Fmn2). Fmn2 regulates actin organization in growth cones, their substrate interaction and motility (Sahasrabudhe et al, 2016). In this context, we have explored the role of Fmn2 in regulation of the traction forces in neuronal growth cones; described in the first part of this thesis.

In this work, using a filopodial bead-pulling assay of neurons plated on deformable gels, we show that Fmn2 depletion compromises filopodial contractility. Increase in retrograde flow in growth cones upon Fmn2 knockdown indicates that Fmn2 regulates clutch engagement and force transmission. Further, measurements of growth cone traction upon Fmn2 knockdown again indicate Fmn2 dependent traction force regulation. Collectively, this work establishes Fmn2 as a regulator of force transmission via regulation of clutch and provides the underlying mechanism of the growth cone motility.

Mechanotransduction is likely to be an important mechanism of signalling in thin, elongated cells like neurons. Maintenance of pre-stress or rest tension may facilitate mechanotransduction in these cells. In recent years, functional roles for mechanical tension in neuronal development and physiology are beginning to emerge

but the cellular mechanisms regulating neurite tension remain poorly understood. Active contraction of neurites is a potential mechanism of tension regulation. In this study, we have explored cytoskeletal mechanisms mediating active contractility of neuronal axons. We have developed a simple assay where we evaluate contraction of curved axons upon trypsin-mediated detachment. We show that curved axons undergo contraction and straighten upon de-adhesion. Axonal straightening was found to be actively driven by actomyosin contractility, while microtubules may subserve a secondary role. We find that while axons show a monotonous decrease in length upon contraction, subcellularly, the cytoskeleton shows a heterogeneous contractile response. Further, using an assay for spontaneous development of tension (without trypsin-induced de-adhesion), we show that axons are intrinsically contractile. These experiments, using novel experimental approaches, implicate the axonal cytoskeleton in tension homeostasis. Our data suggest that while globally the axon behaves as a mechanical continuum, locally the cytoskeleton is remodelled heterogeneously.

So far, this study involves developing assays to look at local regulation of mechanical forces in growth cones and axons. In the future, these assays will allow us to explore force balance between growth cone traction and axonal tension and its functional implications.

1. Synopsis

1.1 Introduction

The nervous system of an organism consists of highly specialized cells called neurons which form a complex stereotyped network driving unique higher-order functions. Regulation of neuronal cell shape, maintenance of its structural integrity and its directed motility are required to achieve precise neuronal connections. Spatiotemporally regulated biochemical signaling is known to drive neuronal elongation and formation of connections during the development. Role of biochemical signaling in neuronal development is very well appreciated [1] but functions of mechanical forces are only beginning to emerge. Underlying cytoskeleton in neurons not only provide structural stability but also plasticity to respond to the extracellular biomechanical cues. How different cytoskeletal organization and their dynamics might regulate mechanical forces is addressed better in different cell types but is still elusive in neurons. In this thesis, cytoskeletal mechanisms driving regulation of mechanical forces in neurons will be discussed. Neurons are highly polarized cells with thin, elongated extensions called axons and at the tip, sensory structures called growth cones. Formation of the functional neuronal network is based on the successful navigation of growth cones to their

respective targets and formation of synapses. Directed growth cone motility requires coordinated cytoskeletal dynamics in response to the guidance cues [2]. Growth cone has two types of protrusive structures: filopodia and lamellipodia. Filopodia are finger-like projections that harbor receptors for the various cues and hence act as antennae to explore the environment. Lamellipodia are flat, veil-like projections at the base of filopodia. Filopodia are formed of parallel bundles of F-actin and lamellipodia have dense meshwork of F-actin and microtubule bundle entering from the axonal shaft [3]. It has been established that these structures and their underlying cytoskeletal drive the directed growth cone motility [4, 5]. Growth cones form contacts with the substrate through integrin-mediated signaling complexes that allow transmission of traction forces on to the substrate in order to move forward. Role of the actin cytoskeleton in growth cone motility has been studied previously. Depolymerization of actin causes impaired growth cone motility suggesting a role of actin dynamics and its regulation in growth cone motility [6, 7]. Actin dynamics and its polymer network is very well regulated by different accessory proteins including actin nucleators, elongators, capping and bundling proteins [8]. How actin regulators orchestrate polymers structures, their dynamics and couple these to substrate adhesions to generate coordinated traction in growth cone motility is poorly understood.

There is a growing list of actin binding proteins in the last few years and how these proteins modulate actin machinery and in turn motility is an active area of investigation. Role of different actin binding proteins in regulating traction forces has been suggested in a few studies [9–11]. Interestingly, some of the actin nucleators involved in nucleation and elongation of actin filaments are shown to regulate traction forces [12, 13]. The primary function of actin nucleators is to

drive actin nucleation which is otherwise thermodynamically unfavorable [14]. In neurons, a class of actin nucleator, formins seems to be playing a critical role. Formins are involved in nucleation and elongation of straight and unbranched actin filaments hence may have a dominant role in filopodia formation [15–17]. In neuronal growth cones; how actin assembly proteins like formins might regulate pulling forces is not known. In this thesis, we will discuss the role of Formin-2 (Fmn2) [18] in regulating traction forces in growth cones (chapter 2).

Neuronal growth cones navigate long distance from their respective cell bodies in order to form connections. It is demonstrated that, in cultures, moving growth cones apply stretch on axons as they advance [19, 20]. Once connections are formed, axons spanned by long distances undergo stretch as the surrounding tissue expands and the animal grows. Axonal stretch is known to affect various functions from neuronal growth [21] to synapse formation [22].

Axons are filled with heavily cross-linked microtubules and neurofilaments [23–25]. Microtubules act as tracks for dyneins and kinesins which move cargoes anterogradely and retrogradely [26], respectively. Actin is mainly present in the cortical region underneath the membrane [27]. Periodic actin rings organized by spectrin underneath the membrane offer mechanical stability to thin axons. Dynamics of the axonal cytoskeleton and its functions are not very well studied. Recently, actin trails and actin patches have been shown to be dynamic actin structures in axons [28]. However, the functional context of these structures is still missing. Though stretch-dependent neuronal functions are characterized; the cytoskeletal dynamics driving different stretch-dependent responses are not very well explored. Stretch-dependent elongation is the only phenomenon which has been addressed to some extent where mechanisms for cytoskeletal dynamics have

been proposed [29]. The focus of the field has been the stretch as a cue to drive various neuronal functions. Intrinsic mechanisms involved in regulating neuronal rest tension and the role of cytoskeleton dynamics remained poorly understood. In this thesis, we propose axonal contraction as a potential mechanism regulating neuronal rest tension and we discuss the cytoskeletal mechanisms of axonal contractility (chapter 3, 4 and 5).

1.2 Objectives

A. Filopodial extension, attachment to the substrate and contractility are important steps in growth cone motility. Through integrin-mediated engagement with the ECM, transient focal contacts are formed and traction forces are transmitted on to the substrate. How filopodia exert pulling forces, how actin dynamics and associated motors regulate it, have been the focus of several studies, in last few years [30]. We investigated this problem in a context of previously characterized actin nucleator of formin family, Fmn2. Fmn2-mediated growth cone motility, its enrichment along filopodial bundles and at the tip of filopodia have been shown previously by our group. Levels of pFAK (Y-397), an activity marker for focal contacts, reduce significantly at the tip of filopodia upon Fmn2 knockdown. The shorter lifetime of filopodia suggests weaker substrate interaction and transmission of forces [18]. Based on these results, we propose to study the role of Fmn2 in regulating filopodial traction dynamics. Interestingly, Fmn2-mediated actin organization not only regulate filopodial dynamics but also growth cone area and its substrate interaction [18]; suggesting the function of Fmn2 in regulating growth cone traction. We propose to test these speculations and understand mechanisms

of Fmn2 dependent growth cone motility using retrograde flow analysis and traction force measurements (chapter 2).

B. Regulation of prestress or rest tension might be important to achieve mechanotransduction in thin, elongated axons. In the field of axonal mechanics, stretch growth and its functions have been studied extensively [21, 29, 31], however, mechanisms regulating axonal rest tension have received relatively little attention. Axonal contraction is a potential mechanism regulating axonal rest tension. Current understanding of axonal tension regulation and contraction is based on the limited set of localized, mechanical perturbations like ablation, microneedle-based pulling or slackening. In the current study, we aim to develop novel paradigms which are less intrusive and globally acting to probe cytoskeletal mechanisms driving regulation of axonal contraction and rest tension (chapter 3 and 4). Further, we propose to understand mechanisms of mechanical tension regulation in the great quantitative details using a novel force measurement technique, Optical fiber-based force transducer (chapter 5).

1.3 Major Findings in this study

1.3.1 Formin-2 (Fmn2) in regulating filopodial contractility and traction forces in growth cones

Growth cone motility is a crucial step in axonal guidance and formation of functional neuronal connections. Our lab has established the role of Fmn2 in growth cone motility [18]. Using biophysical assays like traction force measurements and filopodial pulling assay we show that Fmn2 is involved in regulating growth cone

traction via regulation of the clutch.

Fmn2 regulates Filopodial traction dynamics

It has been shown earlier in the lab that upon morpholino-based Fmn2 knockdown, growth cone motility is compromised. Using pFAK (Y-397) as an activity marker for focal contacts, it has been shown that Fmn2 knockdown leads to the weaker interaction of filopodia with the substrate. Interestingly, this defect was significantly dominant at the tip of filopodia compared to the base [18]. This suggests that force dependent maturation of nascent focal contacts at the tip is affected. We tested this hypothesis using a bead pulling assay to evaluate the filopodial pulling forces.

Using a bead pulling assay, on a compliant gel, we showed that Fmn2 regulates traction dynamics of filopodia. As compared to the control, Fmn2 morphants show reduced pulling velocity, though the frequency of pulling is comparable with the control.

pFAK (Y-397) levels not only drop significantly at the tip of filopodia but also across growth cones suggesting function of Fmn2 in regulating traction in the central region as well. We tested this possibility by measuring retrograde flow in growth cones and estimating traction forces upon Fmn2 knockdown.

Fmn2 regulates transmission of forces via regulation of molecular clutch

Reduced traction dynamics at the tip of filopodia and drop in pFAK (Y-397) activity [18] in growth cones upon Fmn2 knockdown suggested the involvement of Fmn2 in regulating clutch. If F-actin bundles are not engaged very well at the tip then the force will not be transmitted on the substrate and retrograde flow

would increase. To test this hypothesis, we measured retrograde flow in control and Fmn2 morphant growth cones. Upon Fmn2 knockdown, retrograde flow increases suggesting its role in regulating clutch.

Increase in retrograde flow in growth cones and reduction in pFAK (Y-397) levels [18] upon Fmn2 knockdown suggested the role of Fmn2 in regulating growth cone traction. We confirmed this by measuring traction forces in control and Fmn2 morphant growth cones. This data suggest attenuation of traction forces upon Fmn2 knockdown, though this has to be confirmed further with more numbers.

Discussion

Filopodia are important in directional motility of the growth cone [7]. Various actin nucleators of formin family have been implicated in filopodia formation in different cell types [15–17].

Our lab has characterized the role of Fmn2 in growth cone motility and midline crossing [18]. In the current study, we have looked at the mechanistic details of Fmn2-mediated growth cone motility. Reduced pFAK (Y-397) levels at the tip of filopodia [18] and compromised filopodial traction suggest the role of Fmn2 in force transmission at the tip. Increase in retrograde flow, reduction in pFAK (Y-397) levels in growth cones [18] and reduced growth cone traction upon Fmn2 knockdown collectively support the role of Fmn2 in regulating traction dynamics and force transmission in growth cones. Fmn2 localizes to the actin bundles in filopodia and have a role in organizing actin structures in growth cones. Reduction in traction and force transmission could be due to defects in actin bundles. Data from fibroblasts suggests that Fmn2 colocalizes with ventral stress fibers hence may have a direct role in force transmission either by regulating actin bundles or

crosslinking [18]. Another possibility is that Fmn2 dependent actin assembly may regulate force dependent maturation of focal contacts. Interestingly, using optical trap based measurements, a recent study in HeLa cells suggests that formin dependent actin bundles are involved in transmitting actomyosin force at the tip of filopodia [32]. In the future, Fmn2-mediated focal contact dynamics and maturation will be studied to gain more insights into the underlying mechanism.

1.3.2 Cytoskeletal mechanisms of axonal contractility

Axonal contraction is a likely mechanism to achieve length minimization and to maintain the prestress. Using simple cell biological assays; we have investigated the role of cytoskeletal dynamics in regulating axonal contraction. We have characterized underlying cytoskeletal response upon axonal contraction, using docked mitochondria as a cytoskeletal marker. We propose axonal contraction as a potential mechanism to regulate axonal rest tension.

Axons show strain relaxation and straightening upon trypsin-mediated detachment

We have developed an assay wherein we look at straightening or length shortening of curved axon upon trypsin treatment. Neurons display curvature in absence of serum. When these neurons were subjected to trypsin treatment, axons detached and showed a straightening response. This length shortening is calculated as strain. The strain relaxation showed an exponential response in a few cases while other neurons exhibited linear response. Further, we studied cytoskeletal mechanisms of axonal straightening (discussed below).

Axonal strain relaxation is actomyosin dependent

To understand whether this detachment induced straightening is actomyosin dependent, we used specific inhibitors of actin and Myosin- II. Upon Latrunculin A (Lat-A)-mediated depolymerization of actin, straightening is completely abolished. Blebbistatin (Bleb) treated axons fail to show straightening. These two results suggested that axonal strain relaxation is actomyosin dependent. We call this strain relaxation as an actomyosin dependent axonal contraction.

Effect of microtubule depolymerization on axonal contraction

An axonal shaft is filled with heavily cross-linked microtubules. Microtubules dynamics is known to affect various aspects neuronal functions. We asked if microtubules are involved in regulating axonal contraction. Microtubules were depolymerized using a specific inhibitor, Nocodazole (Noco). Axonal beading was observed upon noco treatment which is the characteristic phenotype of microtubule depolymerization in neurons. Despite this beading phenotype, axonal contraction was intact, however, the rate of contraction was reduced. Reduced rate of straightening and contraction could be a secondary effect of morphological changes in neurons. We observe thin tethers along Noco treated axons which hindered straightening kinetics. In the future, how dynamic microtubules participate to sustain the axonal contraction will be studied.

Axons show inherent, spontaneous contractile activity

We have shown that upon de-adhesion, axons show a contractile response. De-adhesion induced axonal contractile response led us to test if axons exhibit inherent, spontaneous contractility. We used microcontact printing assay to ask

this question. Neurons were cultured on the high adhesive islands (Laminin+ Fibronectin) on which growth cone turning towards the island induces curvature along the axon. Live imaging of these neurons showed that axons become straight without induced detachment but at a slower rate. This suggests that inherent, spontaneous contraction is a slow process limited by the rate of detachment. The extent of contraction, however, was comparable with trypsin-induced de-adhesion.

Cytoskeletal strain shows heterogeneous response upon axonal contraction

To understand the nature of cytoskeletal dynamics upon axonal contraction, we used docked mitochondria as a cytoskeletal marker. Interaction of these mitochondria with microtubules [33, 34], neurofilaments [35]and actin [36] have been studied earlier. Docked mitochondria have been used as a cytoskeletal marker in the stretch paradigm earlier [37].

We calculated local strain between two adjacent mitochondria as the axon straightens. Local strains were found to be heterogeneous despite the monotonic drop in the length of axon. The contraction in one pair is occasionally concomitant with an extension is another pair. The overall additive strain is negative at any given point suggesting cumulative contraction. We imaged docked mitochondria without trypsin flow to get heterogeneity due to the baseline mitochondria fluctuations. Heterogeneous strain response is significantly more in trypsin-mediated de-adhesion and straightening paradigm than the baseline confirming that strain heterogeneity is indeed due to the axonal contraction.

This data suggested that there are small contractile units present along the entire length of axons and axonal cytoskeletal is not showing contraction as a whole.

Discussion

Using trypsin-mediated de-adhesion, we show that axons show a contractile response in actomyosin dependent manner. Though microtubule depolymerization doesn't abolish contraction, it happens at a slower rate. We demonstrate inherent, spontaneous contraction of axons using microcontact printing assay.

We propose that axonal contractility is balanced by adhesion along axons and upon spontaneous or induced detachment, actomyosin machinery drives the contraction resulting in length shortening. Such local contractile mechanism might be important for the length minimization in neuronal networks.

Further, we show that subcellular cytoskeleton shows heterogeneous response upon contraction. This heterogeneity might have functional implications in branch dynamics and adhesion dynamics along axons, *in vivo.*

Mechanical forces are important for rapid mechanotransduction and signalling. In the future, how mechanosensory growth cone and the prestressed axon influence each other to achieve the force balance will be studied.

2. Formin-2 in regulating filopodial contractility and traction forces in neuronal growth cones

2.1 Introduction

2.1.1 The growth cone structure and motility

Formation of the precise neuronal connections depends on navigation of growth cones towards their respective targets. Cue-dependent, coordinated growth cone motility is critical for the axonal guidance and in turn for the formation of precise neuronal connections. Growth cones have long finger-like projections called filopodia and veil-like, flat structures called lamellipodia. Filopodia are sensory structures, they have un-branched, parallel bundles of actin and few exploratory microtubules. At the base of filopodia, the lamellipodial region has cross-linked actin network [3] (figure 2.1).

The growth cone filopodia have receptors for detecting attractive and repulsive cues in the environment; substrate-bound or diffusive cues invoke underlying cy-

toskeletal dynamics and this leads to the accurate growth cone navigation. Underlying cytoskeletal dynamics is crucial for the coordinated growth cone movement [2].

It has been shown in different cell types that actin dynamics at the leading edge drives the motility [38]. Role of the actin cytoskeleton and its regulators in the growth cone motility have been studied in last few years [4]. Depolymerization of actin causes impaired growth cone motility; directionality of growth cone is compromised [6, 39]. Myosin-II activity in lamellipodial region and actin assembly at the leading-edge drive the F-actin retrograde flow in growth cones [40]. Retrograde flow of actin [41] and myosin-driven contractility [42] are required for the growth cone motility. The dynamic balance between polymerization at the tip and the retrograde movement of actin decide protrusion or retraction of filopodia [43]. There is a direct evidence that, if this balance is perturbed then the rate of growth cone movement is affected. It has been shown that the growth cone movement is inversely proportional to the retrograde flow [41].

Once filopodial or lamellipodial protrusions are formed, then they are stabilized through the integrin-mediated interaction with the substrate [44]. Focal contacts formed through the integrin receptor engagement with the extracellular matrix (ECM) act as a transient clutch to transmit the intracellular contractile forces onto the substrate as traction forces. Cellular contractility and transmission of traction forces on the substrate are important steps in the cell motility and studied extensively in different cell types [45, 46], however, remained understudied in neurons. In last few years, there are many independent studies suggesting the molecular clutch hypothesis in different cell types [47, 48] and a few studies in neurons [49, 50]. When clutch is engaged; the linkage between F-actin and ECM

is formed through the transmembrane integrin receptors. Retrograde flow attenuates and forces are transmitted on to the substrate. This is followed by polymerization near the membrane that facilitates the protrusion. When clutch is not engaged; then F-actin bundles are not linked to the ECM at the focal contact, retrograde flow of actin increases and traction forces are reduced [51] (figure 2.2). It has been proposed that differential regulation of clutches might allow movement of the cell front while retraction of the rear part.

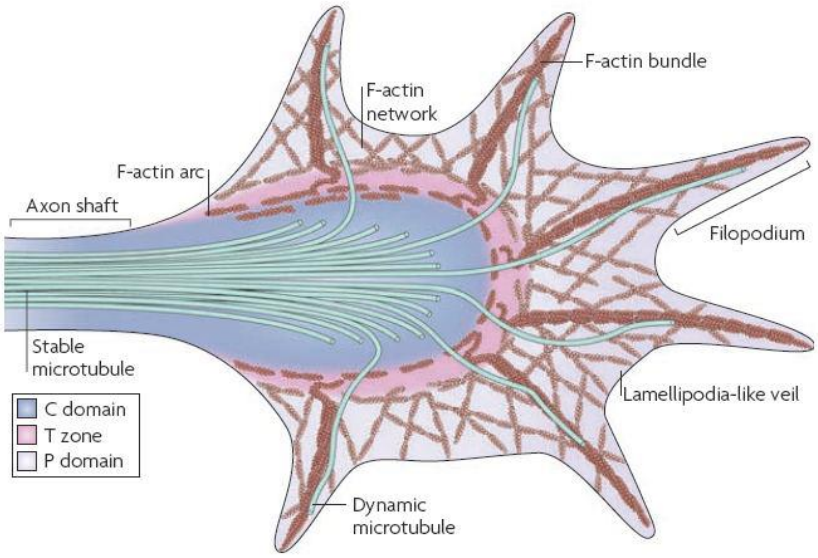

Figure 2.1: The growth cone and its underlying cytoskeletal arrangement. Based on the underlying cytoskeletal arrangement, the growth cone has three regions: central domain, peripheral domain and transition domain. Central domain has microtubule bundle entering from the axonal shaft. The peripheral domain consists of finger-like projections called filopodia and veil-like projections called lamellipodia. Filopodia have parallel bundles of actin and few exploratory microtubules. The lamellipodial region consists of the cross-linked F-actin network. In between C and P domain, actin network is arranged to form the actin arc which constitutes the transition or T domain. (Adapted from [3]).

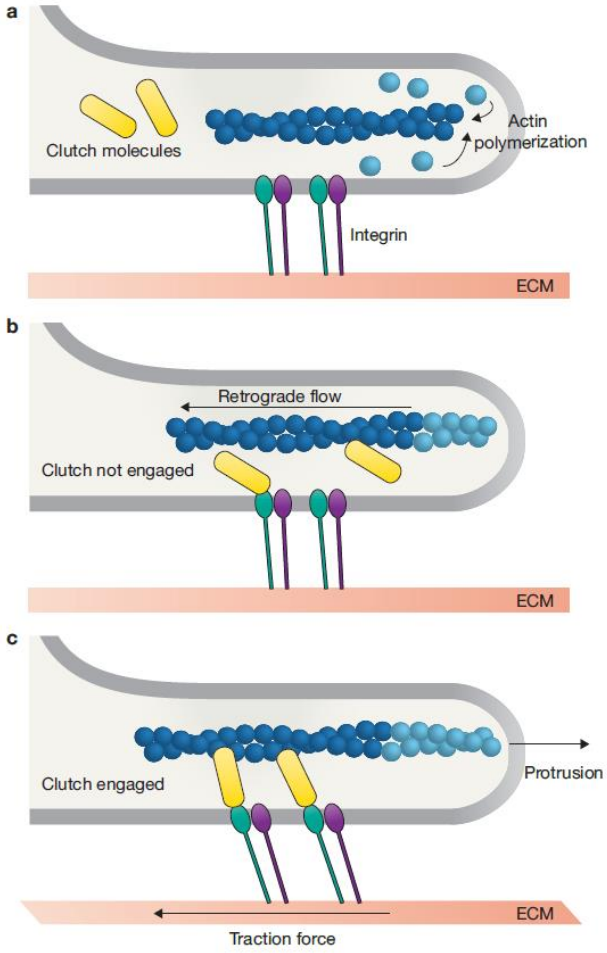

Figure 2.2: The molecular clutch hypothesis. (a) Actin polymerization at the tip (shown in blue). Integrins (green and purple) are bound to the ECM. (b) Retrograde flow increases if the clutch (yellow) is not engaged. (c) If the clutch is engaged, then traction forces are transmitted on to the substrate and retrograde flow attenuates and the protrusion is favored (Adapted from [51])

.

2.1.2 Regulation of filopodial and the growth cone traction forces

Filopodia initiate contacts with the substrate and can reorient growth cones towards or away from the attractive or repulsive guidance cues, respectively. Filopodial traction dynamics is important for initiating directional forces and regulating the growth cone motility [52]. Mechanisms of filopodial pulling are poorly understood and highly dependent on cell types and force measurement techniques [30]. Filopodial pulling forces have been studied more often in the other cell types than neurons, using two different techniques-optical trap based measurements and using the compliant substrates. Based on optical trap measurements in HeLa cells, it is proposed that retrograde flow in the lamellipodial region drives a continuous retrograde flow of the actin network in filopodia. Since actin meshwork is coupled in the filopodial and lamellipodial region, friction between two drives the retrograde flow in the filopodial region and its pulling (figure 2.3). It is proposed that membrane tension may have a secondary role in driving the filopodia retraction [53]. Recently, it has been shown that helical buckling of actin is sufficient to generate filopodial traction on the trapped bead in HEK293 cells [54]. However, such mechanisms have not been studied in growth cone filopodia. Growth cone filopodia dynamics and traction have been studied more often using compliant substrates, as discussed below.

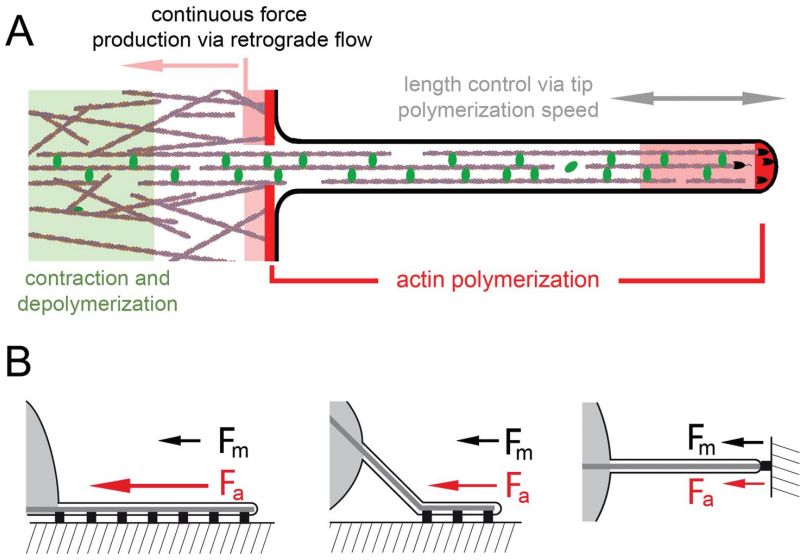

Figure 2.3: Filopodial force regulation. A. Contraction and depolymerization at the base of filopodium drive the retrograde flow. This is coupled to the actin meshwork in filopodia driving its retraction or pulling. Polymerization at the tip drives the protrusion. B. The number of adhesions and geometry regulate traction forces (F_m is membrane tension, F_a is actin retrograde flow) (Adapted from [30])

.

There are significant differences in filopodial force values reported so far for neurons and other cell types [30]. Force measurements of filopodia using compliant substrates report higher values as compared to the optical trap [42, 50]. These differences are excepted since these measurements are in different cell types and the adhesion dynamics in two techniques are different; the shaft adhesions are intact in traction studies on compliant substrates unlike optical trap measurements (figure 2.3 B).

Using traction force measurements of growth cone filopodia from Myosin-II B knockout mice, it has been shown that Myosin-II B is required for the generation

of filopodial traction forces and the growth cone motility [42]. Recently, Myosin dependent filopodial pulling was confirmed in HeLa cells using the optical trap based force measurements and further, it was shown that formin-dependent actin network is required for the filopodial force transmission [32].

Filopodial traction is regulated by various biomechanical cues. Interestingly, clutch dynamics is modulated in response to stiffness of the substrate. Long and sustained pulling with intermittent, sudden detachment have been observed on a compliant substrate. This behavior is called load and fail cycle. On the other hand, on stiffer substrates, only smaller pulls are sustained for the shorter time; this behavior is termed as frictional slippage. These two different modalities suggest that filopodia are mechano-sensitive and regulate traction in stiffness dependent manner [50]. Apart from mechanical signal mentioned above, different biochemical cues can regulate growth cone traction by modulating dynamic interplay between retrograde flow and actin polymerization at the tip, through the receptor signaling. Netrin-1 immobilized on glass beads was sufficient to reorient the spinal growth cone and exert traction in myosin-II-dependent manner. Interestingly, phosphorylation of Focal Adhesion Kinase (FAK) at Y-397 residue is required for the force transmission and recruitment of additional focal adhesions, consistent with other cell types [55]. It has been shown that growth cone traction on a soft substrate coated with laminin increases upon NGF induction [56]. All these studies suggest that upstream biochemical or mechanical cues can modulate the growth cone traction. However, cytoskeletal mechanisms and regulators driving this regulation are not very well explored.

So far, our knowledge regarding force transmission at the focal contacts is based on different cell types and not formally studied in neuronal growth cones in great

details. In this chapter, we have discussed how an actin nucleator, Formin-2 (Fmn2) can regulate traction in spinal growth cones.

2.1.3 Formins and cell motility

Actin-based motility requires nucleation and elongation of the actin filaments. Actin nucleation is a thermodynamically unfavorable process and requires the assistance of proteins called actin nucleators [57]. Formins are the class of actin nucleators which form un-branched, linear actin filaments dominantly found in filopodia (Arp2/3 based nucleation and its role in motility are not discussed here since it is beyond the scope of this study). Formins are characterized by the presence of N-terminal FH1 domain and FH2 domain at C-terminal. The FH2 domain of formins binds to the barbed end and move processively with the growing filaments [14]. Formins regulate wide variety of cellular functions in vertebrate systems like stress fiber assembly [58], cytokinesis [59, 60], oogenesis [61], axonal elongation [62], polarity of the egg [63].

Different classes of formins have been implicated in the filopodia formation in a variety of cells [15–17, 64]. Dia2 (Diaph2) and DAAM [65] shown to be regulating filopodia formation in neuronal growth cones.

Interestingly, actin assembly by formins at focal adhesions has been proposed to regulate traction forces in some reports. Dia-1 is known to regulate focal adhesion and traction forces via filament assembly at focal contacts. The stress fibers formed by the Dia-1 act as the structural template to transmit myosin-driven forces at focal contacts [12]. FHOD-1 formin is shown to regulate actin assembly at integrin clusters and traction forces in fibroblasts [13]. Formin dependent regulation of focal adhesions and traction forces are studied in fibroblasts only in a handful

studies and not reported in neurons.

Fmn2 is enriched in the nervous system [66] and has a potential function in human intellectual and cognitive disabilities, and synaptic functions [67,68]. Earlier work in our lab has suggested functions of Fmn2 in the neuronal development and pathfinding. Using chick spinal neurons, it has been reported earlier [18] that:

1. Fmn2 in enriched in the brain and spinal cord and its expression overlaps with stages of the neuronal outgrowth.

2. Fmn2 is involved in midline crossing during the neuronal development.

3. Fmn2 regulates growth cone motility (figure 2.4) and substrate adhesion (figure 2.5).

These observations prompted us to look at the role of Fmn2 in regulating growth cone traction dynamics and to explore biophysical mechanisms of Fmn2 driven growth cone motility. In this study, we have looked at the role of Fmn2 in regulating filopodial and growth cone traction.

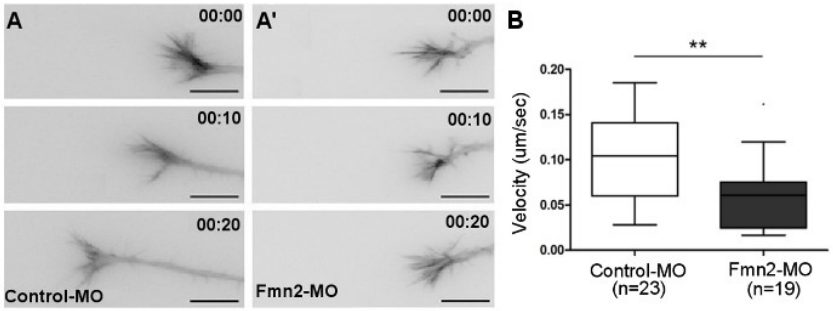

Figure 2.4: Fmn2 regulates growth cone motility. Representative frames from time-lapse imaging for control (A) and Fmn2 morphant (A') growth cones. The time stamp shows minutes elapsed. (B) Fmn2 depletion affects growth cone motility. The line represents the mean and error bars indicate s.e.m. **P$\leqslant$0.01; MannWhitney test. Scale bars: 10 μm. (Adapted from [18]).

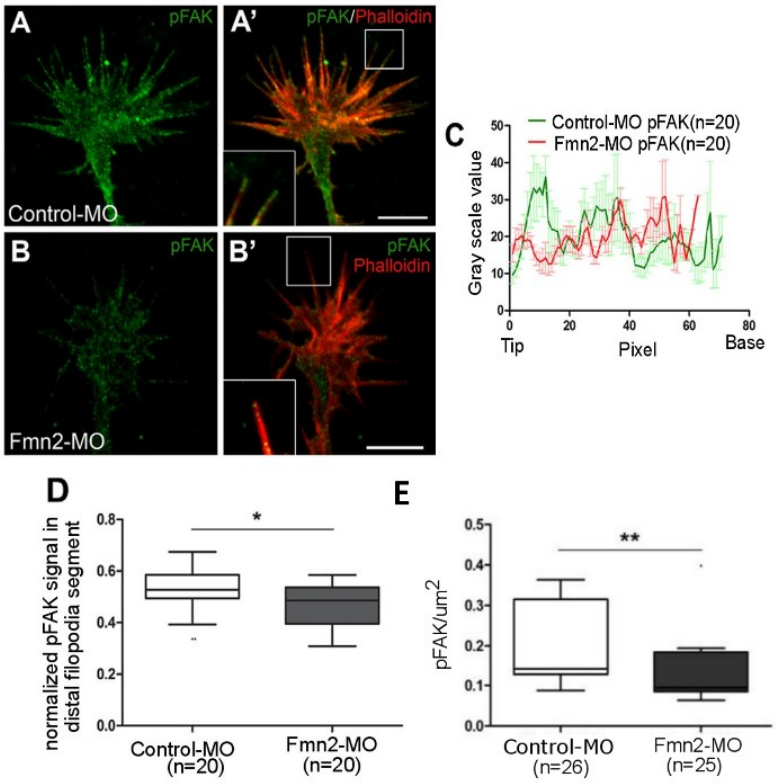

Figure 2.5: Fmn2 knockdown impairs filopodia-substrate interaction. (A-B') Representative micrographs of control morpholino-treated (A, A') and Fmn2 morpholino-treated (B, B') growth cones immuno-stained for pFAK (Y-397) and phalloidin. The pFAK signal seen at filopodial tips in the control is lost in the Fmn2 morphant (insets). (C) The pFAK signal from line traces along the filopodia. The line represents the mean and error bars indicate s.e.m. (D) Normalized pFAK signal in the distal segments of filopodia. (E) Quantification of pFAK (Y-397) intensity in the entire growth cone, normalized to the growth cone area. *P$\leqslant$0.05; MannWhitney test. Scale bars: 10 μm. (Adapted from [18])

.

2.2 Results and discussion

2.2.1 Bead pulling assay to study filopodial traction dynamics

Spinal neurons were cultured on the soft substrate (0.438 kPa) as described in materials and methods in the next section (figure 2.6 A). Filopodium forms an attachment with the substrate and pulls on it. Over time (in few seconds), the tension builds up causing a sudden detachment of filopodium from the substrate. These responses result in deformations of the substrate that are detected by the displacement of gel-embedded fluorescently labeled beads (figure 2.6 A-A"'). The observed load (pulling) and fail (release) behavior of filopodia on a compliant substrate is consistent with the earlier report [50].

Advantages of this assay are:

1. Unlike optical trap where filopodium is detached and trapped on the bead, this assay relies on inherent dynamics and substrate interaction of filopodia. Adhesions along the filopodial shaft are intact.

2. Traction dynamics of many filopodia can be visualized at the same time.

In the initial standardization experiments, growth cones were imaged in DIC mode and with 10 second interval. Frequency analysis gives the distribution of pulling distance and velocity. Pulling distance ranges from 100 nm to 1 μm. Velocity ranges from 10 nm/second to 80 nm/second (figure 2.7). Smaller pull lengths are enriched because of sudden tension build up and release between the pulling events. As a proof of principle, we show the load and fail behavior of filopodia using bead puling assay (figure 2.6 B). In knockdown experiments, we have used the frame rate of 3.3 seconds (Data with 1-second interval also show load and

fail behavior) to be able to image for a longer time without bleaching. We could observe multiple filopodia undergoing bead pulling at any given time. When we compared their pulling velocities, then it was observed that there is a significant variation in bead pulling at the tip vs base of the filopodium. There was a significant variation in the bead pulling by filopodia located at different angles. Within the limits of our analysis, bead pulling and traction seems to be regulated by different factors and highly stochastic. This variation could be due to stochastic attachment-detachment cycles or could also be an experimental variation. A similar observation has been made earlier for chick forebrain neurons cultured on the compliant substrates [50].

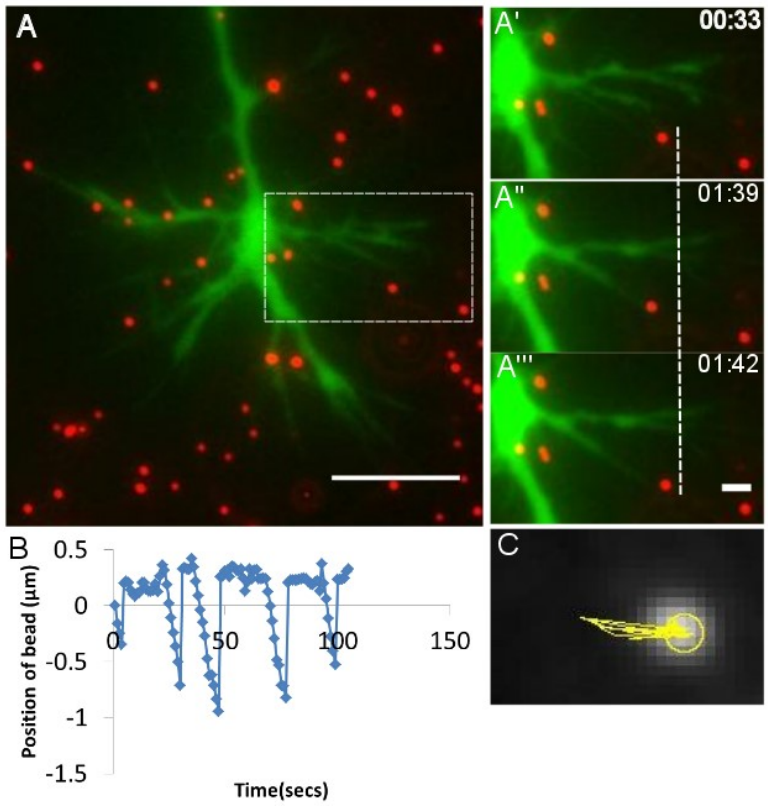

Figure 2.6: Filopodia bead pulling assay. A. Representative micrograph of a mGFP-transfected growth cone plated on polyacrylamide gel (0.438 kPa) with embedded fluorescent beads. The movement of a bead close to the filopodium tip is tracked over time to assess the traction force exerted by the filopodium on the compliant substrate. Scale bar:10 μm. (A'-A''') Representative frames from a time-lapse sequence for the region boxed in A. The time stamp shows minutes elapsed. Scale bar: 2 μm. B. An Example of load and fail behavior of a bead pulled by the filopodium. C. The trajectory of a bead pulled by the filopodium.

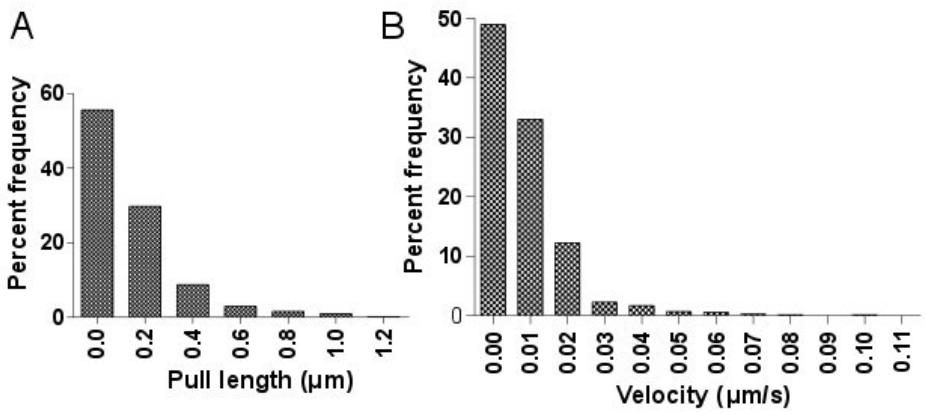

Figure 2.7: Distributions of the pull length and velocity. A. Percent frequency of pull lengths. B. Percent frequency of pulling velocity. Data shown over here is for 10- second intervals (3.3 seconds and 1 second interval data show similar trends). Data are collected from more than 30 filopodia and 700 pulling events.

2.2.2 Filopodia traction dynamics is Myosin-II dependent

Myosin-II has been proposed to be involved in traction force generation previously. An earlier report suggests that Myosin-II B is involved in filopodial pulling [42]. A recent study in HeLa cells confirmed that Myosin-II at the base of filopodia is involved in pulling and retraction of the tip of filopodia. To know whether we see the similar contribution of Myosin-II in our assay, we inhibited Myosin activity using a specific inhibitor of myosin-II, Blebbistatin (30μM). We imaged growth cones to capture filopodia bead pulling in the continuous presence of Blebbistatin. It was noticed that most of the growth cones become filopodia-like, without a central region and filopodia lose contact with the substrate hence the bead (figure 2.8 A-A'). Due to this limitation, we could get data only for 3

growth cones. Upon myosin-II inhibition, lengths of pulls and velocity drop significantly as compared to the matched DMSO control (figure 2.8 B, C). This suggests that myosin-II is involved in filopodia force generation, consistent with the earlier results.

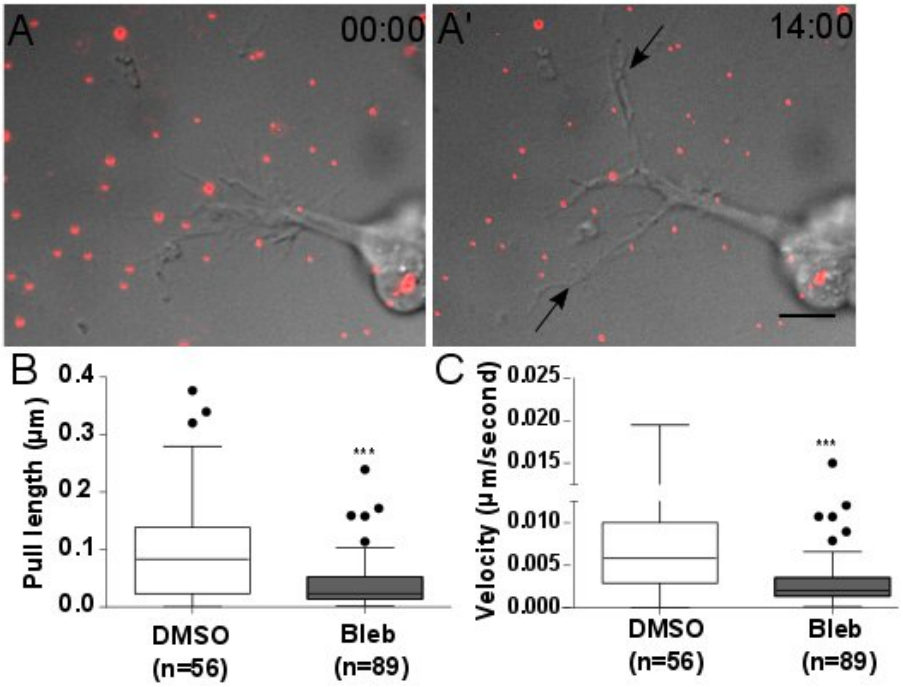

Figure 2.8: Filopodial traction dynamics is myosin-II dependent. A-A'. Representative images of Blebbistatin treated spinal neuron. Scale bar: 10 μm. Arrows show that growth cone collapses and only filopodia remain upon blebbistatin treatment as reported in other studies. Time stamped is in minutes. B-C. Pull lengths and velocity are abrogated upon Blebbistatin treatment. The number of pulling events are shown in brackets on plots. Data are represented as box and whisker plots using the Tukey method. The horizontal line inside the box represents the median. ***P$\leqslant$0.001, MannWhitney test. (With Amrutha Palavalli)

2.2.3 Role of Fmn2 in filopodial traction dynamics

Earlier work in the lab established the role of Fmn2 in midline crossing of commissural neurons *in vivo* and its expression overlaps with the stages of neuronal outgrowth. Further, *in vitro* studies suggested that growth cone motility is affected upon Fmn2 knockdown. pFAK levels reduce significantly at the tip of the filopodia upon Fmn2 knockdown which suggested its role in substrate attachment and traction force generation [18].

Since Fmn2 is a member of formin family, it has a potential role is in regulating parallel bundles of actin in filopodia and filopodial pulling forces. We used bead pulling assay to ask whether Fmn2 has any role in regulating filopodial traction dynamics. Upon Fmn2 knockdown, lengths of pulls and velocity are affected. However, the frequency of pull is comparable with control morpholino (figure 2.10). Data were compared for the pull lengths more than estimated noise; 25 nm (figure 2.9). (Knockdown efficiency was standardized earlier in the lab. 50% knockdown efficiency was estimated after 24 hours. Specificity of phenotype was checked by two different morpholinos. Growth cone morphometric defects and motility defects were rescued using a morpholino resistant construct [18]).

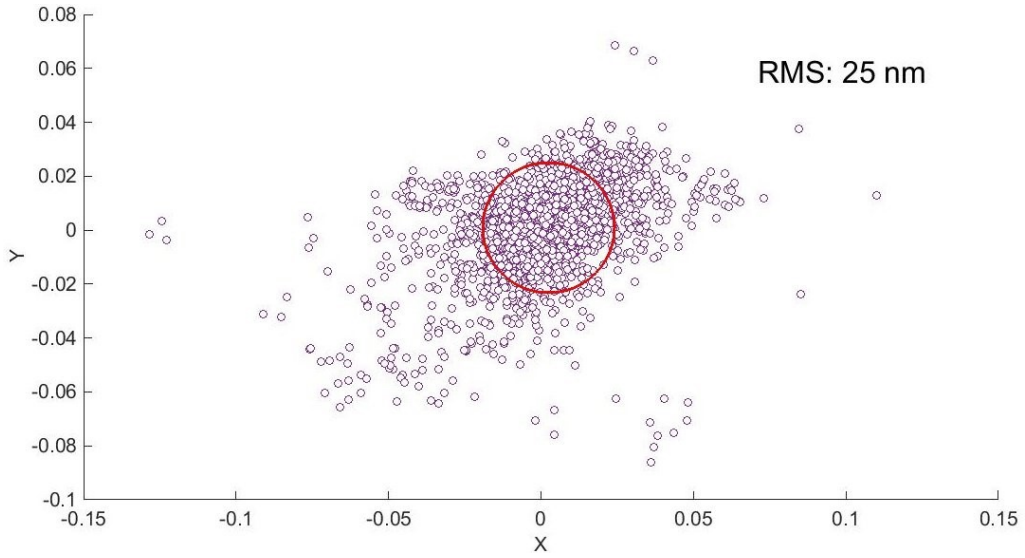

Figure 2.9: Estimation of RMS inaccuracy. The noise was estimated using beads in the background where no cells are present. RMS calculated using 58 beads is 25 nm, shown by the red circle. (Details of calculations are in materials and methods).

This suggests that in Fmn2 morphants, filopodia are able to form a contact in an equal frequency as that of the control morphants but fail to generate sustained traction; filopodium slips quickly before longer pull can be sustained. This opens up following possibilities:

1. As myosin-driven contractility originates from frictional coupling of filopodial actin bundles to the actomyosin network at the base, defects in the actin organization in the central region leads to the poor filopodial contractility. Earlier work using anisotropy measurements in the growth cone suggests defects in actin organization upon Fmn2 knockdown hence supports this hypothesis [18]. Fmn2 has been shown to bundle actin filaments *in vitro* (Priyanka Dutta's unpublished

work) supporting this hypothesis. Fragile actin bundles in Fmn2 morphant filopodia might affect the force transmission. Our qualitative observation from live imaging of actin GFP transfected Fmn2 morphant growth cone show that, filopodia occasionally show sharp bends suggesting defects in actin arrangement upon Fmn2 knockdown. (Data not shown).

2. F-actin bundles are not efficiently engaged with the point contacts resulting in a weak clutch. Earlier work using pFAK(Y-397) seems to indicate the focal contact defect upon Fmn2 knockdown and this could be due to the force dependent focal contact maturation is affected since actin bundles are not engaged at the tip.

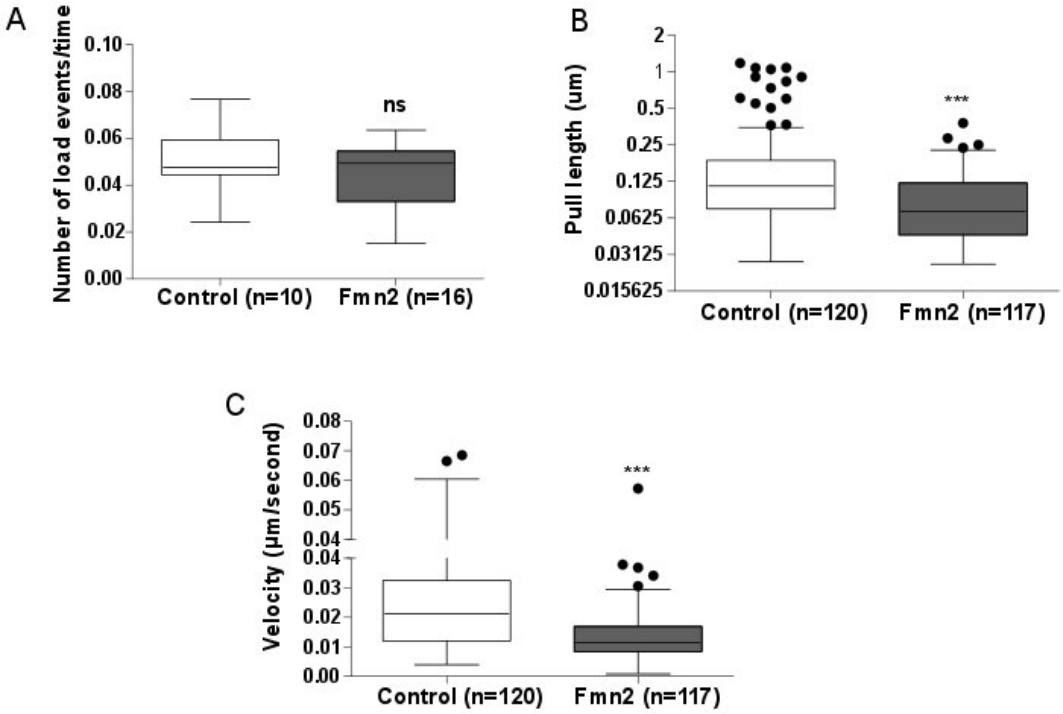

Figure 2.10: Fmn2 knockdown affects traction dynamics. A. Frequency of pulling upon Fmn2 knockdown is comparable with control. B. Pull lengths are reduced upon Fmn2 knockdown. C. Velocity of pulls are attenuated upon Fmn2 knockdown. Data are represented as box and whisker plots using the Tukey method. Numbers in brackets indicate pulling events. Number of filopodia are 10 and 17 for control and Fmn2 morphants respectively. The horizontal line inside the box represents the median. ***P$\leqslant$0.001; ns, non-significant; MannWhitney test.

2.2.4 Fmn2 knockdown results in increase in retrograde flow suggesting weak clutch

As discussed earlier, Fmn2 has a critical role in regulating filopodial contractility. Interestingly, Fmn2 knockdown attenuates levels of pFAK(Y-397) in the central region of growth cones along with filopodia. This indicates that force dependent maturation of focal contacts is affected upon Fmn2 knockdown, as a result of compromized F-actin enggagement at the clutch. The molecular clutch hypothesis suggests that when the clutch is engaged, forces are transmitted and F actin retrograde flow is reduced. When the clutch is not engaged, F-actin retrograde flow increases (figure 2.2). We evaluated F-actin retrograde flow in the growth cones by expressing actin GFP in control and Fmn2 morpholino treated growth cones. These experiments were carried out on the similar compliant gels used in bead pulling assay and in the growth cone traction; discussed in the next section. The retrograde flow was analyzed using flow-tracker code obtained from Dr. David Odde (University of Minnesota). The code gives the kymograph (figure 2.11.B) based on the intensity heat map and hence allows a reliable detection of the flow [50, 69]. Average retrograde flow increases across the growth cone upon Fmn2 knockdown (figure 2.11 C). To know where this defect dominates, we analyzed filopodia and lamellipodia separately.

Interestingly, upon Fmn2 knockdown, retrograde flow increases significantly in the lamellipodial region but not in the filopodial region (figure 2.12. D and E). This could be because of dynamics and differential engagement of filopodia, which mask the effect of Fmn2 knockdown. The transient and weak attachments of filopodia with the substrate leads to heterogeneity in retrograde flow and hence

demand more controlled experiment where filopodium is under controlled force at the tip, e.g. using the optical trap. In the future, this will be confirmed by force measurements of Fmn2 morphant filopodia using the optical trap.

There are studies in HeLa cells suggesting that the pulling at the tip of the filopodia is driven by actomyosin machinery at the base [32, 53]. Increase in retrograde flow in the lamellipodial region (at the base) upon Fmn2 knockdown hence is sufficient to explain weak clutch engagement and reduction in filopodial pulling at the tip due to the poor force transmission from base to the tip. We suggest that, though Fmn2 is involved in filopodial force generation at the tip, its dominant function is in regulating traction in the central region. Reduction in pFAK (Y-397) activity and increase in retrograde flow support this hypothesis. Hence, we evaluated traction forces generated by growth cones upon Fmn2 knockdown (discussed in the next section).

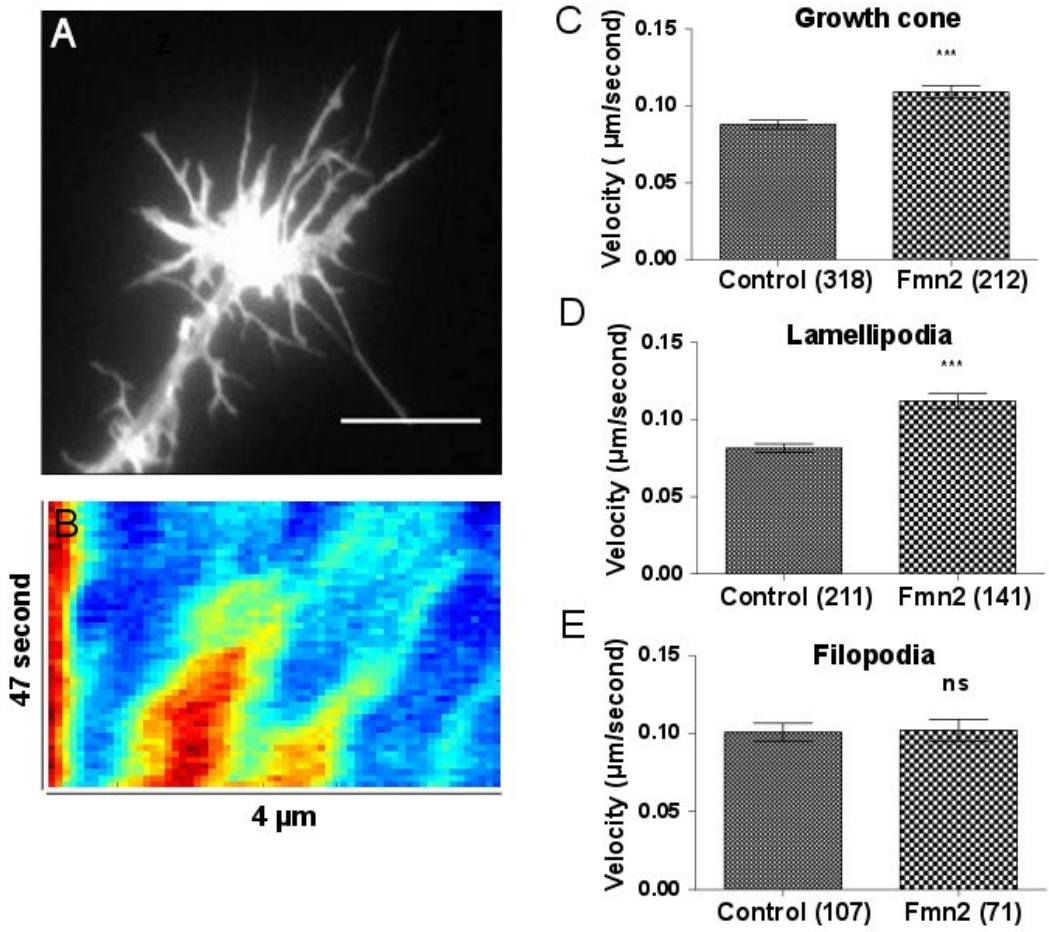

Figure 2.11: Retrograde flow increases upon Fmn2 knockdown. (A) An example of the growth cone transfected with pCAG actin GFP plated on the compliant substrate. (B) Kymograph generated using flow-tracker plugin. (C) Retrograde flow upon Fmn2 knockdown in the whole growth cone. (Number of growth cones for control and Fmn2 morphants are 44 and 36 respectively). (D) Fmn2 knockdown causes an increase in retrograde flow in lamellipodia. (E) No change in retrograde flow in filopodia upon Fmn2 knockdown. Numbers in brackets indicate number of streaks analyzed. ***P$\leqslant$0.001, ns: not significant. Unpaired t-test. Scale bar: 10 μm.

2.2.5 Growth cone traction upon Fmn2 knockdown

As discussed earlier, increase in retrograde flow upon Fmn2 knockdown in the growth cone suggests that Fmn2 is involved regulating not only tip adhesion but also traction across growth cones. Levels of pFAK reduces upon Fmn2 knockdown in the growth cones again support this hypothesis [18] (figure 2.5.E). Using compliant substrates used in earlier assays, we performed traction force experiments to compare traction exerted by control and Fmn2 morphant growth cones (details in Materials and Methods). Though statistically non-significant, the trend suggests that Fmn2 may regulate traction forces exerted by the growth cone (figure 2.12 D). This data needs to be confirmed with more numbers since there is a considerable heterogeneity in estimated traction.

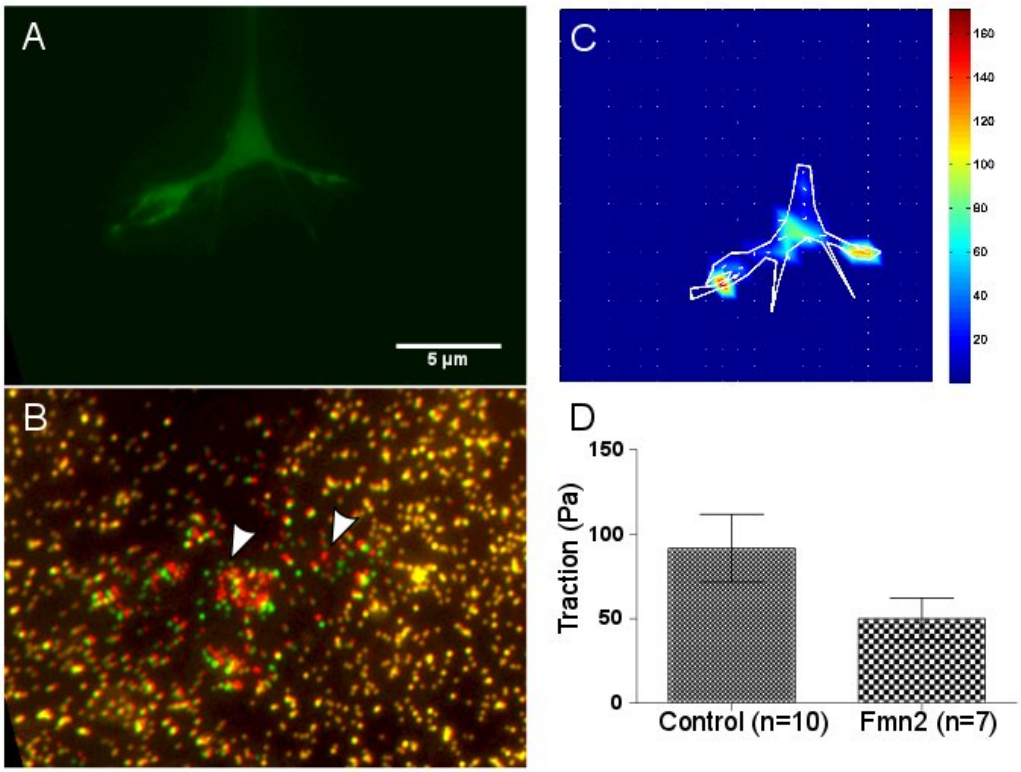

Figure 2.12: Traction force studies. A. Representative micrograph of the growth cone plated on the compliant substrate. B. Corresponding merge of stressed and relaxed images of beads. Green beads represent the relaxed position and red beads represent the stressed position (arrowheads show deformations). Beads away from the growth cone are yellow suggesting that deformations are absent outside the cell area. C. Constrained traction for the growth cone shown in A. Heat map represents traction in Pa. D. Traction drops upon Fmn2 knockdown; more numbers need to be added to confirm this further.

2.3 Summary and conclusions

Actin dynamics and its regulators play a pivotal role in cell motility. Studying these regulators allow the development of testable hypothesis to understand mechanistic details of cell motility in great details. Our lab has shown that an actin nucleator; Fmn2 regulates growth cone motility and *in vivo* midline crossing. Interestingly, Fmn2 does not participate in growth cone filopodia initiation or elongation, however, regulates filopodial tip adhesion maturation and filopodial stability [18]. Using a bead pulling assay, we could show that Fmn2 is involved in regulating filopodial traction dynamics. Increase in retrograde flow upon Fmn2 knockdown confirms that Fmn2 has a role in regulating maturation of focal contacts and force transmission in growth cones. Early attempts on traction force measurements suggest that Fmn2 may regulate traction not only at the filopodial tip but in the entire growth cone.

Earlier work in the lab suggested that Fmn2 regulates actin bundles in growth cones [18]. Reduction in traction upon Fmn2 knockdown could be due to the defects in actin bundles and force transmission. Interestingly, inhibition of formins in HeLa cells affects filopodial pulling forces. In this study, it has been suggested that formins are involved in filopodial force transmission [32]. In fibroblast cells, Fmn2 co-localizes with stress fibers and regulate substrate adhesions. This is consistent with the abrogated pFAK activity upon Fmn2 knockdown in the growth cones [18]. In the current study, increase in retrograde flow and the trend towards reduction in growth cone traction suggest that Fmn2 dependent actin assembly and the focal contact dynamics might regulate traction in growth cones (figure 2.13). Actin assembly at the focal adhesion and its involvement in regulating fo-

cal adhesion maturation and traction has been studied in different cell types for the formin family proteins [12, 13]. Our study provides the first evidence of similar function of formins in neuronal growth cones. Since growth cones form transient, dynamic point contacts that are critical for directional translocation, our study provides novel insights into Fmn2-mediated actin organization in regulating focal contact dynamics and force transmission (figure 2.13).

Fmn2 might regulate traction by regulating clutch dynamics directly. This is a valid explanation since an increase in retrograde flow upon Fmn2 knockdown strongly supports the poor engagement of actin bundles at the focal contacts. In future, this can be confirmed further using talin which cross-links actin and integrins directly and a known mechano-sensory protein. Understanding focal contact dynamics and their signaling upon Fmn2 knockdown will help us unraveling mechanistic details of Fmn2 mediated growth cone motility.

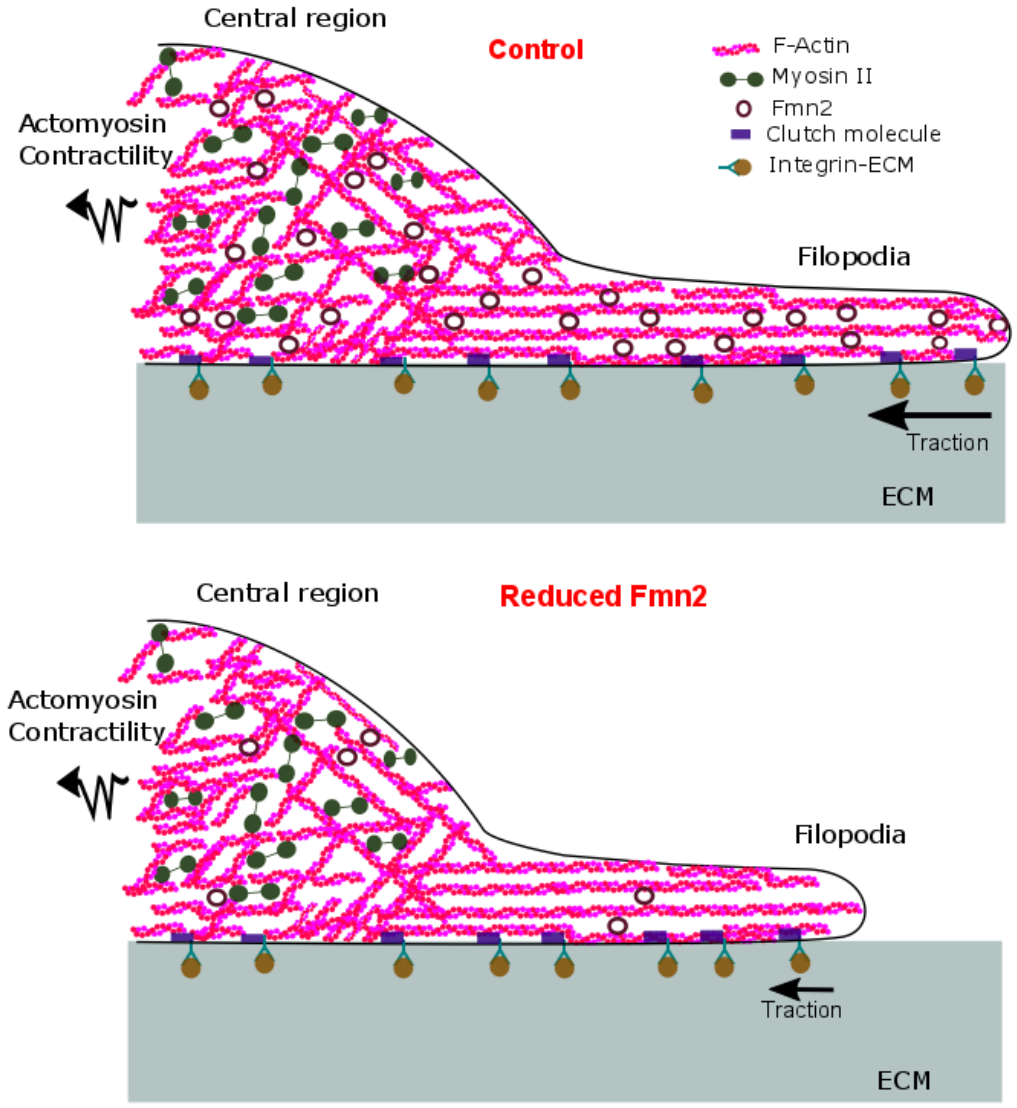

Figure 2.13: Fmn2 in regulating filopodial contractility and traction forces in neuronal growth cones. Based on the earlier results [18] and based on this study, we propose that Fmn2-mediated actin organization is required for substrate interaction, tractin force transmssion and growth cone motility.

2.4 Materials and Methods

2.4.1 Preparation of gels

1. Activation of coverslips:

Coverslips were activated using the protocol described earlier [70]. 28 mm acid-washed coverslips (Fischer Scientific) were treated with 0.5% APMS (3-Aminopropyltrimethoxysilane, Sigma) in water for 10 mins. This was followed by washing with water for 4 to 5 times. These coverslips were baked at 160 °C for 1 hr. Then were pasted on bottoms of 35 mm Petri dishes. Once plates were ready, 200 μl of 0.5% (in water) glutaraldehyde (Sigma) was added in these plates and incubated for 1 hour followed by washing with water for 4 to 5 times.

2. Bead coating on the top coverslips:

1:1 diluted stock of 200 nm beads (Fluospheres carboxylate-modified microspheres) was made. Required numbers of 18 mm coverslips were coated with 100 μl of bead solution (1:20 or 1:50 from the stock) using swinging bucket centrifuge at 3500 rpm for 5 minutes. For the traction force experiments, fibronectin (50 μg/ml, Sigma) coated 18 mm coverslips were used for the same.

3. Preparation of gels:

0.438 $\pm$ 0.064 kPa poly-aryl amide gels (using 3% acrylamide and 0.1% bis-acrylamide.) were made using protocol described earlier [71]. 15μl of gel mix was added on the activated surface of coverslip bottom Petri dish and the bead coated 18 mm coverslip was inverted on that. After gels were solidified, water

was added to avoid drying. 18 mm coverslips were removed from the gel surfaces using a razor blade. The top coverslip with beads is brought in contact with the gel drop as the gel is polymerizing. This leads to the transfer of beads on the gel surface. Coverslips were removed after immersing gels in the water. With this protocol, we robustly get smooth gels and top surfaces uniformly coated with beads without traces of gel on the top coverslips. This suggests that there could be only minimal topological changes and unlikely to affect deformations. However, in the future, the protocol can be improved by avoiding coating of top coverslips and by adding beads in the gel pre-mix.

Stiffness measurements of gels were carried out using the AFM (By Kavitha Sthanam from Dr. Shamik Sens lab at IIT Bombay). Briefly, two technical replicates were used to do the measurements. For each set, minimum 30 readings were taken using a pyramidal cantilever and data was analyzed using Hertz fitting [72].

In this study, the pyramidal cantilevers were used for the stiffness estimation which sometimes overestimates the stiffness values. In the future, it is important to validate stiffness measurements using spherical cantilever.

4. ECM cross-linking:

200 μl of 2 mg/ml sulfo-SANPAH (Thermo Scientific or Covachem) was added on gels and kept under hand-held UV (365 nm) at the distance of 5 to 8 cm for one hour inside the hood. Plates were washed with water 3 times. 250 μl of 50 μg/ml fibronectin (Sigma) was added on gels and incubated overnight at $4\,^{\circ}\mathrm{C}$ till next day, before dissection and culturing.

2.4.2 Dissection and cultures

Fertilized, white Leghorn chicken eggs were obtained from Venkateshwara Hatchery Private Limited, Pune, India. All procedures were approved by the Institutional Animal Ethics Committee, IISER Pune, India. Six-day old chick embryos were used to isolate spinal cord. Dissections were carried out in sterile PBS (137 mM NaCl, 2.7mM KCl, 10 mM Na_2HPO_4, 1.8 mM KH_2PO_4) on the Silgard plate under a dissecting microscope inside a horizontal laminar flow hood. The dissected spinal cord was collected in L15 medium (Gibco). The tissue was centrifuged at 3000 rpm for 3 minutes before the medium was removed and 1x trypsin (Lonza) was added. Trypsinization was undertaken for 20 minutes at $37\,^{\circ}\mathrm{C}$. Following trypsinization, the tissue was centrifuged at 3000 rpm for 3 - 5 minutes before removal of trypsin and washed with L15 medium. The dissociated neurons were plated on pre-made gels in 35 mm cover glass bottomed Petri dishes containing 1.5 ml media (L15 containing 10% FBS, 6 mg/ml glucose (Sigma), 1x glutamine (Gibco), 0.6% methocel (Chemicon),100 ng/ml NGF (Gibco) and 1x Penstrep (Gibco)). The neuronal culture was incubated for 48 hours at $37\,^{\circ}\mathrm{C}$.

For transfections, cells were suspended in 100 μl Optimem containing 10 μg of plasmid and 100 μM control or Fmn2 morpholino.
(Fmn2MO#2 sequence CCATCTTGATTCCCCATGATTTTTC.
Standard control morpholino was used as a negative control:
CCTCTTACCTCAGTTACAATTTATA). Then cell suspension was transferred to the electroporation cuvette and the electric pulse was applied using the following parameters.

Poring pulse:

Voltage (V) - 125

Pulse length (msec) - 5

Pulse interval (msec) - 50

Number of pulses - 2

Decay rate (%) - 10

Polarity - +

Transfer pulse:

Voltage (V) - 20

Pulse length (msec) - 50

Pulse interval (msec) - 50

Number of pulses - 5

Decay rate (%) - 40

Polarity - +/-

After electroporation, cell suspension was transferred in a tube containing 400 μl Optimem (Gibco). After this, the cell suspension was added on the gel surface in culture plates containing the medium (mentioned above).

2.4.3 Imaging

Bead pulling events were captured every 3.3 seconds using a PlanApo 100x/1.4 oil immersion objective on an Olympus IX81 system equipped with a Hamamatsu ORCA-R2 CCD camera. In initial standardization experiments, growth cones were imaged in DIC mode with 10 second interval.

For myosin-II inhibition studies, 30 μM Blebbistatin was used and imaged contin-

uously in presence of Bleb in DIC mode with 6-second interval. Matched DMSO control does not have any effect on pulling velocity (data not shown).
For retrograde flow studies, growth cones on the compliant gels were imaged at 1-second interval using a PlanApo 100x/1.4 oil immersion objective on an Olympus IX81 system equipped with a Hamamatsu ORCA-R2 CCD camera. Morpholino treated growth cones were identified using co-transfected plasmid as a selection marker in all the experiments.

2.4.4 Traction force experiments

For traction force experiments, neurons were plated on gels with the higher bead density. An image of the growth cone and corresponding image of bead distribution were captured (figure 2.12 A, B). This is called the stressed image. After trypsin flow, once growth cone retracts completely, the image of bead distribution was captured again using the similar settings. This is called null force/ relaxed image.

2.4.5 Analysis

1. Bead pulling analysis:

Images were corrected for the drift using image stabilizer plugin in Image J. All filopodia were aligned along X-axis with growth cone at the left and tip of the filopodium at the right side. Beads were tracked in Image J using particle tracker plugin. Bead movement above the calculated RMS inaccuracy of the algorithm considered for the analysis (figure 2.9). To calculate RMS inaccuracy, beads located away from the cells were used (data for 58 beads were used)

$$RMS = \sum \sqrt{1/n((x - x')^2 + (y - y')^2)}.$$

Where x and y are coordinates of beads and x' and y' are mean positions.
All x coordinates were copied in the excel and these absolute positions of beads were used to find out peaks and troughs using following formulae:

$$IF(AND((A2 > A1), (A2 > A3)), "peak", "")$$
$$IF(AND((A2 < A1), (A2 < A3)), "trough", "")$$

Pull steps and velocity were calculated using troughs (movement in the negative direction) in the absolute position of beads.

2. Retrograde flow analysis:

Kymographs were generated in the Metamorph software using a segmented line tool (width: 5 pixels). All kymographs were saved in .tiff format. Flow velocities from kymographs were analyzed using flow-tracker code (Obtained from Dr. D. Odde, University of Minnesota), in the Matlab 2007 (Code doesn't work very well in Matlab 2009 and higher versions). Code generates a heat map of the kymograph which aids reliable detection of the retrograde flow. Retrogradely moving traces were selected using a rectangular selection.
The only parts of the time lapses where growth cone and filopodia are not dynamic and detached from the substrate were used in the analysis.

3. Traction force analysis:

Stressed image, relaxed image and corresponding growth cone image were imported in Image J and corrected for the drift using the image stabilizer or template

matching plugin. Traction values for the growth cones were obtained using the Fourier Transform Traction Cytometry (FTTC) method developed by Butler and colleagues [73]. Briefly, Stressed, relaxed and growth cone images were imported in the code. Stiffness values (0.438 kPa), Poisson ratio for the gel (0.48) and thickness of the gel (60 μm) were set as the input parameters. The code generates displacement fields using the cross-correlation between stressed and relaxed images after regularization and further calculates the traction [73].

Data representation and statistics

Box and Whisker plots and the bars show the spread of the data using the Tukey method. Outliers are represented outside the box as individual data points. For bar graphs, the error bars represent the standard error of mean (SEM). All Box and Whisker plots were compared using Mann-Whitney test. For bar graphs, student's t-test was used to compare the data sets. Comparisons were done in GraphPad Prism. RMS inaccuracy data was plotted using Matlab 2014.

3. Cytoskeletal mechanisms of axonal contractility

3.1 Introduction

3.1.1 The axonal cytoskeleton

Axons are thin, axi-symmetric structures with extreme aspect ratio. Axons grow long distances ranging from micrometers to meters while maintaining a fairly uniform diameter. The axonal cytoskeleton (figure 3.1) is required to maintain these thin structures throughout the lifetime of an organism and abnormal changes in cytoskeleton can lead to the axonal degeneration [74]. The axonal shaft is filled with heavily cross-linked polarized bundles of microtubules [23]. Microtubule-associated motors like kinesin and dynein are involved in the transport of vesicles and organelles in anterograde and retrograde direction respectively [26]. Along with the microtubule network, neurofilaments form an important structural component of the axonal cytoskeleton. Neurofilament sidearm interactions are known to regulate axonal caliber [75, 76]. Recent studies using super-resolution microscopy show that spectrin influences axonal cytoarchitecture by organizing the

cortical actin to periodic, membrane-associated actin rings (figure 3.2) in the mature neurites [27, 77]. The functional aspects of these membrane-associated actin rings are not very well studied yet.

Mechanical properties of axons have been studied using microneedle techniques and AFM measurements. Axons of PC12 cells show initial fast elastic response upon stretching followed by viscoelastic relaxation [78]. Similar responses have been studied in DRG axons in an earlier study [21]. Stiffness measurements of dorsal root and sympathetic ganglia cell axons using the AFM show that microtubules disrupted axons have lowest elastic modulus suggesting that microtubule structure provide a mechanical stability to axons. Further, it has been suggested that microtubules provide a structural scaffold for neurofilaments and microfilaments [79]. However, in PC12 cells neurofilaments are shown to be primarily involved in maintaining the shape [80]. Mechanisms governing the mechanical properties of axons are still unclear since there are only a few studies and need to be confirmed further with more independent experimental approaches.

Based on *in vitro* and *in vivo* studies, the axonal cytoskeleton was considered to be largely stationary for very long time [81, 82]. Dynamic nature of axonal cytoskeletal and its functional implications are slowly emerging in a last two decades [83]. There is an accumulating evidence on a coherent movement of microtubules in a forward direction and it is proposed to have a role in axonal elongation [84]. Recently, a dynamic pool of actin has been observed in axons and have been named actin trails and actin hotspots [28]. The discovery of actin rings and other dynamic actin structures along axons opens up the entire field of axonal cytoskeleton, its dynamics and its implications in neuronal functions [85].

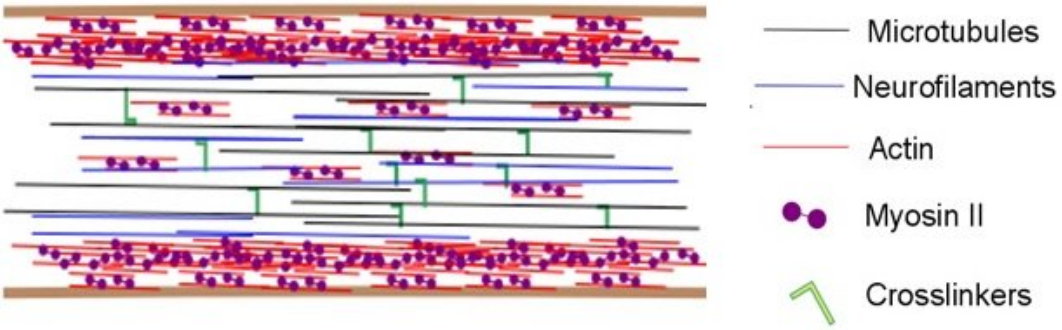

Figure 3.1: The axonal cytoskeleton. The core of an axon is filled with cross-linked microtubules (black) and neurofilaments (blue). Cross-linkers are shown in green. Actin (red) is present cortically beneath the membrane, recently, also shown to be present in the core of axons [28]. The actin-associated Myosin-II motor are shown in purple. Microtubule motors are not shown in this representation. (Based on SEM studies from [23, 24]).

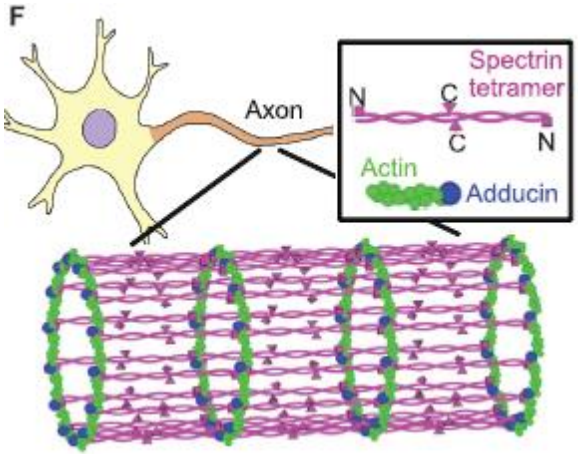

Figure 3.2: Actin rings in the mature neurons. Actin filaments (green), capped by adducin (blue) are arranged in the form of rings. Spectrin tetramers (magenta) connect rings underneath the membrane of axons. The periodicity of this structure is 180 to 190 nm. C terminus (magenta triangles) and N terminus (magenta squares) of spectrin are shown in the inset. (Adapted from [27]).

3.1.2 Role of the mechanical tension in neuronal development

Axons undergo mechanical stretch via growth cone mediated towing [86] and after formation of connections via growth of surrounding tissue, as the animal grows [19, 20]. Mechanical tension has been shown to affect various processes in neuronal development like neuronal growth [31, 87], synapse formation [22], synaptic transmission [88], excitability [89] and also network formation [90–92]. Some of the key findings highlighting the role of mechanical tension in neuronal functions are discussed below.

Role of the mechanical tension in axonal growth and retraction

Stretch-induced growth was first reported more than 50 years ago; the surrounding tissue growth was proposed to induce passive stretching in axons after formation of connections [19]. Later, series of experiments in the 80s and 90s suggested that the growth cone can pull and hence generate tension. Further, applied stretch was shown to induce the axonal growth [31, 93]. Microneedle-based pulling in DRGs suggested that there are tensional set points in axons. Above a threshold force, axons exhibit growth, below this threshold, retraction was observed due to the increase in tension [21]. Based on these studies, it was proposed that mechanical tension can act as a second messenger for the growth of neuronal cells and it can integrate information for the growth or retraction [94]. Neurite retraction can be induced in response to the stiff cantilever suggesting that mechanosensitive growth cone can sense the extracellular mechanical cues to regulate the neurite tension [95]. *In vivo* leg lengthening experiments showed that the nerve can grow in response to the applied stretch by doubling the internodal lengths [96]. In

DRG neurons, stretch application using a magnetic bead on the cell body was sufficient to induce neuronal outgrowth [87], this is consistent with an earlier study on the neurite initiation in DRGs using a microneedle-based pulling [31]. All these studies established the role of mechanical tension in neuronal outgrowth and axonal elongation.

Stretch-dependent growth was further confirmed using an independent approach to look at stretch induced response of many neurons using the stretchable substrates. The stretch grown neurites retain their ability to fire action potentials with a normal amplitude and durations. [97, 98]

Growing body of evidence on the stretch-induced growth led to the studies suggesting mechanisms of stretch-induced mass addition in axons. An intercalated mass addition was proposed mechanism of stretch growth based on *in vitro* experiments using chick DRG neurons [29, 99]. The model suggests that stretch-dependent growth depends on the viscosity and focal adhesion along the axon. Though stretch growth potentially can occur along the entire length of an axon, it is prominently seen in the distal part towards the growth cone since in the proximal part, forces are dissipated due to adhesions [100]. Recently, local protein synthesis in response to the applied strain has been reported as a novel mechanism of mass addition supporting the stretch-induced growth [101].

A neurite growing in response to the applied tension requires continuous membrane addition along with the associated growth. Membrane addition in response to applied stretch has been studied using polyethyleneimine coated microspheres which tightly bind to the plasma membrane. An increase in distance between these microspheres indicates new membrane addition. This study indicates that membrane addition takes place all along the axon but was particularly concen-

trated towards the distal part. Though this study does not comment on vesicle recycling and how membrane is added but provides an evidence for tension induced organization of the membrane. A slackening experiment also suggests the similar trend of the membrane dynamics [31]. Another report on tension induced membrane dynamics suggests the flow of the membrane from growth cone to the cell body, this flow might regulate membrane tension since it is from the region of low tension (due to the accumulation of more membrane near the growth cone) to the region of higher tension [102].

What happens to the cytoskeleton and membrane in stretch growth paradigms is a long-standing question. A recent review by experts who pioneered this field suggests that the thinning of an axon upon stretch would draw microtubules and neurofilaments apart longitudinally, also they will be brought together laterally due to the thinning. Breakage and compaction of filaments in a thinner segment of axons would lead to local assembly and diameter will be recovered again, as it does in stretch-induced growth [103]. This model needs to be confirmed with more experimental evidence pertaining to thinning-thickening cycles as stretch growth happens. Stretch growth paradigm is relatively addressed better compared to the other questions in axonal mechanics. In this chapter and the following, we discuss a novel modality, axonal contraction and straightening which is counteractive of the stretch growth.

Role of the mechanical tension in a synapse formation

In vivo study in *Drosophila* demonstrated that tension developed during the synaptogenesis in an axon is essential for the clustering of neurotransmitter vesicles. Vesicle clustering was reduced if the axon was severed but re-application of ten-

sion was able to restore the clustering. It was found that axons which form neuromuscular junction maintain tension around 1 nN . This report suggests a mechanistic explanation for tension-induced vesicles accumulation. Actin provides a scaffold for vesicle accumulation, rest tension maintains this scaffold and loss of tension leads to the depolymerization of actin and dissemination of vesicles [22]. In frog motor neurons, neurotransmitter release is shown to be regulated by muscle stretch [88]. Stretch-induced increase in synaptic excitability has been reported in brain slices [89]. All these studies, though in different systems, underscore stretch as a potential feedback mechanism in regulating synaptic activity.

A potential role of the mechanical tension in regulating neuronal network

Axonal tension can regulate branch dynamics [90] and decides the position of cell bodies in the network [104]. There are only a few reports suggesting the role of mechanical tension in regulating neuronal network geometry. *In vivo* study on embryonic CNS neuropil of grasshopper *Schistocerca americana*, suggests the role of mechanical tension in neuronal arbor development. Conserved geometries in networks can be achieved by regulation of the tension [105]. Computational modeling study shows that complex, convoluted cortical morphology can be decided by physical forces [106]. A tension-based theory of morphogenesis and compact wiring in the central nervous system has been proposed [107]. These reports suggest that mechanical forces might play a role in higher order organization in neuronal development, however, many more independent approaches need to be developed to explore the tension driven regulation of neuronal networks.

3.1.3 Regulation of the mechanical tension: what is known

As discussed in the earlier section, implications of mechanical tension in various neuronal functions have been addressed, however, intrinsic mechanisms regulating neuronal rest tension remained understudied. Regulation of rest tension in the elongated cells like neurons might be important to maintain the prestress and to achieve long distance mechanical signaling. In this chapter, cytoskeletal mechanisms potentially driving regulation of axonal rest tension will be discussed.

Several studies have demonstrated that neurons actively maintain a rest tension [108, 109]. Neuronal rest tension has largely been studied using microneedle-based manipulations [21], growth cone retraction studies [110] and ablation studies [108]. In microneedle-based axon slackening experiments, the recovery tension often exceeded the initial values suggesting active generation of tension in neurons (figure 3.3), [21]. In axotomy-induced retraction based studies, axonal shortening was found to be ATP-dependent (figure 3.4). [108]. Later, the laser ablation induced axonal retraction was demonstrated to be dependent on actomyosin contractility [111]. In PC12 neurites, retraction studies revealed that actin is involved in generating tension while microtubules had a compressive, resistive function [110]. Myosin-II driven axonal retraction has been shown to be balanced by dynein driven forces suggesting that actin -microtubule motors might be regulating the force balance [112].

Based on microneedle-based pulling in PC12 cells, axons occasionally show initial viscoelastic response followed by the slow contractile response (figure 3.5) [78]. Model suggesting the motor driven contraction of axons was proposed however there was no experimental evidence suggesting the same. Recently acto-

myosin dependent axonal contraction is demonstrated in *Drosophila* neurons, *in vivo* [113].

Though all these studies led to the significant advancement in our understanding on axonal tension regulation, there are intrinsic limitations to these assays. Ablation and microneedle-based studies have employed acute and localized perturbations, which may invoke local responses to these perturbations or damage. For example, axotomy is known to locally elevate calcium [114] and, in turn, may induce activation of myosins [111] and calpain proteases [115]. Though retraction was used as an assay to study the tension, it is an extreme case of contractile activity, where axonal cytoskeletal retracts back into the cell body. While retraction is an important process in the early pruning of branches; these kinds of responses are more relevant in injuries and axon loss [116].

In the current study, we have developed simple assays that are globally acting and less intrusive than microneedle or ablation strategies. We use these methods to investigate the origins of axonal contractility in vertebrate sensory neurons. Unlike retraction which dominates in pruning and leads to the axon loss, this assay allows length minimization of axons while maintaining the structure intact. We have used this assay to understand cytoskeleton-driven axonal contraction (discussed below) and dynamics of the cytoskeleton upon contraction (discussed in the next chapter).

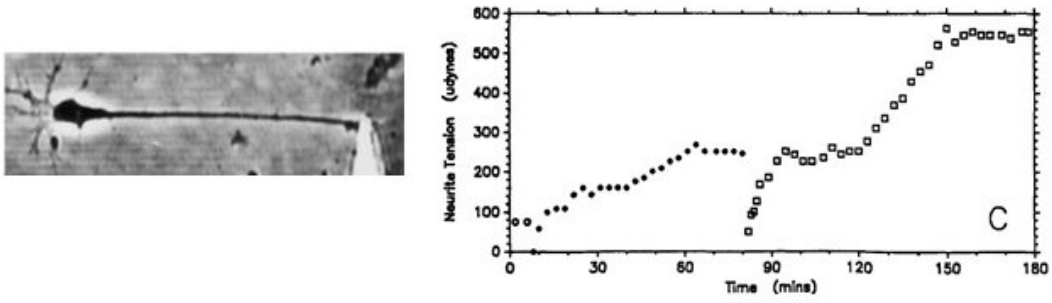

Figure 3.3: Neurite slackening and tension measurements. An example of micro needle attached to the tip of an axon for the slackening experiment (left). Neurite tension increases after slackening. Circles represent before slackening and squares represent after slackening. (right). (Adapted from [21])

Figure 3.4: Ablation leads to the axonal shortening. Upon ablation, DRG axon shows shortening suggesting the contractile activity (Adapted from [108])

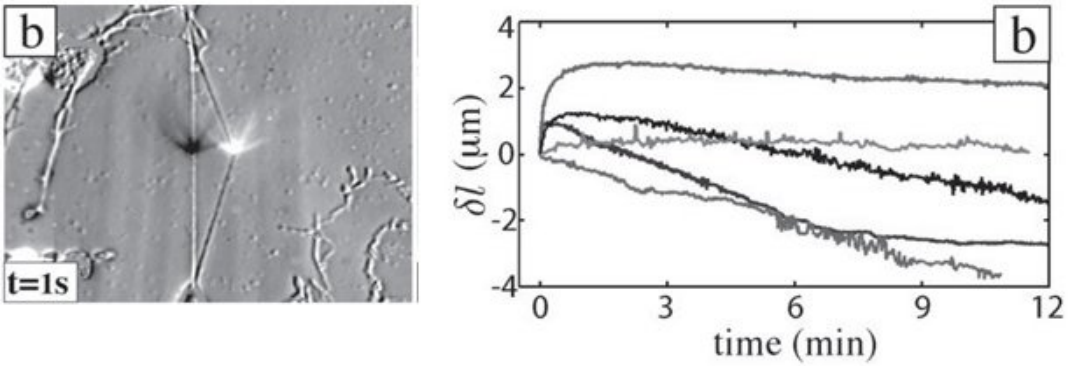

Figure 3.5: The Negative strain suggests axonal contraction. Axonal tension measurement in PC 12 cells using lateral distension (left). Initial viscoelastic relaxation is followed by deflection of the cantilever in negative direction suggesting the contraction (right). (Adapted from [78]).

3.2 Results and discussion

3.2.1 Axons show strain relaxation and straightening upon trypsin-mediated detachment

We have developed a simple cell biological assay to look at the trypsin- mediated de-adhesion and straightening of axons. Chick DRG neurons are cultured on poly-L-lysine coated glass substrates in absence of serum. Axons display curvature in absence of serum presumably due to the compromised growth cone mediated towing and straightening. In the axon relaxation experiments, isolated curved axons were identified and trypsin was added to a final concentration of 5x. Upon trypsin flow, axons detach and show a straightening response (figure 3.6 C-C"). Axons have fewer attachments along their lengths compare to the growth cone

and cell body hence show faster detachment kinetics. We evaluate straightening response by calculating axonal strains. (described in section 3.3.5). Typically, the straightening is apparent within 10-20 seconds of trypsin addition and timescales of straightening ranges from few seconds to eight minutes.

Two different kinds of trends were observed in the strain behavior. Some neurons showed a linear change in the strain with a constant rate (figure 3.8 A) while the other neurons displayed an exponential strain relaxation response (figure 3.8 B). A linear response could arise for neurons having the smaller extent of change and could also be an underestimation due to the end detachment while axonal straightening takes place. For the non-linear cases, strain saturates at different values suggesting the intrinsic differences in the extent of straightening. Similar heterogeneous behavior has been previously documented in chick DRGs in the recovery of rest tension following slackening [21].

These observations were independent of initial length or extent of length change (data not shown). Axons intrinsically grow straight but in a complex environment turning towards or away from the cue could induce curvature along the axonal shaft [117]. Straightening mechanisms might operate in such cases to achieve length minimization.

Initial experiments were done in overnight serum condition. Since serum starvation leads to the more number of curved neurons in culture. Later, all experiments were done with serum starvation followed by 30 minutes serum induction (2-hour serum induction gives comparable average strain rate, (figure 3.7).

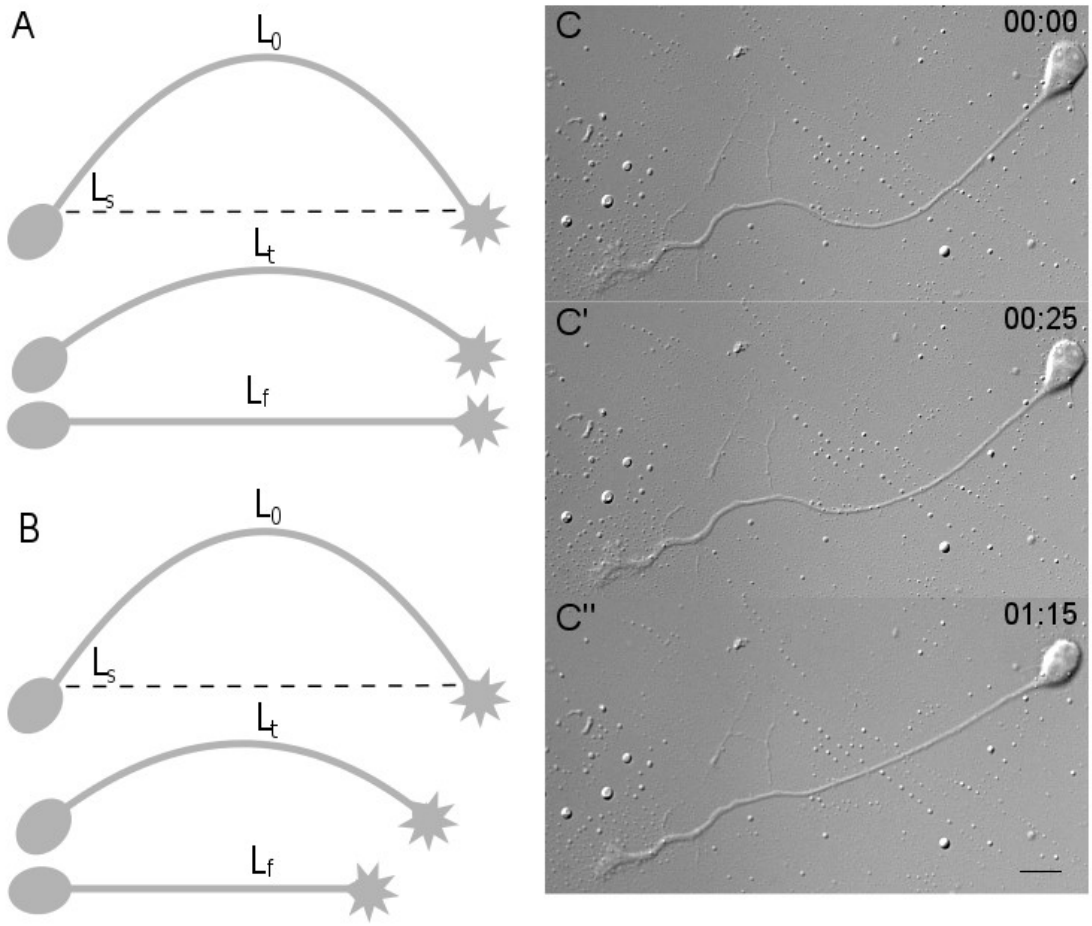

Figure 3.6: Trypsin-induced axonal detachment and straightening. (A) Schematic representation of axonal contraction upon trypsin-induced de-adhesion. (B) Schematic representation of axonal contraction concomitant with tip retraction upon de-adhesion. L_s is the straight-line distance between two ends at time 0. L_0, L_t and L_f are lengths in the first frame, an intermediate frame and the final frame, respectively. (C-C") Representative frames from time-lapse imaging of an axon straightening following trypsin-induced detachment. Trypsin is added at time 0. Time stamp shows minutes:seconds elapsed. Scale bar: 15 μm.

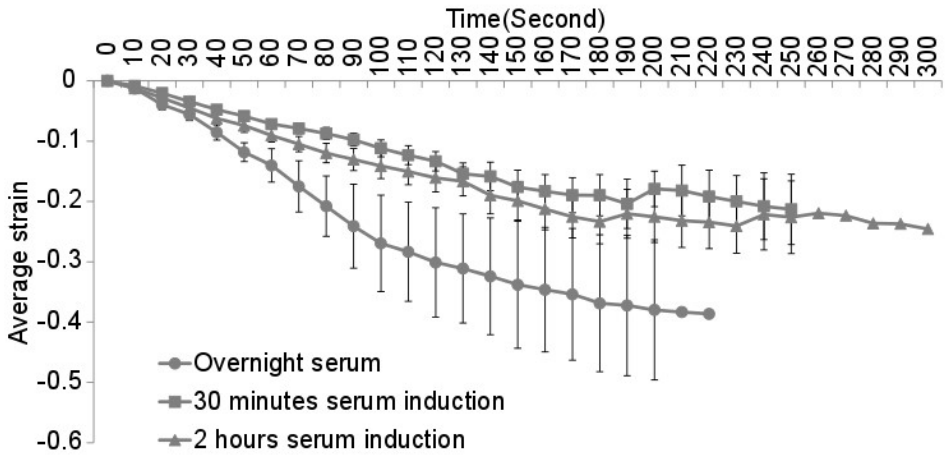

Figure 3.7: Strain relaxation after de-adhesion for axons grown under different serum conditions. Neurons were cultured for 48 hours with either serum-containing media (continuous serum) or in serum-free media. Neurons grown without serum were supplemented with 10% serum for either 2h or 30 mins prior to de-adhesion. $\mathrm{Strain} = (\mathrm{L_t} - \mathrm{L_0})/\mathrm{L_0}$, where $\mathrm{L_0}$ and $\mathrm{L_t}$ are lengths at time 0 and at time t, respectively, as shown in (figure 3.6). An average strain is plotted for continuous serum or serum supplementation for 2 hours or for 30 minutes before trypsin de-adhesion. While the strain rate is slightly larger for neurons grown continuously in serum, the rates for 2 hours and 30 minutes induction were comparable. Short serum induction (2 hours or 30 minutes) resulted in more curved neurons at the time of the experiment compared to those grown in continuous serum. These results prompted us to use the 30 minutes serum induction paradigm for all further experiments. Error bars represent standard error of the mean.

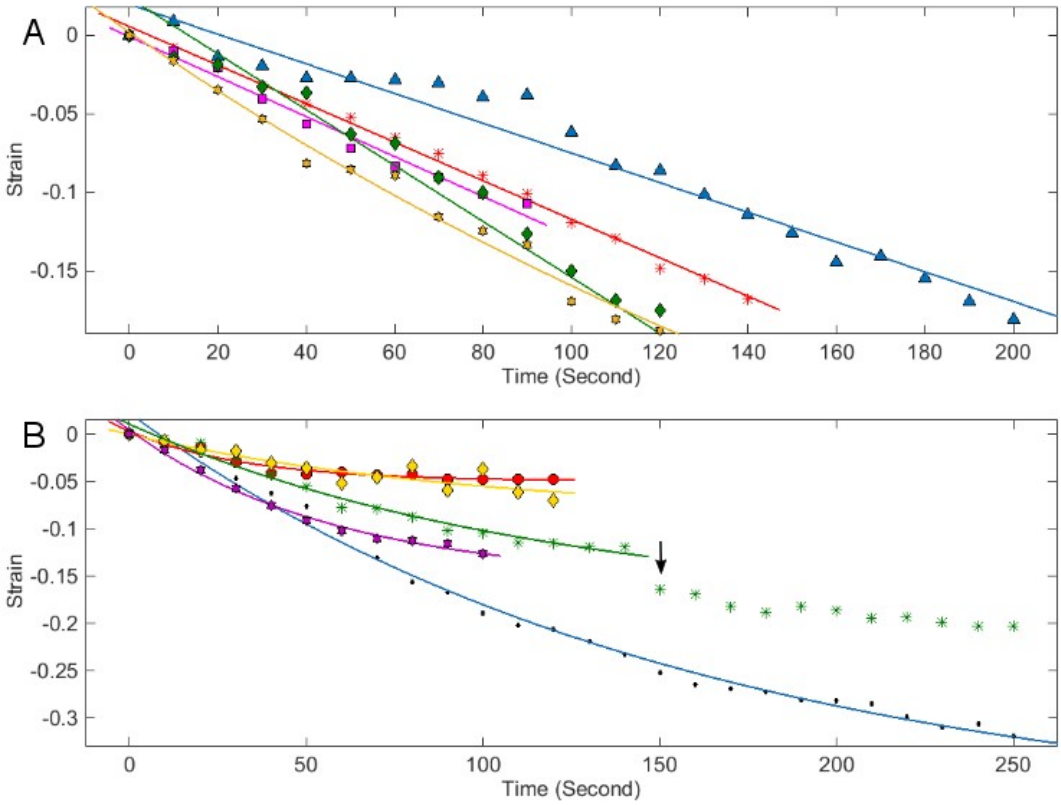

Figure 3.8: Axonal strain relaxation upon de-adhesion. Examples of strain relaxation of axons upon detachment showing both (A) linear and (B) non-linear responses. $\mathrm{Strain} = (\mathrm{L_t} - \mathrm{L_0})/\mathrm{L_0}$, where $\mathrm{L_0}$ and $\mathrm{L_t}$ are lengths at time 0 and at time t, respectively. Different axons are marked in different colors. Symbol indicate actual data while continuous lines are linear and single exponential fits. Arrow indicates a sudden decrease in the strain in that axon as an effect of delayed local detachment; hence data points further are not included in the fit.

3.2.2 Axonal straightening after de-adhesion is actomyosin dependent

Actomyosin dependent contraction has been studied in many different cell types and growth cones [42]. *In vivo* study in *Drosophila* neurons suggests that axonal contraction is actomyosin dependent [113]. To investigate the contribution of Myosin-II in axonal straightening, a specific small molecule inhibitor of myosin II, Blebbistatin (Bleb), was used. Curved neurons pre-treated with 30 μM Bleb for 1 hour failed to straighten upon trypsin-induced de-adhesion (figure 3.9 B, C). Matched DMSO controls, on the other hand, showed the expected axonal straightening (figure 3.9 A). These experiments suggested that axonal strain relaxation observed upon axonal de-adhesion is an active myosin dependent response. (Individual trends are shown in (figure 3.16)).

We next evaluated the contribution of axonal F-actin by using Latrunculin A (Lat A), which depolymerizes F-actin by binding to actin monomers and preventing them from polymerizing. Lat A (0.6 μM) pretreatment for 15 mins was used to inhibit actin polymerization prior to trypsin-induced detachment. Lat A pretreatment completely abolished axonal contractility (figure 3.12 B) while matched DMSO controls showed straightening upon trypsinisation (figure 3.12 A). (Individual trends are shown in (figure 3.17)).

Neurons were imaged for a longer period (10 mins) in order to see if actomyosin contractility was delayed. However, no late response was observed for both bleb and Lat A treated neurons. To ensure trypsin de-adhesion was not affected by drug treatment, the medium was exchanged at the end of the imaging period. The axons were found to be detached and floating indicating trypsin-induced detachment was

unaffected (figure 3.10).

This data suggests that upon induced de-adhesion, actomyosin dependent contraction drives the straightening. Actomyosin activity driven pulling forces have been previously demonstrated in axonal retraction [111, 112]. Recently, in *Drosophila* neurons actomyosin dependent contraction has been shown *in vivo* [113] supporting our results using a different experimental paradigm in the vertebrate neurons.

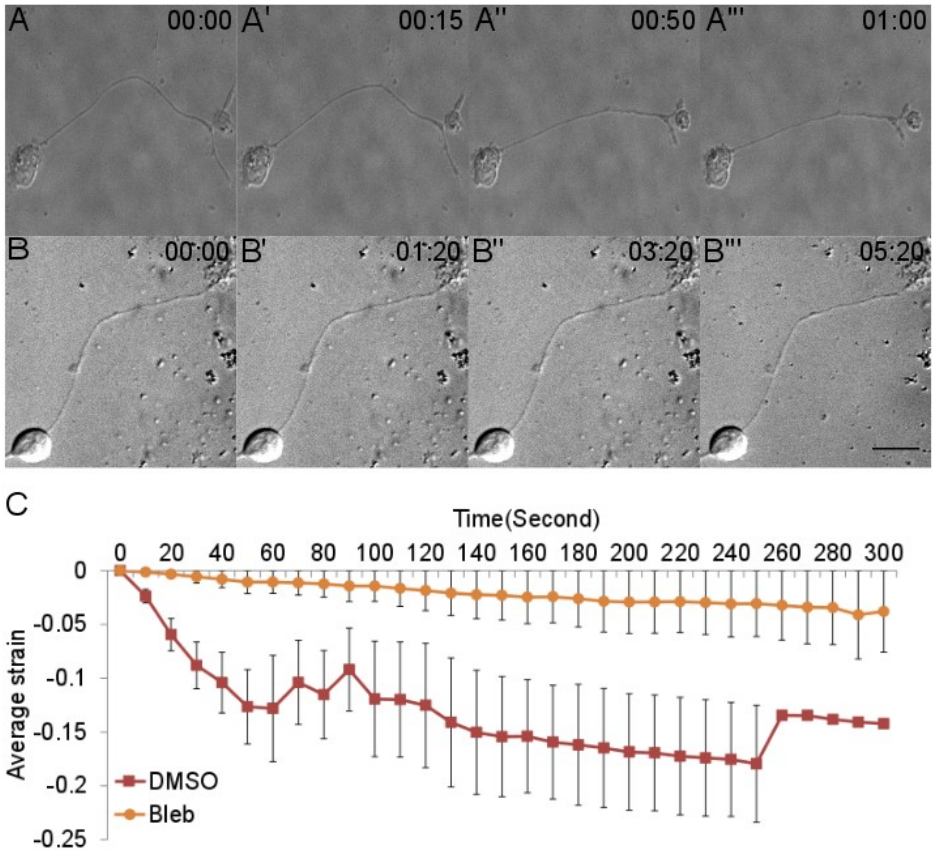

Figure 3.9: Axonal contraction is dependent on myosin-II activity. (A-A"') Representative frames from time-lapse imaging of a DMSO-treated control axon. (B-B"') Representative frames from time-lapse imaging of an axon pretreated with Blebbistatin (30 μM) for 1 hour before trypsin addition. Trypsin is added at time 0 for each treatment. Time stamp shows minutes: seconds elapsed. Scale bar: 15 μm. (C) Average strain rate is reduced upon Blebbistatin (Bleb) treatment (n =10) compared to DMSO-treated controls (n =9). Error bars indicate standard error of the mean.

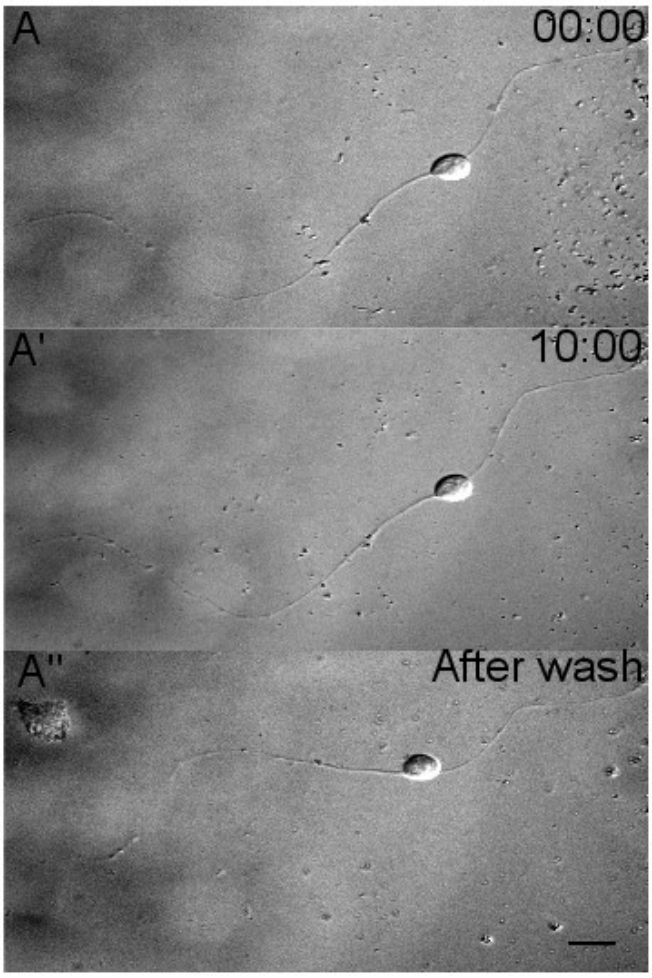

Figure 3.10: Blebbistatin treatment prevents axonal contraction even after longer incubation in trypsin but does not affect trypsin-induced de-adhesion. (A-A") Representative micrographs from time-lapse imaging of an axon pretreated with 30 μM Blebbistatin 1 hour before trypsin addition. Trypsin was added at time 0. Time elapsed is indicated in minutes:seconds. (A') No obvious axonal contraction is seen even after 10 minutes have elapsed after trypsin addition. (A") Upon flowing fresh media at the end of the experiment, the axon is found to be floppy (as evident by the reversed curvature) suggesting the detachment from the substrate. Scale bar: 15 μm.

3.2.3 Effect of microtubule depolymerization on axonal contraction

The axonal shaft is filled with a cross-linked bundle of microtubules which contribute to the structural stability of an axon and also governs various functions including transport and axonal branching. Microtubules breakage along axons is associated with the axonal injury. It is interesting to understand how these stiffest filaments in axons contribute to the axonal contraction. To understand the role of microtubule cytoskeleton in axonal contractility, neurons were pretreated with the microtubule depolymerizing agent, Nocodazole (Noco; 33.3 μM for 15 mins). Interestingly, Nocodazole pretreatment did not block axonal contraction (figure 3.12 C) though the rate of contraction appeared to be reduced compared to the DMSO control (figure 3.12 D). Individual trends are shown in (figure 3.17). Further, we confirmed this using lower concentration of Nocodazole (16 μM for 15 mins).(figure 3.18.)

There is an accumulating evidence suggesting that microtubules and its associated motor dynein have a compressive role and counter-balance the myosin-II driven forces [112]. Recently, the resistive role of microtubules in contraction was shown in *Drosophila* neurons *in vivo* [113]. However, in our assay microtubules depolymerization reduces contraction marginally. Nocodazole treatment resulted in most neurites exhibiting a beaded morphology and tethers along axons (7 out of 9 axons); (figure 3.11). This is consistent with previous observations [118] and confirms the efficacy of Nocodazole. Depolymerization of microtubules results in the formation of thin membrane tethers and these compete with axonal straightening in turn affecting the rate of contraction.

The curved bundles of microtubules in curved axons may play an active role in straightening in conjunction with the actomyosin machinery. In the transition from curve to the straight wherein associated axonal length change ranges from 5% to 35%, change in microtubule curvature is excepted. Sliding of microtubules and change in microtubule curvature may have a role in driving the contraction. Role of the microtubule dynamics in axonal straightening remained to be seen. In the future, it will be interesting to see if microtubule dynamics in involved in driving the contraction.

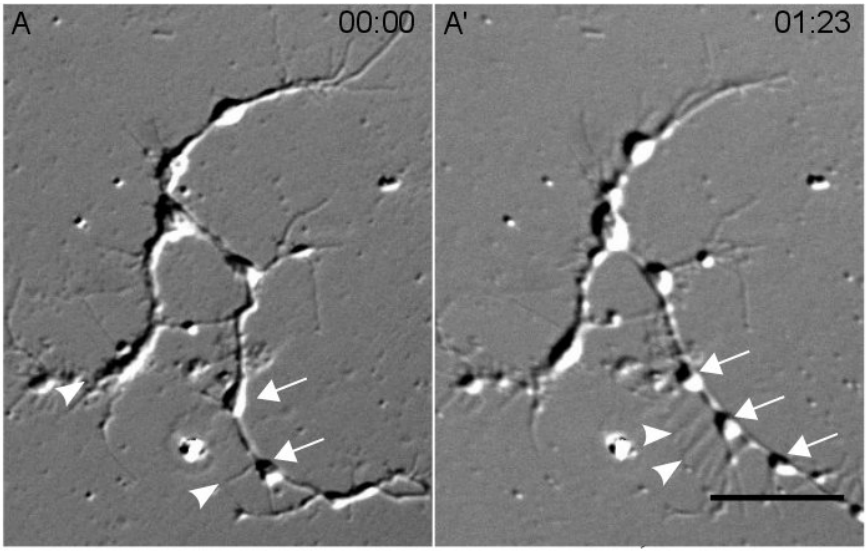

Figure 3.11: Membrane tethers and beads are observed in Nocodazole-treated axons. (A) Representative micrograph of axons pretreated with 33 μM Nocodazole for 15 minutes before trypsin addition at time 0. (A') Micrograph of the same axon after addition of trypsin. Time elapsed is indicated in minutes: seconds. Extensive beading (white arrows) and formation of tethers (white arrowheads) are observed in Nocodazole-treated axons. Scale bar: 15 μm.

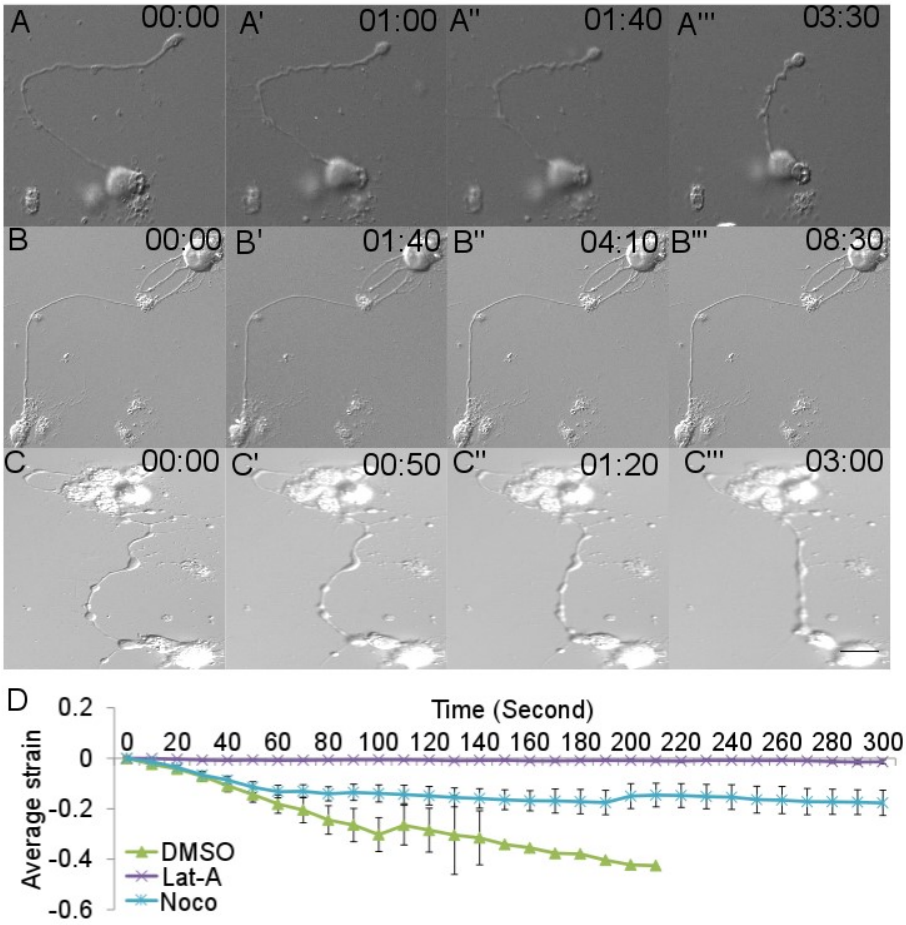

Figure 3.12: Effect of F-actin and microtubule depolymerization on axonal contraction. (A-A"') Representative frames from time-lapse imaging of a DMSO-treated control axon. (B-B"') Representative frames from time-lapse imaging of an axon pretreated with Latrunculin A (0.6 μM) for 15 minutes before trypsin addition. (C-C"') Representative frames from time-lapse imaging of an axon pretreated with Nocodazole (33 μM) for 15 minutes before trypsin addition. Trypsin is added at time 0 for each treatment. Time stamp shows minutes: seconds elapsed. Scale bar: 15 μm. (D) Compared to DMSO controls (n = 7), average strain rate is strongly reduced upon treatment with Latrunculin A (Lat-A; n = 7). Treatment with Nocodazole (Noco; n = 9) also reduces axonal contractility. Error bars indicate standard error of the mean.

3.2.4 Axons show inherent, spontaneous contractility in un-perturbed condition

In straightening experiments discussed so far, contraction is induced upon trypsin-mediated detachment. Next, we asked if axons show inherent, spontaneous straightening response. We used a microcontact printing-based assay to study spontaneous contraction. We grew neurons on patterned substrates with isolated islands of extracellular matrix proteins (laminin and fibronectin). These islands represented isolated sites of high-adhesion relative to the intervening space. The advantages of this assay are: 1. Growth cone turning towards the island induces curvature along axons. 2. Axonal contraction can be looked at reliably without the end movement. It has been shown earlier that axons tend to grow straight intrinsically, however, in a complex environment growth cone tuning often leads to different curved trajectories of axons [117]. We asked whether these curved axons become straight or show shortening response spontaneously (in contrast to trypsin-mediated detachment in experiments described in earlier sections). Using live imaging of these neurons, we showed that axons undergo straightening without trypsin-induced detachment (figure 3.13 A-A", B-B") and we call this contraction inherent, spontaneous contraction. Interestingly, strain relaxation in un-perturbed conditions happens at a much slower rate (figure 3.13 C) suggesting that de-adhesion is the rate-limiting step in spontaneous contraction. We observed straight axonal segments for substantial periods of time and confirmed that straight axons remain straight and the observed spontaneous straightening are not random shape changes (data not shown).

While this assay allowed us to observe spontaneous axonal contractility, the longer

timescales precluded analysis using pharmacological perturbations. However, the trypsin-mediated assay allowed us to undertake pharmacological perturbations of cytoskeletal elements.

To check whether the extent of contraction between two assays (viz., trypsin-deadhesion and spontaneous contraction) is comparable, we used contraction factor (Cr) as a time independent measure of the extent of contraction (also discussed in materials and methods).

$$\mathrm{Cr} = (\mathrm{L_0} - \mathrm{L_f})/(\mathrm{L_0} - \mathrm{L_s})$$

$\mathrm{L_f}$ = saturation length of the axon after de-adhesion, measured from the last frame of recording.

$\mathrm{L_0}$ = length of the axon at the time of trypsinization (t = 0).

$\mathrm{L_s}$ = straight line distance between end points of the axonal segment at time 0.

$\mathrm{L_t}$ = Length of an axon at time t

If there is no length change then Cr will be 0, Cr = 1 indicates straight end-to-end geometry, and values between zero and one indicates partial straightening. And if length reduction is accompanied by tip retraction then Cr could exceed 1.

Cr is comparable between induced contraction (trypsin assay) and spontaneous contraction (microcontact printing assay), in turn validating our trypsin-mediated straightening assay (figure 3.14).

A previous study, using locust neurons, has described a similar assay using islands of carbon nanotubes on quartz sheets. Axonal segments were found to straighten between islands and branches along the contracting segment were retracted concomitant with the development of tension [90].

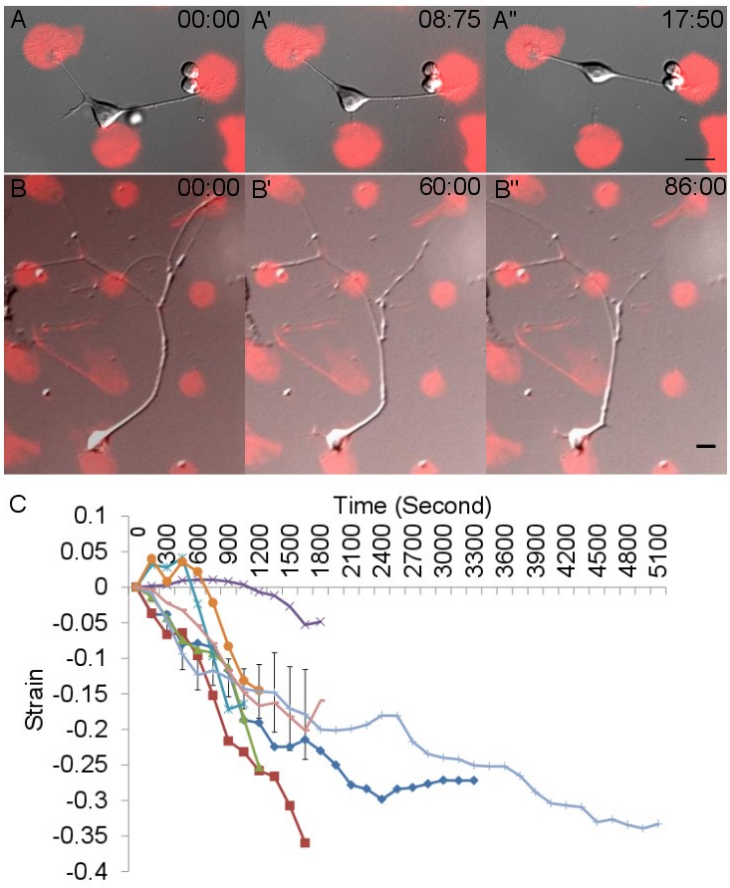

Figure 3.13: Spontaneous contraction of axons. (A-A") Representative micrographs from time-lapse imaging of a pseudobipolar DRG axon spontaneously straightening between two adhesive islands containing laminin and fibronectin (red circles). (B-B") Another example of axonal straightening event. Time stamp shows minutes:seconds elapsed. Scale bar: 15 μm. (C) Evolution of strain with time for 7 axons and the average strain are plotted with error bars indicating standard error of the mean. In some axons, positive strain is initially observed before the axon begins to shorten. This is because this assay relies on slow, spontaneous de-adhesion unlike acute induction of de-adhesion by trypsin.

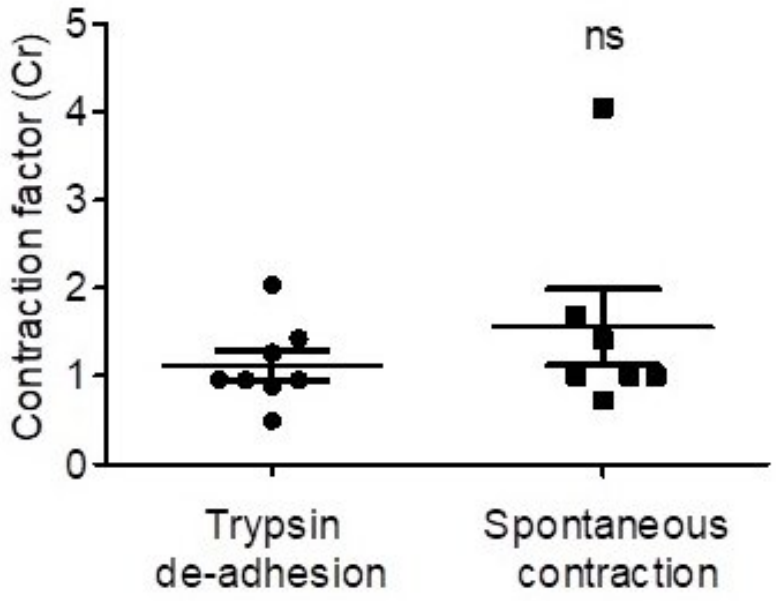

Figure 3.14: The extent of spontaneous contraction is comparable with induced contraction. Comparison of Contraction factor (see Material and Methods for definition) suggest that the extent of spontaneous contraction between adhesive sites (n = 7) is comparable to that observed during trypsin-induced de-adhesion (n = 8). Unpaired t-test was used to compare the means. Error bars represent standard error of the mean. ns: significant.

3.3 Summary and conclusions

We have developed a simple assay to evaluate axonal contractility that avoids local, acute mechanical perturbations and instead uses trypsin to detach axons from the substrate. Additionally, using a microcontact printing-based assay we showed that axons have inherent, spontaneous contractile activity. Spontaneous

axonal contraction is a slow process since it relies on inherent detachment kinetics of axons (figure 3.15).

We propose that axonal contractility is balanced by adhesion along axons and upon spontaneous or induced detachment, actomyosin machinery drives the contraction resulting in detachment from the substrate and shortening. Further, we have looked at subcellular cytoskeleton responses upon contraction, discussed in the next chapter. The local contractile mechanisms might be important for the length minimization for long cells like neurons. Axonal contraction could be a potential mechanism to regulate rest tension of axons, this can be confirmed further, using quantitative force measurements.

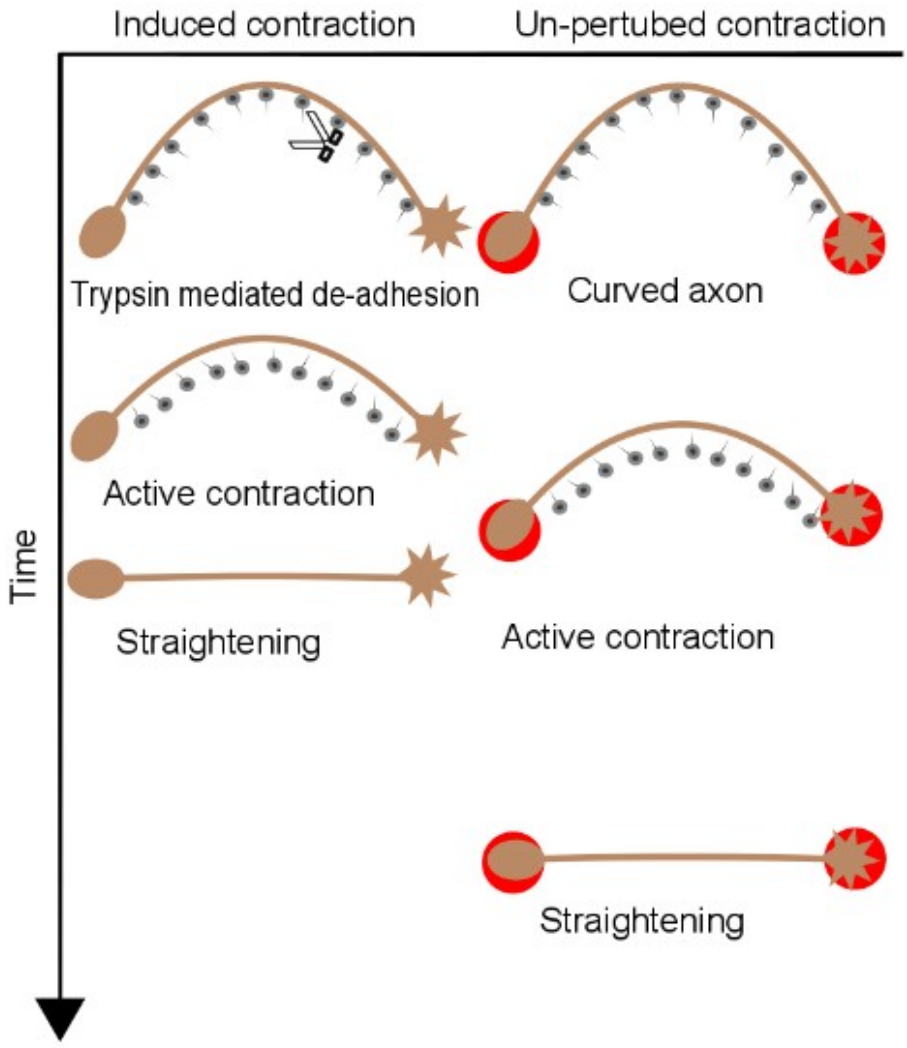

Figure 3.15: Summary of axonal contraction experiments. Actomyosin dependent axonal contraction upon trypsin induced detachment and in un-perturbed condition. The slower rate of contraction in un-perturbed condition suggests detachment is the rate limiting step.

3.4 Materials And Methods

3.4.1 Dissection and cultures

Fertilized, white Leghorn chicken eggs were obtained from Venkateshwara Hatchery Private Limited, Pune, India. All procedures were approved by the Institutional Animal Ethics Committee, IISER Pune, India. Nine or ten-day old chick embryos were used to isolate dorsal root ganglia (DRG). Dissections were carried out in sterile PBS (137 mM NaCl, 2.7mM KCl, 10 mM $\mathrm{Na_2HPO_4}$, 1.8 mM $\mathrm{KH_2PO_4}$) under a dissecting microscope inside a horizontal laminar flow hood. Twelve to fourteen DRGs were removed from both sides of the spinal cord and collected in L15 medium (Gibco). The tissue was centrifuged at 3000 rpm for 3 minutes before the medium was removed and 1x trypsin (Lonza) was added. Trypsinization was undertaken for 20 minutes at $37\,^{\circ}\mathrm{C}$. Following trypsinization, the tissue was centrifuged at 3000 rpm for 3 - 5 minutes before removal of trypsin and washed with L15 medium. The dissociated neurons were plated on poly-L-lysine-coated (1mg/ml PLL; Sigma) 35 mm cover glass bottomed petri dishes in 1.5 ml of serum-free media (L15 containing 6 mg/ml glucose (Sigma), 1x glutamine (Gibco), 1x B27 (Invitrogen), 20 ng/ml NGF (Gibco) and 1x Penstrep (Gibco)). The neuronal culture was incubated for 48 hours at $37\,^{\circ}\mathrm{C}$ before de-adhesion experiments. Cells were grown in serum-free media until half an hour before de-adhesion experiments in order to increase the occurrence of curved axons during the initial growth phase (see next section for details).

For microcontact printing experiments, the cover glasses were patterned (as described below) before plating the neurons. These experiments were performed in

media containing 10% fetal bovine serum (Gibco).

3.4.2 Trypsin de-adhesion, imaging and analysis

To perform experiments, 10% fetal bovine serum (Gibco) was added to the neurons grown in serum-free media and incubated for a further 30 minutes at 37 °C. Immediately prior to trypsin-induced de-adhesion, serum containing media was removed, the cultures were washed thrice in prewarmed serum-free L15 and replaced with 1 ml of serum-free L15. Isolated curved axons were identified and trypsin (Sigma) was added to a final concentration of 5x. Upon trypsin treatment, axons de-adhere and show a straightening response. Neurons were imaged using Differential Interference Contrast (DIC) microscopy using a 40x oil objective on an Olympus IX81 system equipped with a Hamamatsu ORCA-R2 CCD camera. Images were recorded at 1 frame per second acquisition rate using the Xcellence RT (Olympus) software. Typically, straightening starts after 10-20 seconds of trypsin addition and imaging was continued till there is no further length change or the axonal ends (soma or growth cone) detach. Images were exported to ImageJ and lengths were measured using the segmented Line tool at every 10-second interval.

The following inclusion criteria were used to select axons for evaluation of axonal contractility.

1. Axons showing significant curvature, presumably due to attachments along their lengths, were chosen for axon straightening experiments (figure 3.6 A). Axonal segments having obvious branches were not considered as the branches may hinder contraction.

2. If the growth cone retracted concomitantly with a reduction in axonal curvature

then such data were included in our analysis. In these cases, the assumption is that the axonal shortening, evident from the reduction of curvature, is causing the weakly attached growth cone to be pulled backward (figure 3.6 B).

3. If the growth cone or soma detached and retracted before the reduction in axonal curvature then these were not included in the analysis.

In these experiments, the axon lengths ranged from 70 μm to 180 μm and 5 - 35% decrease in length was observed upon de-adhesion.

In initial experiments, we grew DRG neurons in the presence of serum prior to trypsin de-adhesion. However, subsequently, we took advantage of the fact that neurons cultured without serum have a much greater frequency of neurites showing curved trajectories [119] and thus improved the throughput of our experiments. Neurons were grown for 48 hours without serum followed by re-feeding 10% FBS 30 minutes or 2 hours prior to trypsinization. The contractility of 30 minutes and 2 hours serum re-fed axons were comparable. Thus, all inhibitor-based perturbation experiments were conducted following 30 minutes of serum treatment. In all three conditions straightening response was seen in response to axonal de-adhesion ((figure 3.11).

3.4.3 Micropatterning of substrates

Patterned substrates were generated using microcontact printing. Silicon masters with 20 μm diameter depressions spaced 50 μm or 70 μm apart were procured from Bonda Technology Pte. Ltd., Singapore. PDMS (Dow Corning) stamps were made from the master by using a previously published protocol [120]. Sterile PDMS stamps were washed with isopropanol and dried in the laminar flow hood. Laminin (20 μ/ml), fibronectin (100 μg/ml) and rhodamine-labeled BSA

(10 μg/ml) were mixed and used for inking the PDMS stamp. The protein mixture was applied onto the stamp and incubated for 5 minutes at room temperature. After removal of excess protein solution, the stamps were used to pattern cover glass bottomed 35 mm Petri dishes. PBS was added immediately after printing to avoid drying of the patterns until neurons were plated.

For studies involving axons straightening on patterned substrates, axons were imaged after 8 hours or overnight incubation in serum-containing medium. Neurons were imaged in DIC mode using 10x or 40x objective at 15-second intervals. Images were exported to Image J and axonal lengths measured using the segmented line tool.

3.4.4 Drug treatments

Neurons were treated with 30 μM Blebbistatin (- enantiomer; Sigma) for 1 hour prior to the straightening experiments. For actin depolymerization and microtubule depolymerization experiments, 0.6 μM Latrunculin A (Sigma) or 33 μM Nocodazole (Sigma) were added to the cultures 15 minutes prior to trypsin treatment. All drugs were dissolved in DMSO. Control experiments were undertaken to test the effect of similar volumes of DMSO on straightening kinetics.

3.4.5 Definitions of parameters

We characterized the length minimization response by evaluating the evolution of the strain in the axonal segment (figure 3.8 A, B).

$$\mathrm{Strain} = (\mathrm{L_t} - \mathrm{L_0})/\mathrm{L_0}$$

We have used contraction factor (Cr) as a time-independent measure of the extent of axonal shortening,

$$\mathrm{Cr} = (\mathrm{L_0} - \mathrm{L_f})/(\mathrm{L_0} - \mathrm{L_s})$$

$\mathrm{L_f}$ = saturation length of the axon after de-adhesion, measured from the last frame of recording.

$\mathrm{L_0}$ = length of the axon at the time of trypsinization (t = 0).

$\mathrm{L_s}$ = straight line distance between end points of the axonal segment at time 0.

$\mathrm{L_t}$ = Length of an axon at time t

If there is no length change then Cr will be 0, Cr = 1 indicates straight end-to-end geometry, and values between zero and one indicates partial straightening. And if length reduction is accompanied by tip retraction then Cr could exceed 1.

Data representation and statistics

Axonal strain graphs were plotted in Excel (2010). Comparision of contraction factor was carried out GraphPad 5. Curve fitting analysis was done in Matlab 2014 using *cftool*.

3.5 Appendix

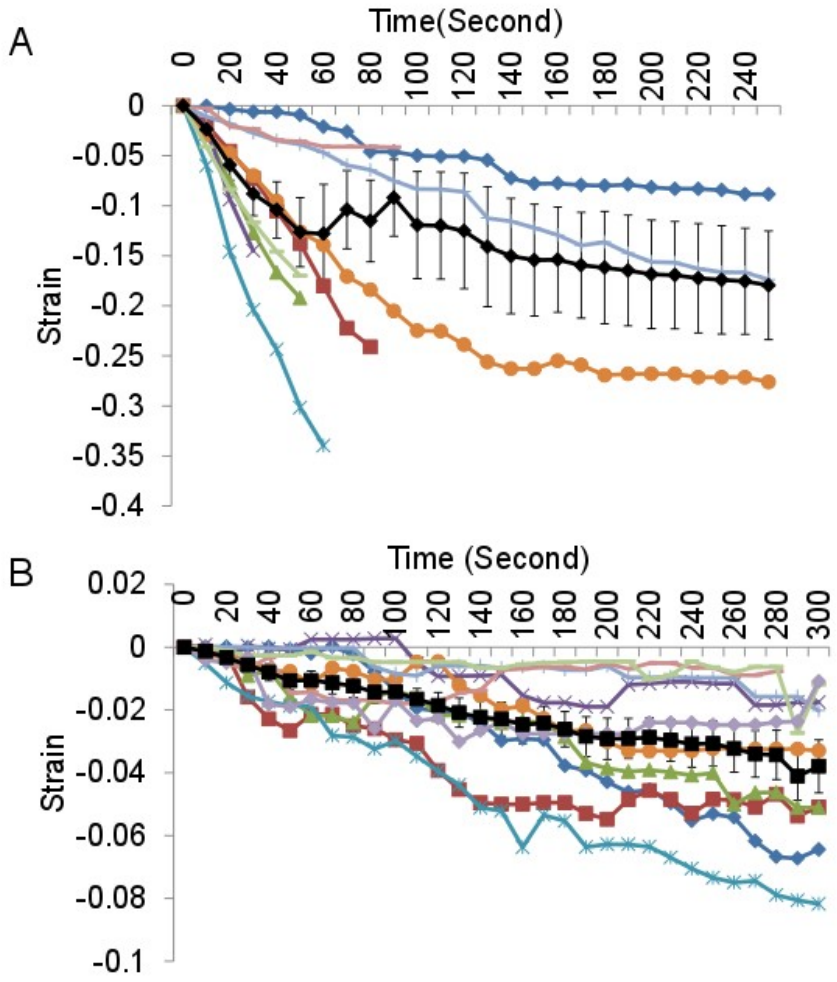

Figure 3.16: Individual datasets of DMSO and blebbistatin treatment. Axonal strains of A. DMSO (0.03 %) and B. Blebbistatin (33 μM) treated axons. Each color indicates an individual axon and the black line shows an average. Error bar represents SEM.

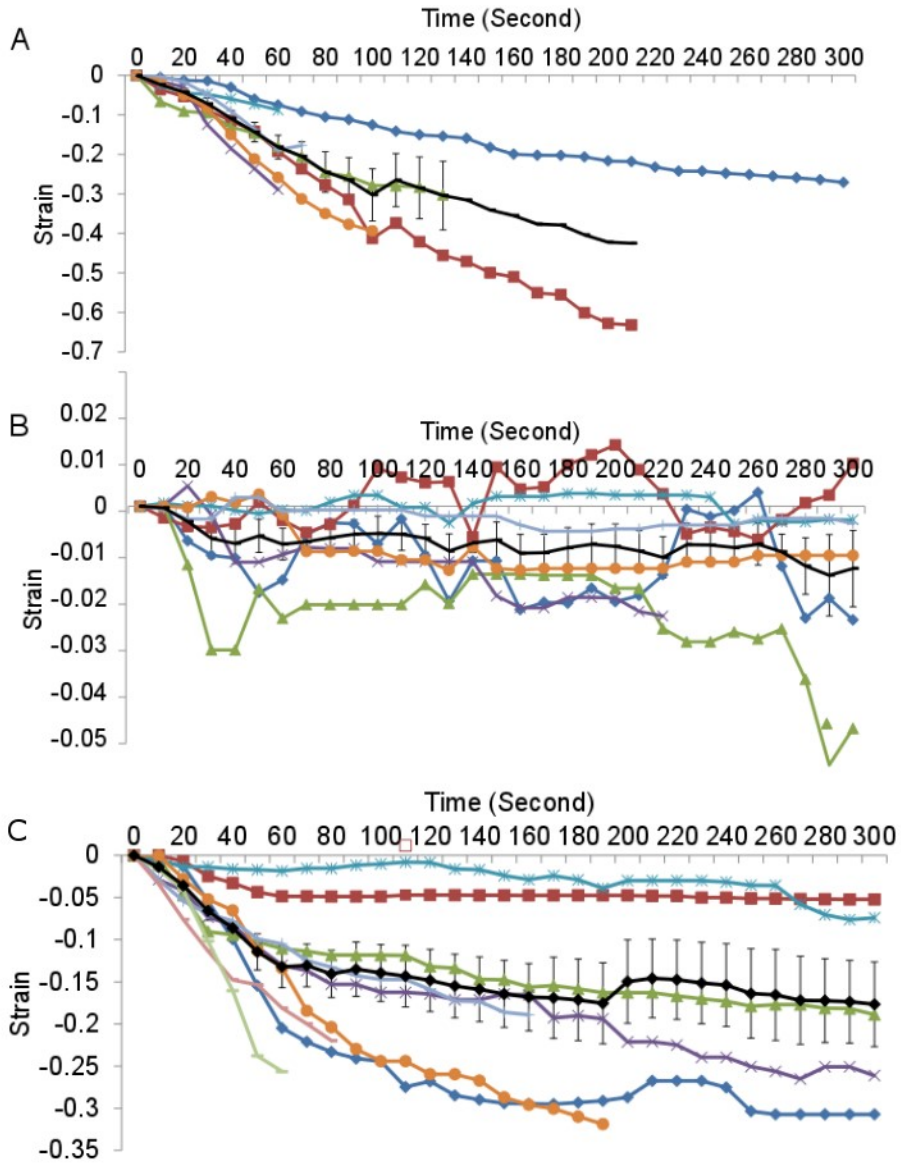

Figure 3.17: Individual datasets of DMSO, Lat A and Noco treatment. Axonal strains of A. DMSO (0.12%) and B. Lat A (0.6 μlM) and Noco (33 μlM) treated axons. Lat A treated axons sometime shows positive strains due to the protrusive activity upon actin depolymerization. Each color indicates individual axon and the black line shows an average. Error bar represents SEM. Higher concentracton of DMSO seems to increase the axonal contraction hence it is important to compare data with the matched DMSO control.

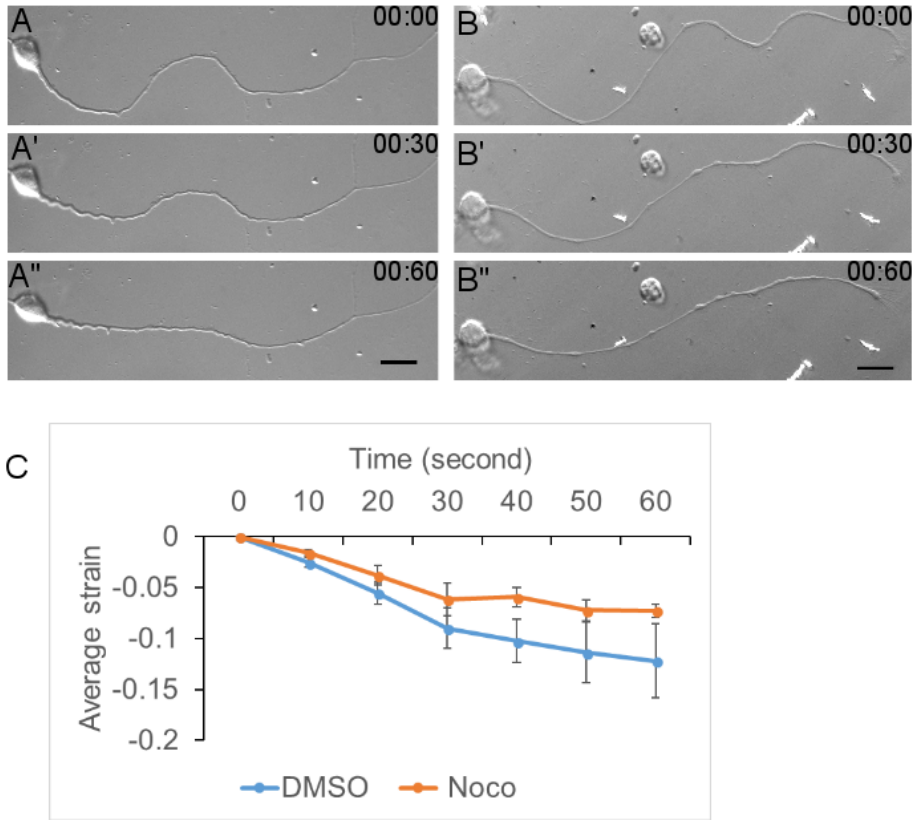

Figure 3.18: Microtubule depolymerization with the lower concentration of Nocodazole reduces the rate of axonal contraction. (A-A") and (B-B") are representative frames from time-lapse imaging of an axon pretreated with DMSO and Nocodazole (16 μM) respectively. Trypsin is added at time 0 for each treatment. Time stamp shows minutes: seconds elapsed. Scale bar: 15 μm. (C) Average strain rate is increased upon Nocodazole (Noco) treatment (n =11) compared to DMSO-treated controls (n =10). Error bars indicate standard error of the mean.

4. Subcellular cytoskeletal dynamics associated with axonal contraction

4.1 Introduction

As described in the last chapter, axonal contraction and straightening are acto-myosin dependent processes and microtubule remodeling may occur to sustain the length shortening. How axonal cytoskeleton remodels upon trypsin-mediated de-adhesion to drive straightening is an intriguing question. In this chapter, we discuss the subcellular cytoskeleton dynamics underlying the axonal contraction. Dynamics of axonal cytoskeletal remained controversial for a long time [81, 83, 121]. Some of the early studies used photobleaching and photoactivation techniques to investigate the dynamics of axonal cytoskeleton [122]. These approaches could not be used in our study since axonal shaft itself moves in our straightening experiments.

We used docked mitochondria as a general cytoskeletal marker to study subcellular responses in axonal contraction.

4.1.1 Interaction of mitochondria with the axonal cytoskeleton

Proper mitochondrial distribution along the axonal length is critical for various neuronal functions and defects in mitochondria positioning is associated with major neurological disorders [123]. Mitochondria can pause or become stationary at various subdomains of axons based on the metabolic demand [124]. It is known that only one-third of mitochondria are motile rest of them are stationary [34]. Stationary mitochondria remain docked on the cytoskeleton and move at an extremely slow rate. Docked mitochondria were defined as those that moved slower than 0.1 μm/s (i.e., 360 μm/h), based on the lower limits of dyneins and kinesins [99, 125]. They are associated with microtubules, neurofilaments by cross-linkers (figure 4.1). Microtubules-mitochondria interactions have been studied extensively, Syntaphilin is known to play a role in docking of mitochondria on microtubules [33, 34]. Interaction of neurofilaments with mitochondria depends on mitochondrial membrane potential, the phosphorylation status of the neurofilaments and neurofilament sidearm interactions [35]. It has been suggested that mitochondria retention requires actin cytoskeleton in the cortical region [36]. NGF induces inhibition of mitochondrial motility along axons. Mitochondrial retention in this study is shown to be actin-dependent suggesting the role of the actin cytoskeleton in retention of mitochondria [126].

All these studies suggest the stable association between axonal cytoskeleton and mitochondria underscoring the reliability of docked mitochondria as a cytoskeletal marker.

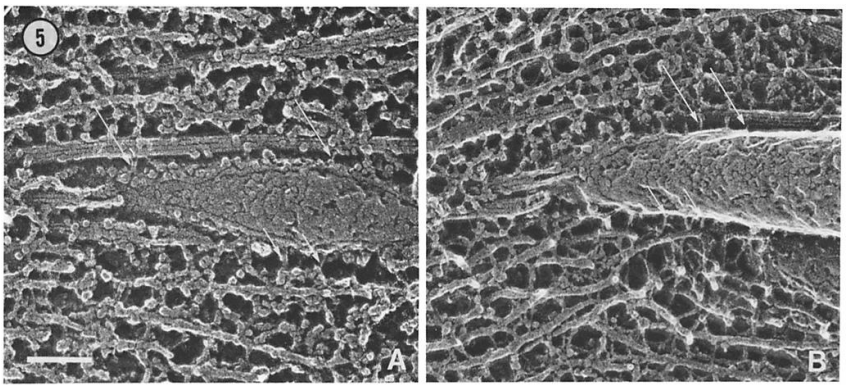

Figure 4.1: The crosslinking of mitochondria with microtubules and neurofilaments. Interactions of the mitochondria with microtubules (left) and neurofilaments (right) by the cross-linkers (white arrows) in the frog axon observed using electron microscopy. Scale bar: 0.1 μm. (Adapted from [24]).

4.1.2 Docked mitochondria as a cytoskeletal marker

Due to the traceability and ease of labeling, docked mitochondria have been used extensively in neurons [37, 84, 99, 127, 128]. Docked mitochondria have been used to study the underlying cytoskeletal dynamics in axonal growth. Due to the limitations in employing photobleaching and photoactivation techniques in axons, docked mitochondria approach became popular especially for the paradigms where dynamics is associated with the axonal length changes like axonal elongation. Docked mitochondria were validated as a cytoskeletal marker in the growth paradigm. In this study, the pattern of mitochondrial dynamics is consistent with dynamics of cortical actin flow, shown by polystyrene bead cross-linked to the axonal cortical actin [99].

Stretch-induced cytoskeletal dynamics have been studied using docked mitochon-

dria in DRG neurons growing on the stretchable substrates. This study suggests strain heterogeneity in axonal cytoskeleton due to the applied stretch [37]. Axonal elongation and underlying cytoskeletal response have been studied in recent years using docked mitochondria approach, these studies suggest forward *en bloc* movement of the cytoskeleton during elongation [84,127,128]. Though cytoskeletal dynamics in growth and elongation has been studied; it has remained unexplored in axonal contraction paradigm. Use of docked mitochondria in our assay for axonal contraction (discussed in chapter 3) gives us the unique opportunity to evaluate subcellular cytoskeletal dynamics underlying axonal contraction.

4.2 Result and discussion

4.2.1 Subcellular strain analysis upon contraction

We used docked mitochondria as a cytoskeletal marker to understand underlying cytoskeletal dynamics driving the contraction. Trypsin-mediated straightening experiments were done on neurons labeled with mitotracker green (figure 4.3 A-A"). We could not use conventional kymography tool for this analysis since axonal segment shortens during the course of the experiment. Thus, we developed a custom written code to track the position of mitochondria and calculate local strains between adjacent mitochondria pairs as a function of time (figure 4.2, figure 4.3 B). This local strain in this analysis is defined as:

Local strain = $[\Delta L_{i(t)} - \Delta L_{i(0)}] / \Delta L_{i(0)}$

Where ΔL_i is a distance between the i^{th} pair of adjacent mitochondria (indexed sequentially from one end) and t is time.

Though the axonal strain drops monotonously, local cytoskeletal strain showed

the heterogeneous response (n=8). Each pair of mitochondria showed contractile-extensile behavior. Occasionally, contraction in one pair is concomitant with extension in another pair. While the cumulative sum of the local strains was negative, at any given time both positive and negative strains were observed along the same axon and these values fluctuated with time (figure 4.4). These data suggest that the axonal cytoskeletal in not contracting as a uniform whole but is highly heterogeneous (figure 4.7).

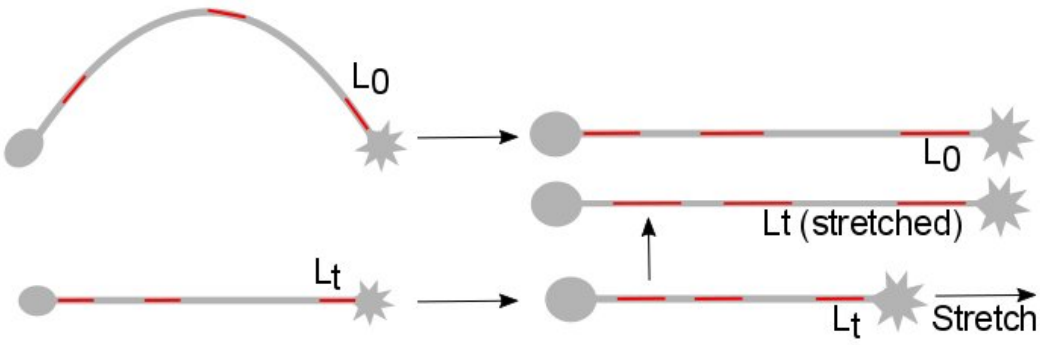

Figure 4.2: Schematic explaining mitochondria analysis. L_0 (curved axon), L_t (straight axon). Using a matlab based code, both curved and straight axons are interpolated. L_t (stretched) is a stretched image and interpolated with L_0 to allow reliable detection of mitochondria. Mitochondria are shown in red.

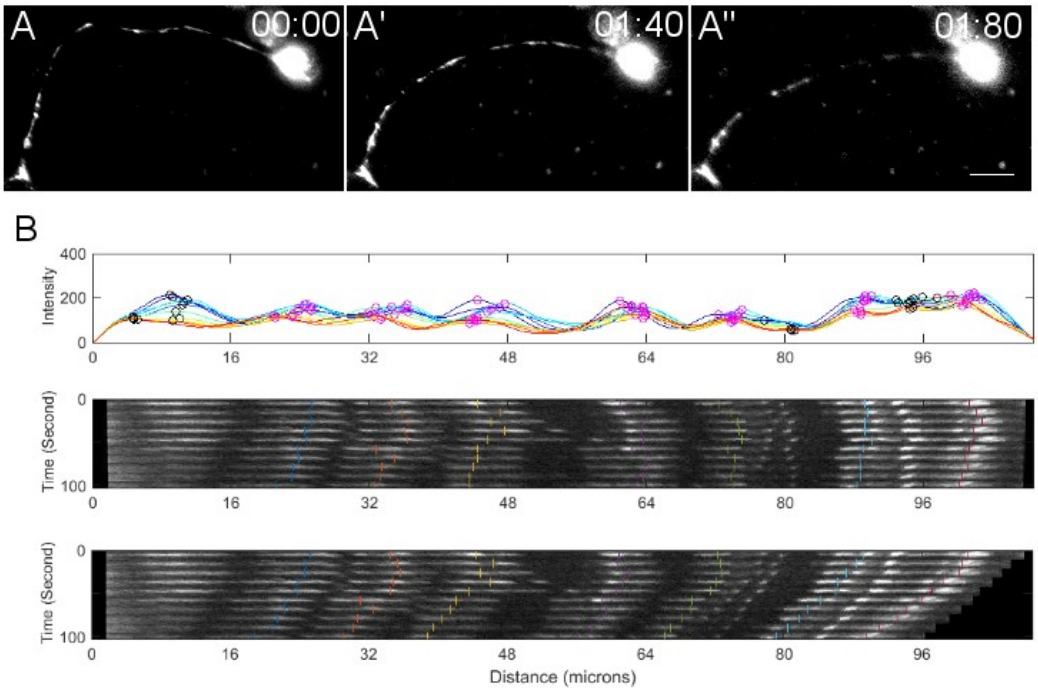

Figure 4.3: Mitochondria tracking and analysis. (A-A") Representative time frames of an axon with labeled mitochondria undergoing straightening due to induced de-adhesion. Trypsin was added at time 0. Time elapsed is in minutes: seconds. Scale bar: 15 μm. (B) Intensity-based detection of mitochondrial position along the axon, from the cell body to the distal end (see Materials and Methods for details). The top panel shows the intensity traces for different time points (represented in different colors) along the axon. The intensity trace of each time point is resampled to have the same length as the first time point (longest). The positions of the detected local maxima are indicated by circles. Pink circles indicate maxima selected for analysis. The middle panel shows a kymograph of the fluorescent mitochondria with the axonal contours at each timepoint stretched to the same length. This procedure serves as a visual aid to reliably identify peaks corresponding to mitochondria that are reliably present across all time points. The bottom panel shows a kymograph in the original scale with the location of the selected mitochondria, which were used to calculate local strain.

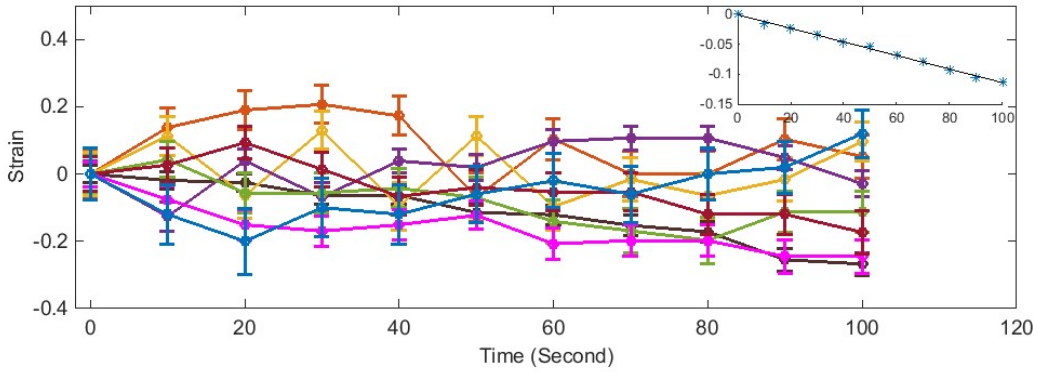

Figure 4.4: Intermitochondrial strains show heterogenous response. Plotting the evolution of strain between mitochondrial pairs (adjacent pairs numbered from soma to growth cone) of a randomly selected axon as it straightens. The data reveals instances of contraction in one pair of mitochondria being concomitant with an extension in another pair and occasionally contraction/extension in two pairs occur together. Inset shows that the net axonal strain decreases steadily with time compared to the local strains. Error bars are standard deviations of natural mitochondrial fluctuations observed in six live axons recorded for a similar period of time without inducing de-adhesion.

4.2.2 Axonal cytoskeleton shows heterogeneous response upon axonal contraction

In order to distinguish the strain dynamics upon contraction from baseline mitochondrial fluctuations, we imaged mitochondria labeled axons without trypsin flow. It was noticed that mitochondria have minimal strain fluctuations in the similar time scales (figure 4.5). In order to compare strain heterogeneity between control (without trypsin) and straightening paradigm (with trypsin), we used in-

stantaneous strain (figure 4.6) since it is calculated between adjacent frames of a fixed time interval (10 seconds). Strain heterogeneity increases upon de-adhesion and straightening suggesting that cytoskeletal strain dynamics is indeed due to the contraction and not because of the strain evolving due to the random fluctuations (figure 4.7). We have also estimated the error in the tracking using fixed mitochondria data to validate our analysis, strain fluctuations are minimal in this case (data not shown).

Next, we asked whether local strains in mitochondrial pair depend on the initial separation between mitochondria. Data for instantaneous strain were pooled and binned to have groups of similar bin width. We could reliably compare the bins of 20-40 μm between without trypsin data (baseline fluctuation) and with trypsin (deadhesion and straightening). In this analysis, data were binned with a fixed bin width for all possible separations. However, we analyzed the data in only the 20-40 μm bin as there were limited data points available in bins lesser or greater than the 20-40 μm. Heterogeneity in instantaneous strain was compared for initial separation ranging from 20-40 μm using O' Brien's method and it increases during contraction suggesting that cytoskeletal contractility at this length scales (figure 4.8).

Collectively, this analysis shows that monotonous axonal contraction is driven by heterogeneous cytoskeletal dynamics. Within the limits of our resolution of the technique, heterogeneity is seen at 20-40 μm.

In vivo, the heterogeneous response seen along axons might be important for localized regulation of various processes like a branch and the adhesion dynamics. So far, axonal contraction studies have been largely limited to the evaluation average properties like for force or bulk strain. We show that actomyosin-based

contractility drives axonal contraction but the subcellular response is heterogeneous. The subcellular strain has been evaluated in stretch paradigm and similar heterogeneity in the strain is shown [37]. We could demonstrate it in exactly opposite contraction paradigm. In this study, signaling through focal adhesion was proposed to be a mechanism to drive strain responses. In our assay, this possibility is ruled out since it is induced upon de-adhesion. This opens a possibility of other globally acting signaling mechanisms involved in cytoskeletal dynamics in contraction.

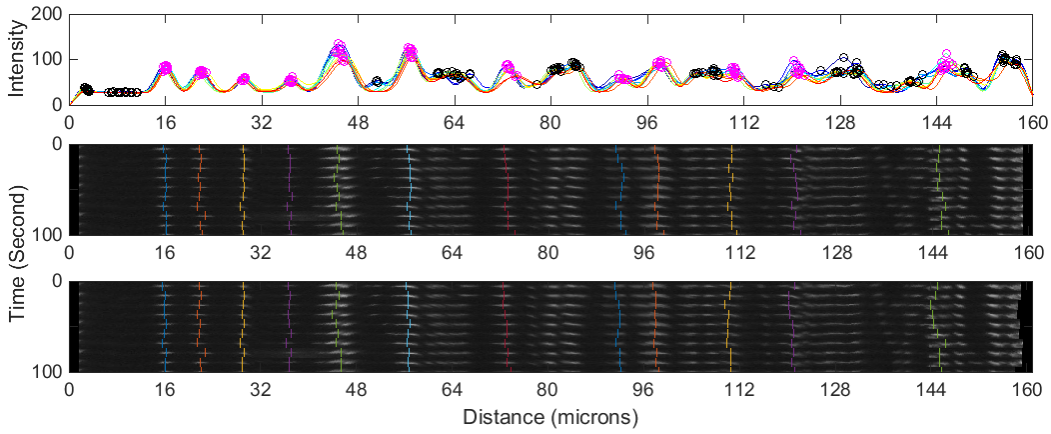

Figure 4.5: An example of baseline mitochondria fluctuations without the trypsin flow. The top panel is an intensity profile of mitochondria for the axon without detachment and straightening. The middle panel shows a kymograph of the fluorescent mitochondria with the axonal contours at each timepoint stretched to the same length. The bottom panel shows a kymograph in the original scale with the location of the selected mitochondria (rescaled to the actual scale).

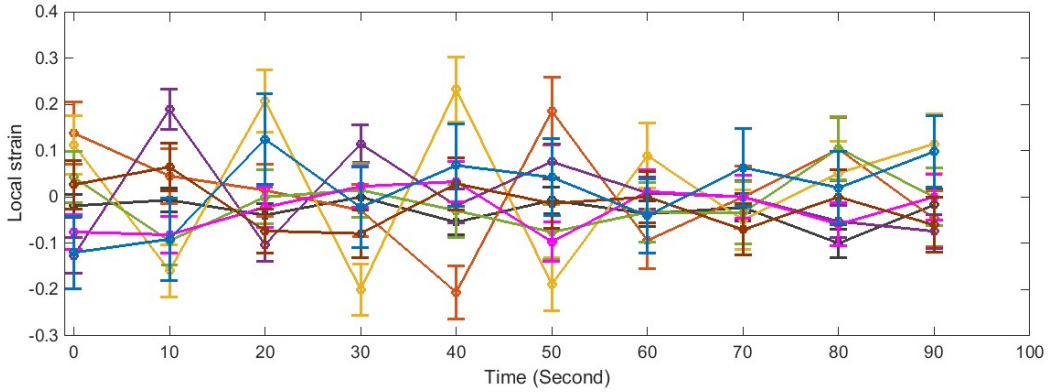

Figure 4.6: Instantaneous strain vs time plot for axonal mitochondria. Instantaneous strain= $[\Delta L_{i(t+\delta t)}\text{-}\Delta L_{i(t)}]$ / $\Delta L_{i(t)}$, between pairs of mitochondria for the same axon shown in (figure 4.4). $\Delta L_{i(t+\delta t)}$ and $\Delta L_{i(t)}$ are distances between i^{th} pair of mitochondria at time t+δt and t, respectively. Color coding for mitochondrial pairs is the same as in (figure 4.4).

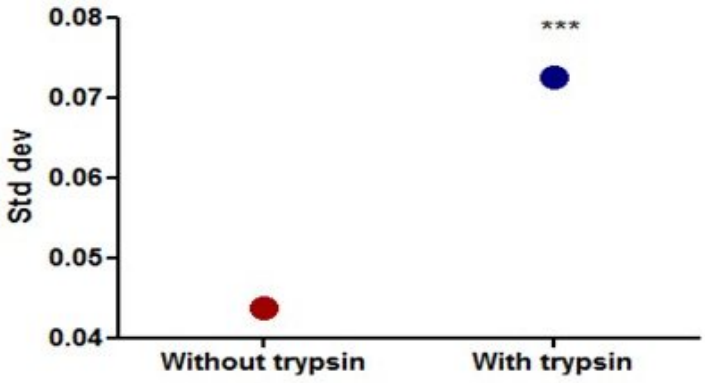

Figure 4.7: Strain heterogeneity increases upon contraction. Strain is calculated at every 10 second interval for straightening data (n=8) and without trypsin control (n=6). All instantaneous strain values were pooled and compared (each treatment has more than 500 data points). O' Brien's test: p=0.0001.

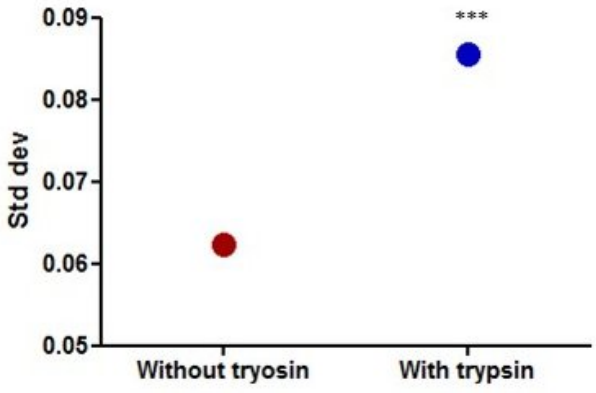

Figure 4.8: Strain heterogeneity increases at 20-40 μm initial separation upon contraction. The strain is calculated at every 10 second interval for straightening data (n=8) and without trypsin control (n=6). All instantaneous strain values were pooled for initial separation of 20-40 μm and compared (each treatment has more than 500 data points). O' Brien's test: p=0.0001

4.3 Summary and conclusions

Analysis of subcellular strain using docked mitochondria to evaluate cytoskeletal deformations suggests that the cytoskeleton does not contract as a whole, instead, contractility is heterogeneously distributed along the axonal length. Our data suggest that axons have small contractile units (figure 4.9) distributed along the axonal length and their dynamics is invoked upon detachment, during the contraction.

Future studies should focus on spatiotemporal regulation of the organization and activity of the actomyosin system in axons.

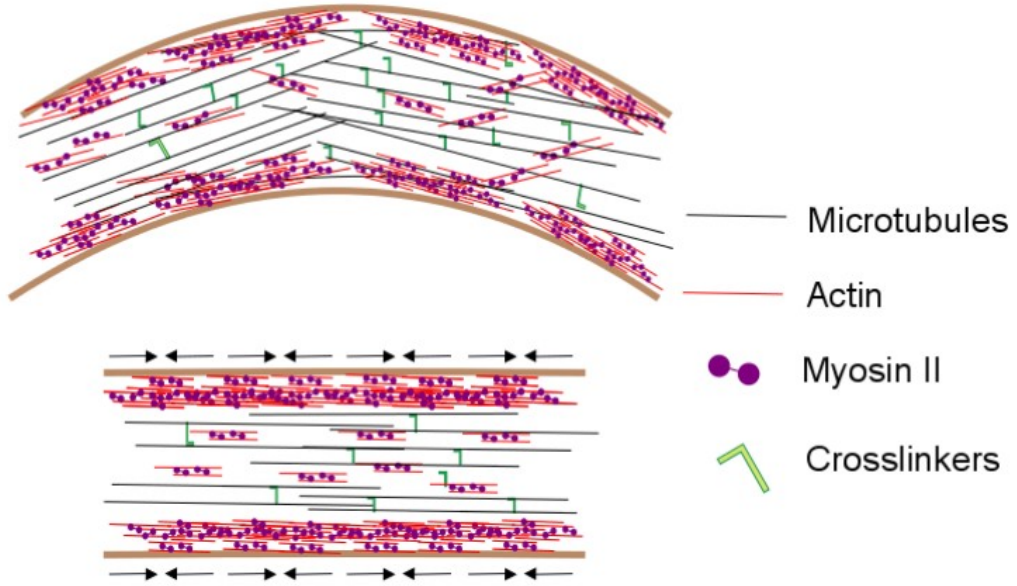

Figure 4.9: Model for cytoskeletal mechanisms mediating axonal straightening. Cortical actomyosin network contracts (as discussed in Chapter 3) upon detachment induced by unknown feedback mechanism leading to the straightening of axons. Microtubules sliding and re-arrangement is likely to be necessary in order to accommodate the contraction. The axon appears to consist of small contractile units whose activity is heterogeneously distributed along its length.

4.4 Materials and methods

4.4.1 Dissection and cultures

As described in chapter 3.

4.4.2 Labeling of mitochondria

Neurons were cultured for 48 hours followed by serum induction as described above. After 30 minutes of serum induction, cells were incubated with 50 nM MitoTracker Green FM (Thermo Scientific) for 2 minutes followed by 2 washes using L15 (Gibco) and minimum 30 minutes incubation in L15 before imaging. Images were acquired at every one second interval in GFP channel using a 40x oil objective on an Olympus IX81 system equipped with a Hamamatsu ORCA-R2 CCD camera.

4.4.3 Mitochondria tracking and analysis

Together with Dr. J. Joseph, Unversity of Hyderabad, India we developed a MATLAB-based code to track labeled mitochondria. Mitochondria were tracked every 10 seconds as this was optimal for differentiating docked and mobile mitochondria. Simple Neurite Tracer plugin was implemented in Fiji to trace the axon and obtain the coordinates along its length at each time point. These images, with their corresponding coordinate files were saved as .jpg and .swc files, respectively. Images and their corresponding .swc files were imported to MATLAB. Coordinates from the .swc files were used to obtain the normal to the path forming the neurite trajectory at each point and the vector of pixels along this normal was determined. The location of the intensity maxima along this vector of pixels at each point was used as the coordinate of the neurite at that point. The vectors of pixels along the normal were also stored for making kymograph plots. The intensity values per pixel along the neurite, using the coordinates obtained by the procedure described above, were used to identify the locations of the mi-

tochondria. To eliminate detection of small spurious local peaks as mitochondria a smoothing filter was used. Intensity series from all images of a neurite were resampled to have the same length as the longest (the first image). These interpolated series were used to reliably identify peaks corresponding to mitochondria that were consistently present throughout the experiment (figure 4.2, figure 4.4). The coordinates of the detected mitochondria were scaled back to get their coordinates on the original scale. These position data were used to calculate local strains.

4.4.4 Data representation and statistics

Intensity based kymographs and strain vs time graphs were generated in Matlab (2014). Strain values obtained from the mito-tracker code were further used for heterogeneity analysis in JMP software (trial version). O' Brien's test was used for this analysis. When variances of two groups are not equal and equality of variances are not satisfied then O'Briein's test is used. O' Brien analysis is suitable for pairwise comparisons of variances and hence also used earlier in the stretch paradigm [37].

5. Preliminary work on axonal tension measurements using an Optical fiber-based force transducer

5.1 Introduction

Neuronal cells have been an attractive model system to understand mechanical properties due to their unique shape and geometry. How thin, axi-symmetric axons utilize underlying cytoskeletal dynamics to maintain their structures is an active area of investigation. In last few decades, the mechanical responses of neurons, including both passive and active, have been studied using various quantitative force measurement techniques. This includes techniques like AFM based measurements on cell bodies [129, 130] and growth cones [131] and neuronal tissues [132, 133], microneedle-based pulling of axons [21, 31], [93]. *In vivo*, in *Drosophila* neurons, active forces were measured using calibrated force sensor [109]. Neurite initiation and elongation have been studied using a magnetic bead coated with the antibody that elicits neurite initiation in presence of magnetic field [87].

Microneedle based pulling is the most extensively used tool to study axonal mechanics including viscoelastic properties of axons [78], axonal initiation, growth [21, 31]. So far, the field has been relying on the microneedle technique (with few exceptions) to understand the mechanical responses of axons and role of underlying cytoskeletal dynamics [84, 113]. But there are certain limitations of this technique which need to be considered. Application of controlled force or strain is not possible using microneedles. Most of these studies do not talk about noise in the system which may affect the nature of responses. It is important to have more precise approaches than microneedle to understand the robustness of results documented so far for neurons and in general to study cell mechanics.

In last two chapters, we discussed the actomyosin dependent axonal contraction as a potential mechanism of tension regulation and this needs to be confirmed with direct and quantitative force measurements. With this motivation, we attemted to use an Optical fiber-based force transducer developed in the laboratory of our collaborator, Dr. Pramod Pullarkat (RRI, Bangalore, India). [134]. This setup (figure 5.1) has been recently modified to allow measurement of axonal mechanical response by applying controlled deformations (constant strain). In this chapter, our early attempts to characterize the set up to study active responses of axons will be discussed. In the future, this set up will allow us to understand mechanisms of axonal contraction (discussed in last two chapters), in great quantitative details.

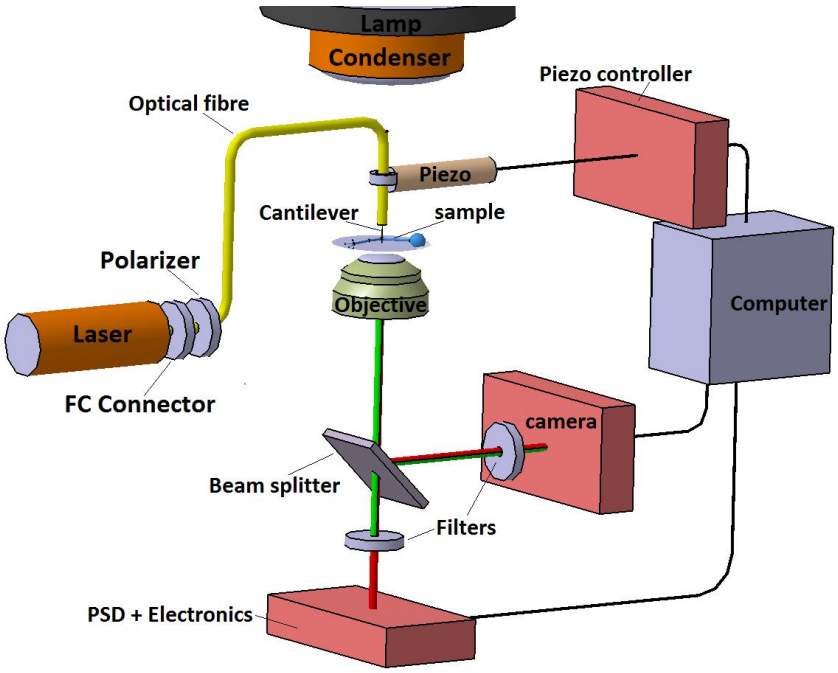

Figure 5.1: Optical fiber-based force transducer. An etched optical fiber is used to apply stretch on an axon. The rigid end of the cantilever is controlled using a piezo. Movement of the piezo is programmed through the computer. An etched optical fiber connected to a laser source. Light coming through the optical fiber is tracked using a position sensitive detector and a camera (Adapted from [134])

5.2 Results and discussion

Slackening experiments using a microneedle suggested that axons can regulate their rest tension [21]. Later, motor based active contraction of axons was proposed in PC12 cells [78]. Our trypsin-mediated de-adhesion and straightening experiments suggest an active, actomyosin dependent contraction as a potential mechanism to regulate the rest tension. In order to study active contraction and

axonal tension generation quantitatively, we used the optical fiber-based force transducer. Since this involves measurements lasting several minutes, as a first step, we characterized drift in the system.

5.2.1 Design of the stage incubator

In order to study active responses, a stage incubator was fabricated (figure 5.2, figure 5.3) to maintain $37\,^{\circ}\mathrm{C}$ throughout the force measurements. There are two heating coils one in the base and one in the lid. Voltage set for the base coil and for the lid was 12V. A resistor of $18\,\Omega$ was attached in series in the base coil. This is to keep the lid temperature slightly higher than base in order to suppress convection since there could be some heat loss from the window which was made to insert the cantilever.

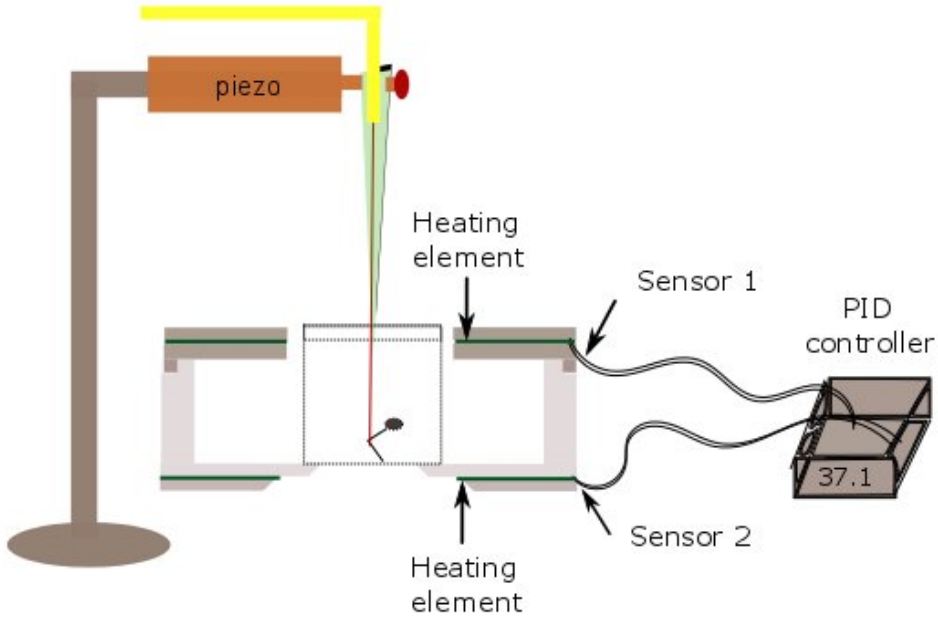

Figure 5.2: Design of the stage incubator.

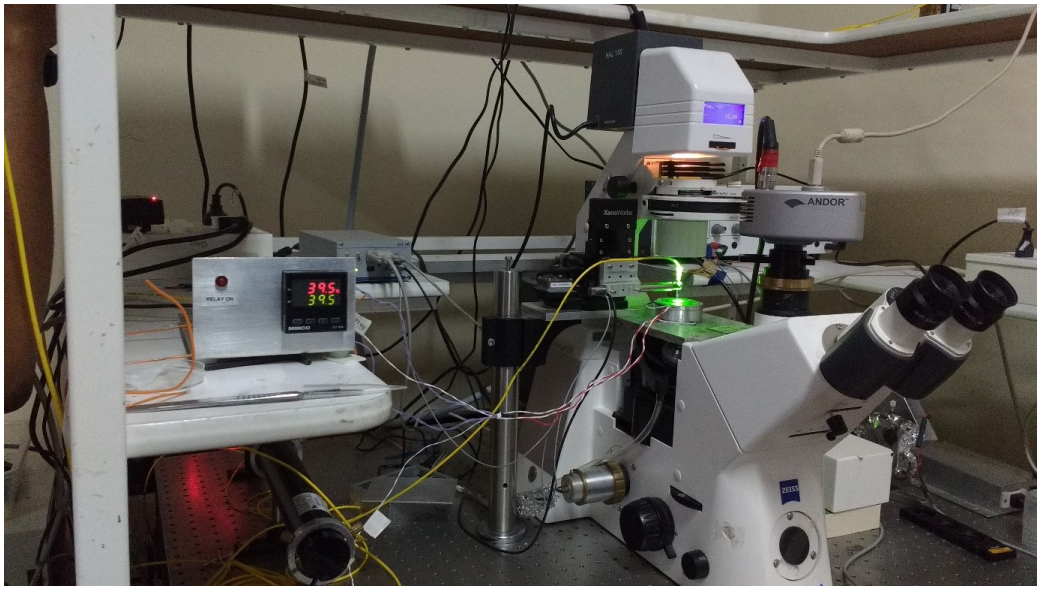

Figure 5.3: Optical fiber force measurement set up with the stage incubator.

5.2.2 Calibration of the temperature sensors and characterization of thermal drift

Platinum resistance sensors (Pt100) were kept in the hot air oven at varying temperature, ranging from 40 to 70 degrees and also at 4 degrees in the refrigerator. The exact temperature was measured using a thermometer (with 0.1-degree accuracy) and the corresponding resistance was measured using a multimeter. Resistance values obtained from multimeter vs temperature shows a linear plot (figure 5.4, figure 5.5). After setting up of temperature controller and checking its stability, convection was checked by putting chalk dust particles in the medium and movement of these particles were tracked using the microscope. Only Brownian motion without any appreciable drift was detected.

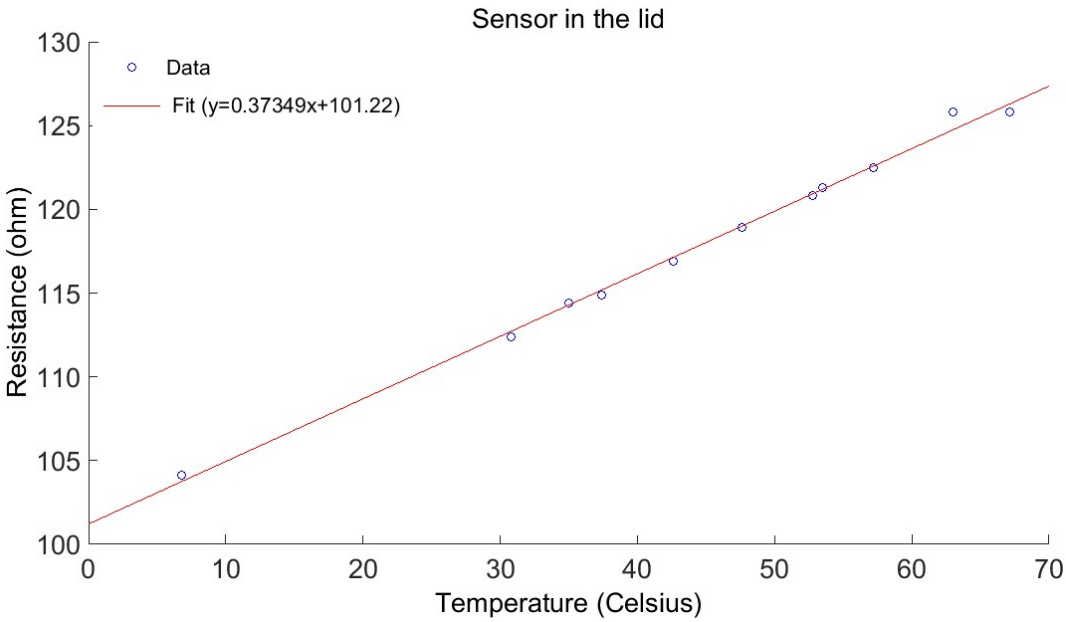

Figure 5.4: Calibration of Pt100 temperature sensors.

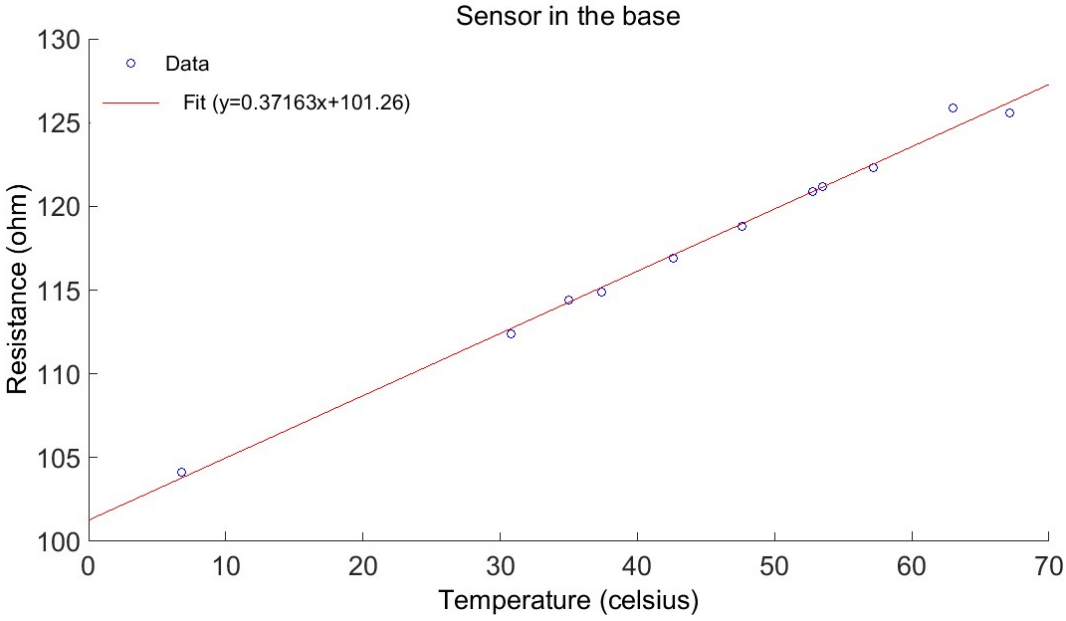

Figure 5.5: Calibration of Pt100 temperature sensors.

5.2.3 Characterization of the mechanical drift

To understand the mechanical drift in the system, a rigid cantilever was used at room temperature. Long-term drift of 1 μm was observed in 20 to 30 minutes. Also, short-term drift of 20 to 100 seconds was noticed. The region marked in red in (figure 5.6) shows short-term drift. Similar drift pattern was observed at 37 °C.

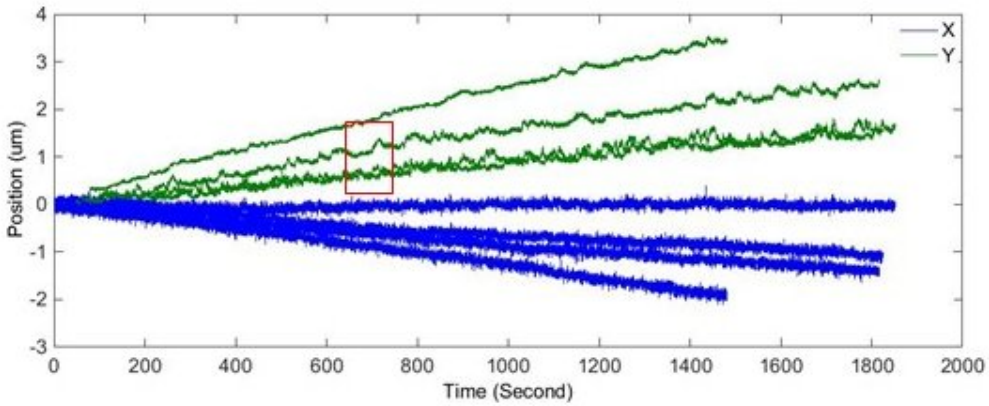

Figure 5.6: The mechanical drift. Change in position of the stiff cantilever at room temperature. Short-term drift happens at the time scale of 20-100 seconds as shown in a red box.

Since the pattern of the drift is similar at room temperature and 37 °C, it is likely to be mechanical in origin. Based on these observations we decided to systematically evaluate contribution of each mechnical component causing the drift. Rigid fiber at room temperature was used for these experiments and multiple runs were done for each test.

Mechanical drift check by systematically changing each component:

Table 5.1. Drift characterization

Tests	Results
1. Switching of the piezo.	Piezo movement causes the drift and switching it off reduces it but not always. There is no pattern to this.
2. Use of the short needle.	No change in the drift pattern.
3. Mounting of cantilever without the piezo, on the aluminum block.	The direction of the drift changes, magnitude remains the same.
4. Laser source was changed to access whether the drift is due to intensity fluctuations.	No change in the drift pattern.
5. Switching of the micromanipulator.	No change in drift pattern.
6. Tracking of the intensity spot on the Camera and PSD at the same time.	This is to check the detection accuracy. The camera and PSD tracking show similar patterns suggesting the accurate detection.

There was no detectable source of the drift. In the future, it is important to estimate noise everytime long term force measurements are done.

5.2.4 Axon pulling experiments

Since there was no detectable source of the drift, we decided to check noise everytime we do force measurements on axons. Axonal pulling was carried out using soft cantilever with the stiffness range 0.00026 N/m to 0.002 N/m. Using a constant extension mode, axons were displaced by 5 microns then the position of the

cantilever was recorded (figure 5.7). Axons occasionally show an initial viscoelastic response followed by an increase in force. The initial viscoelastic response is consistent with the force measurements at 25 degree, this is possibly due to the dissipation of the forces caused by crosslinker detachment (P.P. lab, unpublished work). In few cases, where we could do force measurements successfully (n=5), we occassionaly saw an increase in tension (about 1 nN) after initial viscoelastic relaxation. Reverse steps were given to the piezo (e.g. from 15 μm extension to 10 μm, as shown in figure 5.8.A and B) to assess the force response. In the reverse pull, increase in force could be due to the sudden release of tension in axons (figure 5.8 A). This data needs to be confirmed further with more numbers to understand the transition from passive to active behavior and axonal contraction and tension build up in a detailed quantitative manner.

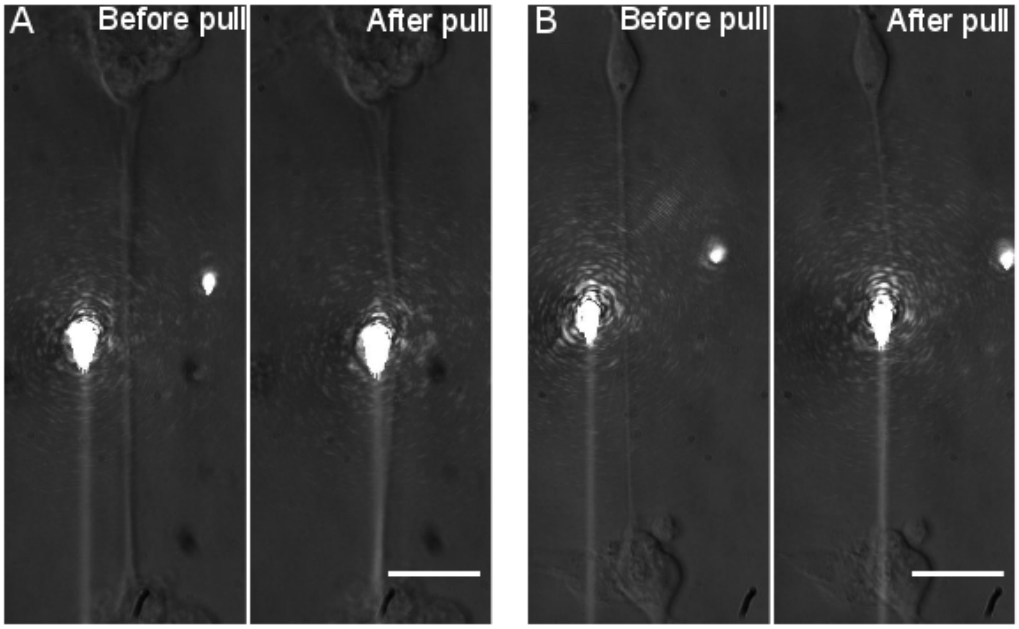

Figure 5.7: Axon pulling experiments. A and B are two different examples of axon pulling experiments. The bright spot is the laser light exiting the optical fiber cantilever. Stiffness of the cantilever: 0.002 N/m. Scale bar: 5 μm.

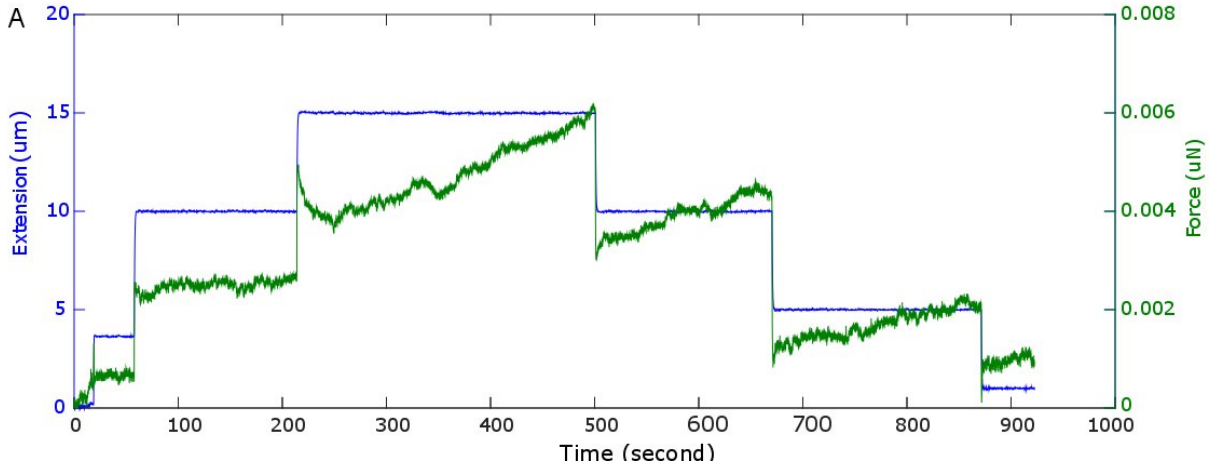

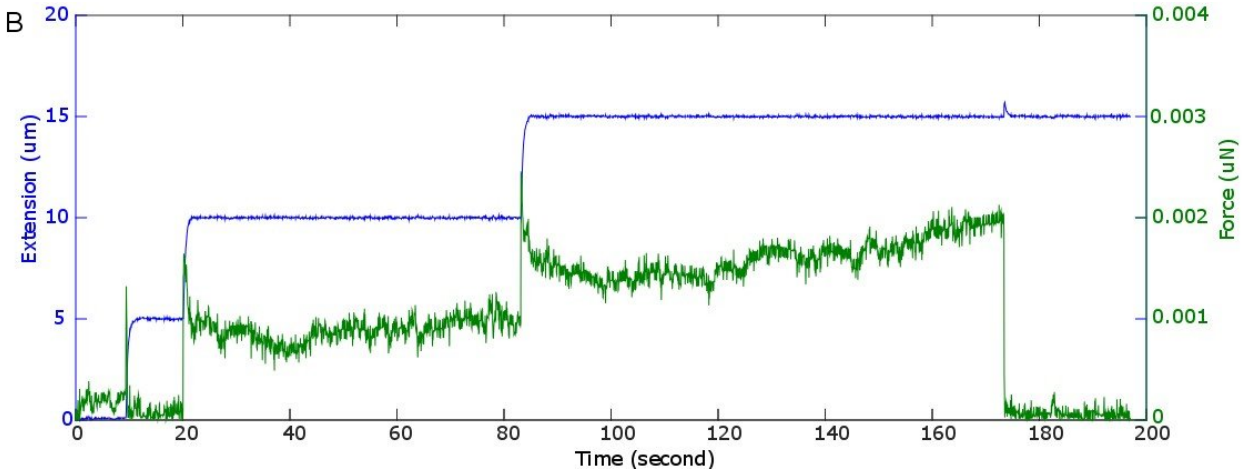

Figure 5.8: Step pulls of axons using a constant extension mode. A. Occasionally the initial viscoelastic force relaxation is followed by an increase in tension. B. Axon loses contact with the cantilever and hence force drops to 0 suggesting that increase in force is indeed coming from the axon and not the drift. (Data for the same axons shown in (figure 5.7))

5.3 Summary and conclusions

1. Drift in the system is not of thermal origin but rather mechanical.

2. We checked all mechanical components including piezo, laser, cantilever holder etc. but we don't see a reduction in the drift with any of these consistently.

3. We also ruled out thermal drift by checking the temperature stability of incubator and by checking convection.

4. We ruled out that something is happening at the level of detection by checking on camera and PSD at the same time.

Based on these studies, we considered the drift as a limitation of the setup. In order

to overcome the drift problem, we decided to use extremely soft cantilever (since drift is mechanical, it is assumed that use of soft cantilever will increase the force signal without changing the overall drift). In order to distinguish between drift and actual data, we quantified the drift every time we performed force measurements on neurons.

5. In a few successful trials, we saw an increase in force but this a preliminary data and begs more confirmatory experiments.

In earlier chapters, the axonal contraction was studied using axonal strains. The pulling device is a more sensitive and a complementary approach to the earlier studies. Though axonal pulling using an optical fiber is again a localized perturbation similar to ablation and microneedle experiments, it is likely to provide quantitative data that will be central to understanding the finer details of mechanisms underlying axonal contraction.

In the future, optical fiber based force transducer will allow us to do mechanical perturbations using controlled force or controlled strain modes and simultaneous observation of detailed microscopic dynamics along thin axons which are not possible with the conventional mechanical perturbations.

5.4 Materials and methods

5.4.1 Cantilever preparation

The optic fiber comes with the two layers of plastic sheaths. An outer layer is removed by a scalpel. Fiber is passed through a needle with the piezo holder in a way that required length of the cantilever is coming out from the distal tip of the needle. Next, second plastic layer was removed by exposing it to flame so that

glass fiber is exposed. The base of the cantilever with both plastic sheets intact was packed with aluminum foil in the needle's part meant to fit a syringe. The needle was coated with a nail paint properly then dipped in Hydrofluoric Acid (HF, Merck, India) for one hour with stirring to achieve 9-10 μm diameter. The diameter was checked under the microscope before use. Before etching, the fiber diameter is originally 120 microns. Length of the fiber ranges from 6-7mm.

5.4.2 Dissection and culture

DRGs were cultured using the protocol mentioned earlier, in chapter 3, using the medium containing 0.6 mg/ml Methocel (Colorcon), 10% FBS (Gibco) and 6 mg/ml D-glucose (Sigma), 20 ng/ml NGF (Invitrogen) and PSG antibiotic (Invitrogen) at 1X concentration.

To avoid the convection and drift, cells were cultured in glass rings of around 1 cm outer diameter and 1 cm height so that the cantilever is completely immersed in the medium.

5.4.3 Axonal pulling experiments

The medium was replaced with L15 media without Methocel followed by 30 minutes incubation in the stage incubator. An etched optical fiber is mounted in a way that it is dipped in the medium and dish was covered using a split acrylic disc in a way that only 1 mm hole is open from where cantilever passes through. Then axon is focused and aligned vertically by moving the incubator. Axons were pulled by using a step pull protocol in which 5 μm steps were given to the piezo and position of the cantilever was recorded on the PSD. The experiments were done in constant extension mode.

5.4.4 Analysis

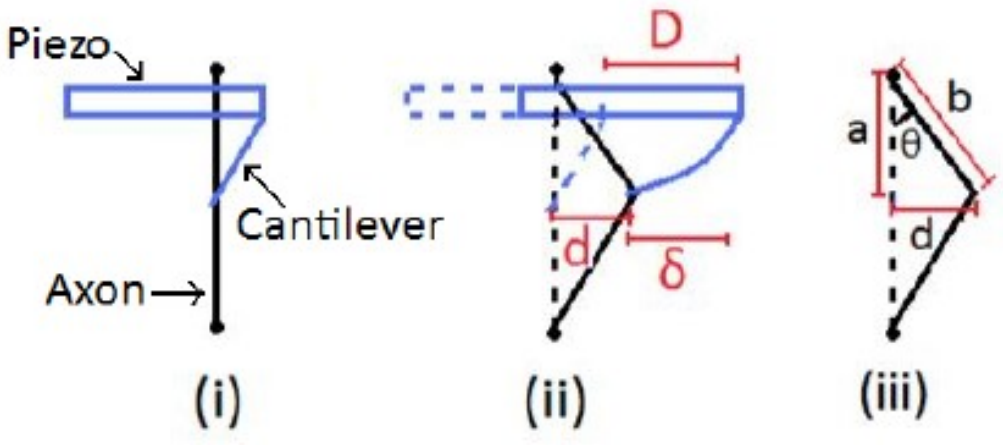

Figure 5.9: Schematic of force measurements. Piezo is moved by distance D which leads to extension of axon by the cantilever attached to it, by the distance d (Adapted from [135])

The defection of the cantilever is obtained as follows:

$$\delta = D - d$$

Using Hookes law,

$$Fc = Kc \times \delta$$

Kc is the stiffness of the cantilever and is calculated based on its length and diameter.

$$Kc = 8.5 \times 10^{-5}(d^4/l^3)$$

(Please refer to the [134] for the details of the calibration)

6. Summary and future directions

Mechanical forces influence various aspects of neuronal functions and development due to the unique shape and mechanical properties of neurons. Cytoskeletal driven forces generated intracellularly can regulate neuronal shape and motility. In this thesis, we have discussed two different problems pertaining to cytoskeletal functions in the regulation of mechanical forces in neurons:

6.1 Fmn2 mediated regulation of traction forces in neuronal growth cones.
6.2 Cytoskeletal mechanisms of axonal contractility.

6.1 Fmn2 mediated regulation of traction forces in neuronal growth cones

In this study, we have shown that Fmn2 is involved in regulating filopodial traction dynamics and growth cone traction force transmission. We propose Fmn2 as a potential regulator of clutch and transmission of forces.
To test, how Fmn2 regulates clutch engagement; dynamics of focal contact upon Fmn2 knockdown can be studied. Dynamics of focal contacts can be studied using photoactivation of photobleaching techniques.

To address Fmn2-mediated clutch regulation, the intra-molecular tension of component proteins of adhesion sites can be measured by using recently developed tension sensors like that for talin [136]. Fmn2-dependent actin organization can be studied using transmission electron microscopy studies. This will be a direct evidence for defects in actin organization upon Fmn2 knockdown and hence will provide insight into mechanisms.

Fmn2 has been implicated in axonal guidance including, the mid-line crossing of spinal commissural neurons. It will be interesting to explore the biophysical mechanisms underlying this. It has been shown earlier that netrin coated beads can reorient the growth cone and modulate the traction [137]. It will be of interest to see if Fmn2 regulates this; whether Fmn2 is involved in a cue- dependent force transmission.

Using general inhibitor of formins, SMIFH2, we would like to see if the FH2 domain is involved in this regulation and whether this is generic a function of formins. Interestingly, optical trap-based measurements in HeLa cells suggests that formins are involved in regulating filopodial pulling forces [32].

How filopodia pull is an intriguing question due to their unique actin organization. How parallel actin bundles show a contractile response is still not clear. Though helical buckling [54] and coupling with the contractile forces generated in the central region [30] have been proposed; mechanistic details are still missing. Fmn2 perturbation may affect actin organization selectively without affecting motor activity and may be useful to understand filopodial force generation mechanisms.

In this thesis, we have attempted to understand biophysical mechanisms of force transmission and growth cone motility in the context of Fmn2. In the future, these assays will allow us to study growth cone mechanics in greater details.

6.2 Cytoskeletal mechanism of axonal contractility

We developed a simple cell biological assay for axonal contraction and showed that axonal contraction is actomyosin dependent. Axons have intrinsic, spontaneous contractile activity and it is limited by the rate of de-adhesion. Microtubule depolymerization did not prevent axonal contraction, however, affected the rate.

Using docked mitochondria as a marker for bulk cytoskeleton dynamics, we show that underlying cytoskeletal contracts heterogeneously with the contraction-extension cycles. This heterogeneity may offer plasticity to axonal cytoskeleton to regulate various functions. In the future, Myosin-II and actin can be imaged to confirm mitochondria strain dynamics.

So far, in the trypsin-mediated de-adhesion assay, we have been relaying on curved axonal trajectories on the poly-L-lysine substrate in absence of serum. However, this approach cannot be scaled up and is low throughput. In the future, it may be possible to grow neurons on curved micropatterns to ensure more curved neurons at the same time. As a proof of principle, we have data where axons constrained to follow curved trajectories spontaneously detach and straighten (figure 6.1). This preliminary data suggests the feasibility of the approach. In these experiments, the curvature and time of incubation to get enough number of curved axons will have to be optimized. This assay will allow us to evaluate spontaneous detachment due to the contraction, as shown in (figure 6.1) and can also be used in combination with trypsin-mediated de-adhesion of axons with predefined curvature.

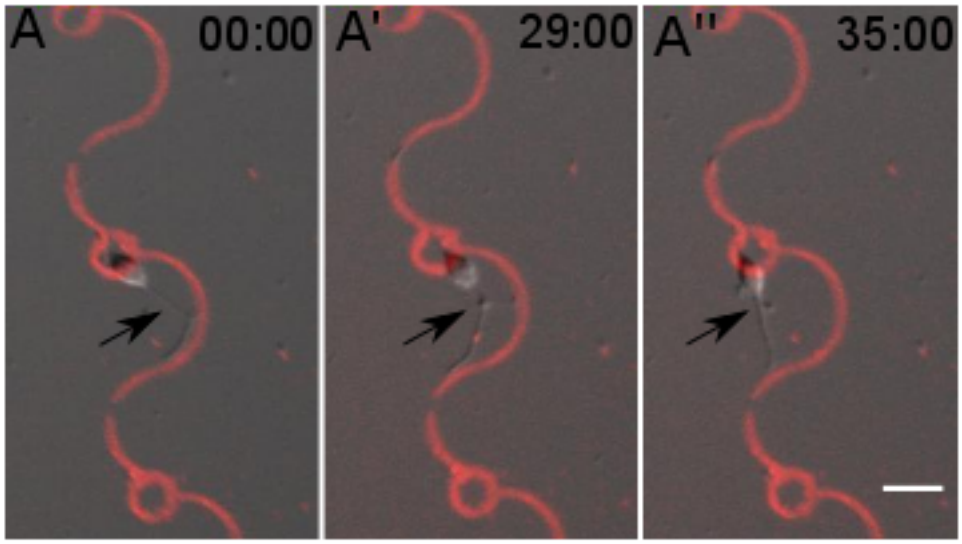

Figure 6.1: Example of an axon (arrow) detaching from a curved extracellular matrix pattern and straightening. (A-A"). In time, the axon reduces the curvature and becomes straight. Scale bar: 25 μm.

Interestingly, straight axons often show a pulsatile contractile response (data not shown). Straight axons with their growth cones immobilized on discrete adhesive patterns will allow evaluation of contraction when growth cones pause. In combination with labeled mitochondria, it may be possible to understand contraction of straight axons; a baseline contractile activity.

Straightening on the soft substrates with beads embedded in the gel will allow us to measure forces involved in axonal de-adhesion and straightening; however, the stiffness of the gel has to be standardized to appropriately evaluate these responses.

How the actomyosin machinery drives the axonal contraction is a really fascinating question. Cortical F-actin network might play a pivotal role in driving con-

traction. It will be interesting to study if spectrin dependent actin rings are present at this stages of neurons and whether spectrin dependent actin organization drives axonal contraction. This will confirm whether the circumferential contraction is coupled to the axial contraction.

Axonal rest tension and growth cone traction are interdependent. Recent work suggests that unbalanced traction decides axonal rest tension [138]. We have developed assays to look at axonal contractility and growth cone traction separately. In the future, combination of these assays will allow us to explore the neuronal force balance and its functional implications.

Publications

Sahasrabudhe, A., Ghate, K.,**Mutalik, S.**, Jacob, A. and Ghose, A. (2016) Formin-2 regulates stabilization of filopodial tip adhesions in growth cones and affects neuronal outgrowth and pathfinding in vivo. Development, 143, 449-460. http://dev.biologists.org/content/143/3/449.long

Mutalik, SP., Joseph, J., Pullarkat, PA. and Ghose, A. (2017) Cytoskeletal mechanisms of axonal contractility. bioRxiv, doi: 10.1101/227777. (Under review). https://www.biorxiv.org/content/biorxiv/early/2017/12/10/227777.full.pdf

Bibliography

[1] Andrea B Huber, Alex L Kolodkin, David D Ginty, and Jean-François Cloutier. Signaling at the growth cone: ligand-receptor complexes and the control of axon growth and guidance. *Annual review of neuroscience*, 26(1):509–563, 2003.

[2] Erik W Dent and Frank B Gertler. Cytoskeletal dynamics and transport in growth cone motility and axon guidance. *Neuron*, 40(2):209–227, 2003.

[3] Laura Anne Lowery and David Van Vactor. The trip of the tip: understanding the growth cone machinery. *Nature reviews Molecular cell biology*, 10(5):332, 2009.

[4] Timothy M Gomez and Paul C Letourneau. Actin dynamics in growth cone motility and navigation. *Journal of neurochemistry*, 129(2):221–234, 2014.

[5] Eric A Vitriol and James Q Zheng. Growth cone travel in space and time: the cellular ensemble of cytoskeleton, adhesion, and membrane. *Neuron*, 73(6):1068–1081, 2012.

[6] Paul Forscher and Stephen J Smith. Actions of cytochalasins on the organization of actin filaments and microtubules in a neuronal growth cone. *The Journal of cell biology*, 107(4):1505–1516, 1988.

[7] L Marsh and Paul C Letourneau. Growth of neurites without filopodial or lamellipodial activity in the presence of cytochalasin B. *The Journal of cell biology*, 99(6):2041–2047, 1984.

[8] CG Dos Remedios, D Chhabra, M Kekic, IV Dedova, M Tsubakihara, DA Berry, and NJ Nosworthy. Actin binding proteins: regulation of cytoskeletal microfilaments. *Physiological reviews*, 83(2):433–473, 2003.

[9] Sari Tojkander, Gergana Gateva, Amjad Husain, Ramaswamy Krishnan, and Pekka Lappalainen. Generation of contractile actomyosin bundles depends on mechanosensitive actin filament assembly and disassembly. *Elife*, 4, 2015.

[10] Hanshuang Shao, James H-C Wang, Martin R Pollak, and Alan Wells. α-actinin-4 is essential for maintaining the spreading, motility and contractility of fibroblasts. *Public Library of Science one*, 5(11):e13921, 2010.

[11] Mikheil Azatov, Silvia M Goicoechea, Carol A Otey, and Arpita Upadhyaya. The actin crosslinking protein palladin modulates force generation and mechanosensitivity of tumor associated fibroblasts. *Scientific reports*, 6:28805, 2016.

[12] Patrick W Oakes, Yvonne Beckham, Jonathan Stricker, and Margaret L Gardel. Tension is required but not sufficient for focal adhesion maturation without a stress fiber template. *J Cell Biol*, 196(3):363–374, 2012.

[13] Thomas Iskratsch, Cheng-Han Yu, Anurag Mathur, Shuaimin Liu, Virginie Stévenin, Joseph Dwyer, James Hone, Elisabeth Ehler, and Michael Sheetz. FHOD1 is needed for directed forces and adhesion maturation during cell spreading and migration. *Developmental cell*, 27(5):545–559, 2013.

[14] Melissa A Chesarone and Bruce L Goode. Actin nucleation and elongation factors: mechanisms and interplay. *Current opinion in cell biology*, 21(1):28–37, 2009.

[15] J Block, TEB Stradal, J Hänisch, R Geffers, SA Köstler, E Urban, JV Small, K Rottner, and J Faix. Filopodia formation induced by active mDia2/Drf3. *Journal of microscopy*, 231(3):506–517, 2008.

[16] Wah Ing Goh and Sohail Ahmed. mDia1-3 in mammalian filopodia. *Communicative & integrative biology*, 5(4):340–344, 2012.

[17] Richa Jaiswal, Dennis Breitsprecher, Agnieszka Collins, Ivan R Corrêa, Ming-Qun Xu, and Bruce L Goode. The formin Daam1 and fascin directly collaborate to promote filopodia formation. *Current Biology*, 23(14):1373–1379, 2013.

[18] Abhishek Sahasrabudhe, Ketakee Ghate, Sampada Mutalik, Ajesh Jacob, and Aurnab Ghose. Formin 2 regulates the stabilization of filopodial tip adhesions in growth cones and affects neuronal outgrowth and pathfinding in vivo. *Development*, 143(3):449–460, 2016.

[19] Ross G Harrison. The croonian lecture on the origin and development of the nervous system studied by the methods of experimental embryology.

In *Proc. R. Soc. Lond. B*, volume 118, pages 155–196. The Royal Society, 1935.

[20] Paul Weiss. Nerve patterns: the mechanics of nerve growth. In *Dynamics of Development: Experiments and Inferences*, pages 445–485. Elsevier, 1968.

[21] Timothy J Dennerll, Phillip Lamoureux, Robert E Buxbaum, and Steven R Heidemann. The cytomechanics of axonal elongation and retraction. *The journal of cell biology*, 109(6):3073–3083, 1989.

[22] Scott Siechen, Shengyuan Yang, Akira Chiba, and Taher Saif. Mechanical tension contributes to clustering of neurotransmitter vesicles at presynaptic terminals. *Proceedings of the National Academy of Sciences*, 106(31):12611–12616, 2009.

[23] Rajendrani Mukhopadhyay, Sanjay Kumar, and Jan H Hoh. Molecular mechanisms for organizing the neuronal cytoskeleton. *Bioessays*, 26(9):1017–1025, 2004.

[24] Nobutaka Hirokawa. Cross-linker system between neurofilaments, microtubules and membranous organelles in frog axons revealed by the quick-freeze, deep-etching method. *The Journal of cell biology*, 94(1):129–142, 1982.

[25] Josta T Kevenaar and Casper C Hoogenraad. The axonal cytoskeleton: from organization to function. *Frontiers in molecular neuroscience*, 8:44, 2015.

[26] Ronald D Vale. The molecular motor toolbox for intracellular transport. *Cell*, 112(4):467–480, 2003.

[27] Ke Xu, Guisheng Zhong, and Xiaowei Zhuang. Actin, spectrin, and associated proteins form a periodic cytoskeletal structure in axons. *Science*, 339(6118):452–456, 2013.

[28] Archan Ganguly, Yong Tang, Lina Wang, Kelsey Ladt, Jonathan Loi, Bénédicte Dargent, Christophe Leterrier, and Subhojit Roy. A dynamic formin-dependent deep f-actin network in axons. *J Cell Biol*, pages jcb–201506110, 2015.

[29] Daniel M Suter and Kyle E Miller. The emerging role of forces in axonal elongation. *Progress in neurobiology*, 94(2):91–101, 2011.

[30] Thomas Bornschlögl. How filopodia pull: what we know about the mechanics and dynamics of filopodia. *Cytoskeleton*, 70(10):590–603, 2013.

[31] Jing Zheng, Phillip Lamoureux, Vivian Santiago, Timothy Dennerll, Robert E Buxbaum, and Steven R Heidemann. Tensile regulation of axonal elongation and initiation. *Journal of Neuroscience*, 11(4):1117–1125, 1991.

[32] Naila O Alieva, Artem K Efremov, Shiqiong Hu, Dongmyung Oh, Zhongwen Chen, Meenubharathi Natarajan, Hui Ting Ong, Antoine Jegou, Guillaume Romet-Lemonne, Jay T Groves, et al. Force dependence of filopodia adhesion: involvement of myosin II and formins. *bioRxiv*, page 195420, 2017.

[33] Qian Cai and Zu-Hang Sheng. Mitochondrial transport and docking in axons. *Experimental neurology*, 218(2):257–267, 2009.

[34] Jian-Sheng Kang, Jin-Hua Tian, Ping-Yue Pan, Philip Zald, Cuiling Li, Chuxia Deng, and Zu-Hang Sheng. Docking of axonal mitochondria by syntaphilin controls their mobility and affects short-term facilitation. *Cell*, 132(1):137–148, 2008.

[35] Oliver I Wagner, Jonathan Lifshitz, Paul A Janmey, M Linden, TK McIntosh, and J-F Leterrier. Mechanisms of mitochondria-neurofilament interactions. *Journal of Neuroscience*, 23(27):9046–9058, 2003.

[36] Istvan R Boldogh and Liza A Pon. Interactions of mitochondria with the actin cytoskeleton. *Biochimica et Biophysica Acta (BBA)-Molecular Cell Research*, 1763(5):450–462, 2006.

[37] Joshua Chetta, Cecilia Kye, and Sameer B Shah. Cytoskeletal dynamics in response to tensile loading of mammalian axons. *Cytoskeleton*, 67(10):650–665, 2010.

[38] Thomas D Pollard and Gary G Borisy. Cellular motility driven by assembly and disassembly of actin filaments. *Cell*, 112(4):453–465, 2003.

[39] David Bentley and Alma Toroian-Raymond. Disoriented pathfinding by pioneer neurone growth cones deprived of filopodia by cytochalasin treatment. *Nature*, 323(6090):712, 1986.

[40] Nelson A Medeiros, Dylan T Burnette, and Paul Forscher. Myosin II functions in actin-bundle turnover in neuronal growth cones. *Nature cell biology*, 8(3):216, 2006.

[41] Chi-Hung Lin and Paul Forscher. Growth cone advance is inversely proportional to retrograde F-actin flow. *Neuron*, 14(4):763–771, 1995.

[42] Paul C Bridgman, Sonya Dave, Clara F Asnes, Antonella N Tullio, and Robert S Adelstein. Myosin IIB is required for growth cone motility. *Journal of Neuroscience*, 21(16):6159–6169, 2001.

[43] Aneil Mallavarapu and Tim Mitchison. Regulated actin cytoskeleton assembly at filopodium tips controls their extension and retraction. *The Journal of cell biology*, 146(5):1097–1106, 1999.

[44] Jonathan P Myers, Miguel Santiago-Medina, and Timothy M Gomez. Regulation of axonal outgrowth and pathfinding by integrin–ECM interactions. *Developmental neurobiology*, 71(11):901–923, 2011.

[45] Margaret L Gardel, Benedikt Sabass, Lin Ji, Gaudenz Danuser, Ulrich S Schwarz, and Clare M Waterman. Traction stress in focal adhesions correlates biphasically with actin retrograde flow speed. *J cell Biol*, 183(6):999–1005, 2008.

[46] Benedikt Sabass, Margaret L Gardel, Clare M Waterman, and Ulrich S Schwarz. High resolution traction force microscopy based on experimental and computational advances. *Biophysical journal*, 94(1):207–220, 2008.

[47] Alberto Elosegui-Artola, Roger Oria, Yunfeng Chen, Anita Kosmalska, Carlos Pérez-González, Natalia Castro, Cheng Zhu, Xavier Trepat, and Pere Roca-Cusachs. Mechanical regulation of a molecular clutch defines force transmission and transduction in response to matrix rigidity. *Nature cell biology*, 18(5):540, 2016.

[48] Grégory Giannone, René-Marc Mège, and Olivier Thoumine. Multi-level molecular clutches in motile cell processes. *Trends in cell biology*, 19(9):475–486, 2009.

[49] Lucie Bard, Cécile Boscher, Mireille Lambert, René-Marc Mège, Daniel Choquet, and Olivier Thoumine. A molecular clutch between the actin flow and N-cadherin adhesions drives growth cone migration. *Journal of Neuroscience*, 28(23):5879–5890, 2008.

[50] Clarence E Chan and David J Odde. Traction dynamics of filopodia on compliant substrates. *Science*, 322(5908):1687–1691, 2008.

[51] Lindsay B Case and Clare M Waterman. Integration of actin dynamics and cell adhesion by a three-dimensional, mechanosensitive molecular clutch. *Nature cell biology*, 17(8):955, 2015.

[52] Steven R Heidemann, Phillip Lamoureux, and Robert E Buxbaum. Growth cone behavior and production of traction force. *The Journal of cell biology*, 111(5):1949–1957, 1990.

[53] Thomas Bornschlögl, Stéphane Romero, Christian L Vestergaard, Jean-François Joanny, Guy Tran Van Nhieu, and Patricia Bassereau. Filopodial retraction force is generated by cortical actin dynamics and controlled by reversible tethering at the tip. *Proceedings of the National Academy of Sciences*, 110(47):18928–18933, 2013.

[54] Natascha Leijnse, Lene B Oddershede, and Poul M Bendix. Helical buckling of actin inside filopodia generates traction. *Proceedings of the National Academy of Sciences*, 112(1):136–141, 2015.

[55] Simon W Moore, Xian Zhang, Christopher D Lynch, and Michael P Sheetz. Netrin-1 attracts axons through FAK-dependent mechanotransduction. *Journal of Neuroscience*, 32(34):11574–11585, 2012.

[56] Stephen G Turney, Mostafa Ahmed, Indra Chandrasekar, Robert B Wysolmerski, Zoe M Goeckeler, Robert M Rioux, George M Whitesides, and Paul C Bridgman. Nerve growth factor stimulates axon outgrowth through negative regulation of growth cone actomyosin restraint of microtubule advance. *Molecular biology of the cell*, 27(3):500–517, 2016.

[57] Jan Faix and Robert Grosse. Staying in shape with formins. *Developmental cell*, 10(6):693–706, 2006.

[58] Naoki Watanabe, Takayuki Kato, Akiko Fujita, Toshimasa Ishizaki, and Shuh Narumiya. Cooperation between mDia1 and ROCK in Rho-induced actin reorganization. *Nature cell biology*, 1(3):136, 1999.

[59] Diego H Castrillon and Steven A Wasserman. Diaphanous is required for cytokinesis in drosophila and shares domains of similarity with the products of the limb deformity gene. *Development*, 120(12):3367–3377, 1994.

[60] Julien Dumont, Karine Million, Kelsey Sunderland, Pascale Rassinier, Hyunjung Lim, Benjamin Leader, and Marie-Hélène Verlhac. Formin-2 is required for spindle migration and for the late steps of cytokinesis in mouse oocytes. *Developmental biology*, 301(1):254–265, 2007.

[61] Benjamin Leader, Hyunjung Lim, Mary Jo Carabatsos, Anne Harrington, Jeffrey Ecsedy, David Pellman, Richard Maas, and Philip Leder. Formin-2,

polyploidy, hypofertility and positioning of the meiotic spindle in mouse oocytes. *Nature cell biology*, 4(12):921, 2002.

[62] Yoshiki Arakawa, Haruhiko Bito, Tomoyuki Furuyashiki, Takahiro Tsuji, Sayaka Takemoto-Kimura, Kazuhiro Kimura, Kazuhiko Nozaki, Nobuo Hashimoto, and Shuh Narumiya. Control of axon elongation via an SDF-1α/Rho/mDia pathway in cultured cerebellar granule neurons. *J Cell Biol*, 161(2):381–391, 2003.

[63] Steven Emmons, Huy Phan, John Calley, Wenliang Chen, Brian James, and Lynn Manseau. Cappuccino, a drosophila maternal effect gene required for polarity of the egg and embryo, is related to the vertebrate limb deformity locus. *Genes & development*, 9(20):2482–2494, 1995.

[64] Jennifer Block, Dennis Breitsprecher, Sonja Kühn, Moritz Winterhoff, Frieda Kage, Robert Geffers, Patrick Duwe, Jennifer L Rohn, Buzz Baum, Cord Brakebusch, et al. Fmnl2 drives actin-based protrusion and migration downstream of cdc42. *Current biology*, 22(11):1005–1012, 2012.

[65] Erik W Dent, Adam V Kwiatkowski, Leslie M Mebane, Ulrike Philippar, Melanie Barzik, Douglas A Rubinson, Stephanie Gupton, J Edward Van Veen, Craig Furman, Jiangyang Zhang, et al. Filopodia are required for cortical neurite initiation. *Nature cell biology*, 9(12):1347, 2007.

[66] Benjamin Leader and Philip Leder. Formin-2, a novel formin homology protein of the cappuccino subfamily, is highly expressed in the developing and adult central nervous system. *Mechanisms of development*, 93(1):221–231, 2000.

[67] Rosalind Law, Tracy Dixon-Salazar, Julie Jerber, Na Cai, Ansar A Abbasi, Maha S Zaki, Kirti Mittal, Stacey B Gabriel, Muhammad Arshad Rafiq, Valeed Khan, et al. Biallelic truncating mutations in FMN2, encoding the actin-regulatory protein Formin 2, cause nonsyndromic autosomal-recessive intellectual disability. *The American Journal of Human Genetics*, 95(6):721–728, 2014.

[68] Khyobeni Mozhui, Daniel C Ciobanu, Thomas Schikorski, Xusheng , Lu Lu, and Robert W Williams. Dissection of a qtl hotspot on mouse distal chromosome 1 that modulates neurobehavioral phenotypes and gene expression. *Public Library of Science genetics*, 4(11):e1000260, 2008.

[69] L Ji and G Danuser. Tracking quasi-stationary flow of weak fluorescent signals by adaptive multi-frame correlation. *Journal of microscopy*, 220(3):150–167, 2005.

[70] Yu-Li Wang and Robert J Pelham Jr. Preparation of a flexible, porous polyacrylamide substrate for mechanical studies of cultured cells. In *Methods in enzymology*, volume 298, pages 489–496. 1998.

[71] Justin R Tse and Adam J Engler. Preparation of hydrogel substrates with tunable mechanical properties. *Current protocols in cell biology*, pages 10–16, 2010.

[72] Joanna L MacKay and Sanjay Kumar. Measuring the elastic properties of living cells with atomic force microscopy indentation. In *Cell Imaging Techniques*, pages 313–329. 2012.

[73] James P Butler, Iva Marija Tolic-Nørrelykke, Ben Fabry, and Jeffrey J Fredberg. Traction fields, moments, and strain energy that cells exert on their surroundings. *American Journal of Physiology-Cell Physiology*, 282(3):C595–C605, 2002.

[74] Matthew TK Kirkcaldie and Jessica M Collins. The axon as a physical structure in health and acute trauma. *Journal of chemical neuroanatomy*, 76:9–18, 2016.

[75] Sylvie M De Waegh, Virginia M-Y Lee, and Scott T Brady. Local modulation of neurofilament phosphorylation, axonal caliber, and slow axonal transport by myelinating schwann cells. *Cell*, 68(3):451–463, 1992.

[76] Joseph R Marszalek, Toni L Williamson, Michael K Lee, Zuoshang Xu, Paul N Hoffman, Mark W Becher, Thomas O Crawford, and Don W Cleveland. Neurofilament subunit NF-H modulates axonal diameter by selectively slowing neurofilament transport. *The Journal of cell biology*, 135(3):711–724, 1996.

[77] Jiang He, Ruobo Zhou, Zhuhao Wu, Monica A Carrasco, Peri T Kurshan, Jonathan E Farley, David J Simon, Guiping Wang, Boran Han, Junjie Hao, et al. Prevalent presence of periodic actin–spectrin-based membrane skeleton in a broad range of neuronal cell types and animal species. *Proceedings of the National Academy of Sciences*, 113(21):6029–6034, 2016.

[78] Roberto Bernal, Pramod A Pullarkat, and Francisco Melo. Mechanical properties of axons. *Physical review letters*, 99(1):018301, 2007.

[79] Hui Ouyang, Eric Nauman, and Riyi Shi. Contribution of cytoskeletal elements to the axonal mechanical properties. *Journal of biological engineering*, 7(1):21, 2013.

[80] Brian T Helfand, Melissa G Mendez, Jason Pugh, Claude Delsert, and Robert D Goldman. A role for intermediate filaments in determining and maintaining the shape of nerve cells. *Molecular biology of the cell*, 14(12):5069–5081, 2003.

[81] Nobutaka Hirokawa, Sumio TeradaTakeshi Funakoshi, and Sen Takeda. Slow axonal transport: the subunit transport model. *Trends in cell biology*, 7(10):384–388, 1997.

[82] Anthony Brown. Slow axonal transport: stop and go traffic in the axon. *Nature Reviews Molecular Cell Biology*, 1(2):153, 2000.

[83] Yitao Ma, Dinara Shakiryanova, Irina Vardya, and Sergey V Popov. Quantitative analysis of microtubule transport in growing nerve processes. *Current biology*, 14(8):725–730, 2004.

[84] Douglas H Roossien, Phillip Lamoureux, and Kyle E Miller. Cytoplasmic dynein pushes the cytoskeletal meshwork forward during axonal elongation. *J Cell Sci*, 127(16):3593–3602, 2014.

[85] Christophe Leterrier, Pankaj Dubey, and Subhojit Roy. The nano-architecture of the axonal cytoskeleton. *Nature Reviews Neuroscience*, 18(12):713, 2017.

[86] Philip Lamoureux, Robert E Buxbaum, and Steven R Heidemann. Direct evidence that growth cones pull. *Nature*, 340(6229):159, 1989.

[87] Joseph N Fass and David J Odde. Tensile force-dependent neurite elicitation via anti-β1 integrin antibody-coated magnetic beads. *Biophysical journal*, 85(1):623–636, 2003.

[88] Bo-Ming Chen and Alan D Grinnell. Kinetics, ca2+ dependence, and biophysical properties of integrin-mediated mechanical modulation of transmitter release from frog motor nerve terminals. *Journal of Neuroscience*, 17(3):904–916, 1997.

[89] Anthony Fan, Kevin Ambrose Stebbings, Daniel Adolfo Llano, and Taher Saif. Stretch induced hyperexcitability of mice callosal pathway. *Frontiers in cellular neuroscience*, 9:292, 2015.

[90] Sarit Anava, Alon Greenbaum, Eshel Ben Jacob, Yael Hanein, and Amir Ayali. The regulative role of neurite mechanical tension in network development. *Biophysical journal*, 96(4):1661–1670, 2009.

[91] Daniel Šmít, Coralie Fouquet, Frédéric Pincet, Martin Zapotocky, and Alain Trembleau. Axon tension regulates fasciculation/defasciculation through the control of axon shaft zippering. *eLife*, 6, 2017.

[92] MA Breau, I Bonnet, J Stoufflet, J Xie, S De Castro, and S Schneider-Maunoury. Extrinsic mechanical forces mediate retrograde axon extension in a developing neuronal circuit. *Nature communications*, 8(1):282, 2017.

[93] Dennis Bray. Axonal growth in response to experimentally applied mechanical tension. *Developmental biology*, 102(2):379–389, 1984.

[94] Steven R Heidemann and Robert E Buxbaum. Tension as a regulator and integrator of axonal growth. *Cytoskeleton*, 17(1):6–10, 1990.

[95] Kristian Franze, Jens Gerdelmann, Michael Weick, Timo Betz, Steve Pawlizak, Melike Lakadamyali, Johannes Bayer, Katja Rillich, Michael Gögler, Yun-Bi Lu, et al. Neurite branch retraction is caused by a threshold-dependent mechanical impact. *Biophysical journal*, 97(7):1883–1890, 2009.

[96] Ichiro Abe, Naoyuki Ochiai, Harumitsu Ichimura, Akihito Tsujino, Jia Sun, and Yuki Hara. Internodes can nearly double in length with gradual elongation of the adult rat sciatic nerve. *Journal of orthopaedic research*, 22(3):571–577, 2004.

[97] JR Loverde and BJ Pfister. High magnification imaging of neuronal somata undergoing axon stretch growth in vitro. In *Bioengineering Conference (NEBEC), 2012 38th Annual Northeast*, pages 45–46. IEEE, 2012.

[98] Joseph R Loverde and Bryan J Pfister. Developmental axon stretch stimulates neuron growth while maintaining normal electrical activity, intracellular calcium flux, and somatic morphology. *Frontiers in cellular neuroscience*, 9:308, 2015.

[99] Phillip Lamoureux, Steven R Heidemann, Nathan R Martzke, and Kyle E Miller. Growth and elongation within and along the axon. *Developmental neurobiology*, 70(3):135–149, 2010.

[100] Matthew OToole, Phillip Lamoureux, and Kyle E Miller. A physical model of axonal elongation: force, viscosity, and adhesions govern the mode of outgrowth. *Biophysical journal*, 94(7):2610–2620, 2008.

[101] James M Love, Brian G Bober, Elisabeth Orozco, Amanda T White, Shannon N Bremner, Richard M Lovering, Simon Schenk, and Sameer B Shah. mTOR regulates peripheral nerve response to tensile strain. *Journal of neurophysiology*, 117(5):2075–2084, 2017.

[102] Jianwu Dai and Michael P Sheetz. Mechanical properties of neuronal growth cone membranes studied by tether formation with laser optical tweezers. *Biophysical journal*, 68(3):988–996, 1995.

[103] Steven R Heidemann and Dennis Bray. Tension-driven axon assembly: a possible mechanism. *Frontiers in cellular neuroscience*, 9:316, 2015.

[104] Y Hanein, O Tadmor, S Anava, and A Ayali. Neuronal soma migration is determined by neurite tension. *Neuroscience*, 172:572–579, 2011.

[105] Barry G Condron and Kai Zinn. Regulated neurite tension as a mechanism for determination of neuronal arbor geometries in vivo. *Current biology*, 7(10):813–816, 1997.

[106] Claus C Hilgetag and Helen Barbas. Role of mechanical factors in the morphology of the primate cerebral cortex. *Public Library of Science, Computational Biology*, 2(3):e22, 2006.

[107] David C Van Essen. A tension-based theory of morphogenesis and compact wiring in the central nervous system. *Nature*, 385(6614):313, 1997.

[108] EB George, BF Schneider, RJ Lasek, and MJ Katz. Axonal shortening and the mechanisms of axonal motility. *Cytoskeleton*, 9(1):48–59, 1988.

[109] Jagannathan Rajagopalan, Alireza Tofangchi, and M Taher A Saif. Drosophila neurons actively regulate axonal tension in vivo. *Biophysical journal*, 99(10):3208–3215, 2010.

[110] Harish C Joshi, Dan Chu, Robert E Buxbaum, and Steven R Heidemann. Tension and compression in the cytoskeleton of PC 12 neurites. *The Journal of cell biology*, 101(3):697–705, 1985.

[111] Gianluca Gallo. Myosin II activity is required for severing-induced axon retraction in vitro. *Experimental neurology*, 189(1):112–121, 2004.

[112] Fridoon J Ahmad, Jessica Hughey, Torsten Wittmann, Anthony Hyman, Marion Greaser, and Peter W Baas. Motor proteins regulate force interactions between microtubules and microfilaments in the axon. *Nature cell biology*, 2(5):276, 2000.

[113] Alireza Tofangchi, Anthony Fan, and M Taher A Saif. Mechanism of axonal contractility in embryonic drosophila motor neurons in vivo. *Biophysical journal*, 111(7):1519–1527, 2016.

[114] ME Spira, R Oren, A Dormann, N Ilouz, and S Lev. Calcium, protease activation, and cytoskeleton remodeling underlie growth cone formation and neuronal regeneration. *Cellular and molecular neurobiology*, 21(6):591–604, 2001.

[115] Daniel Gitler and Micha E Spira. Real time imaging of calcium-induced localized proteolytic activity after axotomy and its relation to growth cone formation. *Neuron*, 20(6):1123–1135, 1998.

[116] Liqun Luo and Dennis DM O'Leary. Axon retraction and degeneration in development and disease. *Annu. Rev. Neurosci.*, 28:127–156, 2005.

[117] Michael J Katz. How straight do axons grow? *Journal of Neuroscience*, 5(3):589–595, 1985.

[118] Yan He, Wenqian Yu, and Peter W Baas. Microtubule reconfiguration during axonal retraction induced by nitric oxide. *Journal of Neuroscience*, 22(14):5982–5991, 2002.

[119] Marilyn A Ludueña. The growth of spinal ganglion neurons in serum-free medium. *Developmental biology*, 33(2):470–476, 1973.

[120] Manuel Théry and Matthieu Piel. Adhesive micropatterns for cells: a microcontact printing protocol. *Cold Spring Harbor Protocols*, 2009(7):pdb–prot5255, 2009.

[121] Soo-Siang Lim, Paul J Sammak, and Gary G Borisy. Progressive and spatially differentiated stability of microtubules in developing neuronal cells. *The Journal of cell biology*, 109(1):253–263, 1989.

[122] Shigeo Okabe and Nobutaka Hirokawa. Differential behavior of photoactivated microtubules in growing axons of mouse and frog neurons. *The Journal of Cell Biology*, 117(1):105–120, 1992.

[123] Zu-Hang Sheng and Qian Cai. Mitochondrial transport in neurons: impact on synaptic homeostasis and neurodegeneration. *Nature Reviews Neuroscience*, 13(2):77, 2012.

[124] Andrew F MacAskill and Josef T Kittler. Control of mitochondrial transport and localization in neurons. *Trends in cell biology*, 20(2):102–112, 2010.

[125] Anthony Brown. Axonal transport of membranous and nonmembranous cargoes: a unified perspective. *The Journal of cell biology*, 160(6):817–821, 2003.

[126] Sonita R Chada and Peter J Hollenbeck. Mitochondrial movement and positioning in axons: the role of growth factor signaling. *Journal of Experimental Biology*, 206(12):1985–1992, 2003.

[127] Kyle E Miller and Michael P Sheetz. Direct evidence for coherent low velocity axonal transport of mitochondria. *The Journal of cell biology*, 173(3):373–381, 2006.

[128] Ahmad IM Athamneh, Yingpei He, Phillip Lamoureux, Lucas Fix, Daniel M Suter, and Kyle E Miller. Neurite elongation is highly correlated with bulk forward translocation of microtubules. *Scientific reports*, 7(1):7292, 2017.

[129] Elise Spedden, James D White, Elena N Naumova, David L Kaplan, and Cristian Staii. Elasticity maps of living neurons measured by combined fluorescence and atomic force microscopy. *Biophysical journal*, 103(5):868–877, 2012.

[130] Elise Spedden and Cristian Staii. Neuron biomechanics probed by atomic force microscopy. *International journal of molecular sciences*, 14(8):16124–16140, 2013.

[131] Ahmad IM Athamneh, Alexander X Cartagena-Rivera, Arvind Raman, and Daniel M Suter. Substrate deformation predicts neuronal growth cone advance. *Biophysical journal*, 109(7):1358–1371, 2015.

[132] David E Koser, Amelia J Thompson, Sarah K Foster, Asha Dwivedy, Eva K Pillai, Graham K Sheridan, Hanno Svoboda, Matheus Viana, Luciano da F Costa, Jochen Guck, et al. Mechanosensing is critical for axon growth in the developing brain. *Nature neuroscience*, 19(12):1592, 2016.

[133] Elias H Barriga, Kristian Franze, Guillaume Charras, and Roberto Mayor. Tissue stiffening coordinates morphogenesis by triggering collective cell migration in vivo. *Nature*, 554(7693):523, 2018.

[134] RV Seshagiri Rao, Chirag Kalelkar, and Pramod A Pullarkat. Optical fiber-based force transducer for microscale samples. *Review of Scientific Instruments*, 84(10), 2013.

[135] Jagruti Pattadkal. A study of neuronal response to mechanical tension. *Master thesis submitted to IISER, Pune*, 2013.

[136] Abhishek Kumar, Mingxing Ouyang, Koen Van den Dries, Ewan James McGhee, Keiichiro Tanaka, Marie D Anderson, Alexander Groisman, Benjamin T Goult, Kurt I Anderson, and Martin A Schwartz. Talin tension sensor reveals novel features of focal adhesion force transmission and mechanosensitivity. *J Cell Biol*, 213(3):371–383, 2016.

[137] Simon W Moore, Nicolas Biais, and Michael P Sheetz. Traction on immobilized netrin-1 is sufficient to reorient axons. *Science*, 325(5937):166–166, 2009.

[138] Callen Hyland, Aaron F Mertz, Paul Forscher, and Eric Dufresne. Dynamic peripheral traction forces balance stable neurite tension in regenerating aplysia bag cell neurons. *Scientific reports*, 4:4961, 2014.